# Groundwater Flow Model of the Church Rock Site and Local Area Church Rock, New Mexico

October 2012

United Nuclear Corporation
Church Rock Tailings Site
Church Rock, New Mexico

CHESTER ENGINEERS

United Nuclear Corporation

Gallup, New Mexico

# Groundwater Flow Model of the Church Rock Site and Local Area Church Rock, New Mexico

October 2012

CHESTER ENGINEERS

United Nuclear Corporation
Gallup, New Mexico

# Groundwater Flow Model of the Church Rock Site and Local Area Church Rock, New Mexico

October 2012

Prepared by: James A. Ewart, Ph.D., P.G.

Approved by: Mark D. Jancin, Ph.D., P.G.

Project No.: 12-6209-SC-122

CHESTER ENGINEERS

# Table of Contents

**Page Nos.**

# List of Tables

# List of Figures

# List of Figures, cont'd

# List of Appendices

# List of Acronyms and Abbreviations

| | |
|---|---|
| ACL | alternate concentration limit |
| DEM | digital elevation model |
| EPA | U.S. Environmental Protection Agency |
| ET | evapotranspiration |
| ft amsl | elevation in feet above mean sea level |
| ft/d | feet per day |
| ft/yr | feet per year |
| $ft^3/d$ | cubic feet per day |
| gpm | gallons per minute |
| GMS | Groundwater Modeling System (computer software) |
| KM CR | Kerr McGee Church Rock Mine |
| LPF | layer-property flow |
| mg/L | milligrams per liter |
| NE CR | Northeast Church Rock Mine |
| NRC | U.S. Nuclear Regulatory Commission |
| RI | remedial investigation |
| ROD | Record of Decision |
| TDS | total dissolved solids |
| UNC | United Nuclear Corporation |

# Section 1

## *Introduction*

On behalf of United Nuclear Corporation (UNC), Chester Engineers has prepared this report on the development of a three-dimensional, numerical groundwater flow model (Flow Model) of UNC's Church Rock Mill and Tailings Site and the adjacent down-gradient region northeast of Gallup, New Mexico. The purpose of this report is to describe the Flow Model: its conceptual basis, the methods of its development, its capabilities, and its limitations.

The principal objective of the Flow Model is to support decision making related to Alternate Concentration Limit (ACL) applications that may potentially be submitted to the NRC. As the potential for such applications is anticipated to be greatest for the Zone 3 hydrostratigraphic unit, that unit is the focus of interest of the Flow Model. The definition of this unit and its context with respect to the Site and the broader groundwater flow system are described in this report.

To support decision-making for Zone 3 ACL applications, the Flow Model should have the more general capability of predicting the future disposition of three genetic classes of groundwater. Two of these classes are anthropogenic and have been defined in the Record of Decision (ROD) (EPA, 1988b) and subsequent Site documents: post-mining/pre-tailings (background) and post-mining/post-tailings (commonly referred to as tailings-impacted or seepage-impacted). The third class of groundwater is derived from natural recharge and is described by the ROD as pre-mining/pre-tailings (natural). This general objective directed the scale of the model in its spatial and time dimensions.

The historic disposition of seepage-impacted groundwater has been subject to direct observation, beginning with monitor well sampling by UNC in the early 1980s and continuing through the 1985-1987 remedial investigation (RI) (EPA, 1988a), and subsequent (1989-2011) annual sampling and reporting by UNC (Canonie Environmental Services Corp. [Canonie], 1989, 1990, 1991, 1992, 1993 and 1995; Smith Technology Corporation, 1995 and 1996; Rust Environment and Infrastructure, 1997; Earth Tech, 1998, 1999, 2000, 2002a and 2002b; USFilter, 2004a; N.A. Water Systems, 2004, 2005, 2007, and 2008a; and Chester Engineers, 2009, 2010, 2011, 2012). In contrast, the entry and migration of background groundwater through geologic media began in 1968 and had extended beyond the area of water-level observations in monitoring wells by the time such observations began in the early 1980s. This increasingly became the case in subsequent decades, because the monitoring well network was expanded to delineate the extent of seepage-impacted, rather than background groundwater. Nevertheless, understanding the disposition of background groundwater from the past through the future is a requisite for predicting the future disposition of seepage-impacted groundwater, because background groundwater is in contact with seepage-impacted groundwater and occupies portions of the geologic media between up-gradient impacted groundwater and down-gradient natural groundwater. This made it necessary to initiate the model with the start of mine water discharge in 1968.

Areas saturated by natural groundwater were and are largely down-gradient of the Site monitor wells. However, key observations made during the sinking of the Northeast Church Rock Mine

(NE CR mine) Shaft 1, and subsequently in the most down-gradient monitor wells in the Zone 1 hydrostratigraphic unit, enable the delineation of the natural groundwater table in Zones 1 and 3. As explained further in the report, this delineation dictated the spatial scale of the Flow Model.

The Flow Model was developed using two industry standard computer programs: MODFLOW, 2000 version (Harbaugh et al., 2000) and MODPATH (Pollock, 1994). The specific versions of these programs are those included in the Groundwater Modeling System software (GMS, version 5.3, Aquaveo publ.), which was used for pre- and post-processing of model data. Surfer (version 10, Golden Software) was also used for pre- and post-processing. The use of MODFLOW and MODPATH imparted important capabilities, but also limitations on the Flow Model. Most generally, the Flow Model is fully three-dimensional, and incorporates the geometries and hydraulic characteristics of each Site hydrostratigraphic zone that was subject to transient saturation by the two anthropogenic classes of groundwater described above. The Flow Model makes extensive use of the MODFLOW cell rewetting process, which is procedural rather than physics-based. While this capability was essential for the model simulation, it can only approximate the propagation of an unconfined wetting front through previously unsaturated geologic media. The model is limited to groundwater flow and purely convective (i.e. non-reactive, non-dispersive) transport. Purely convective transport is simulated by the method of particle tracking. Specific limitations imparted by the choice of modeling method and model error characteristics are described further in the report.

## 1.1 Site Location

The Church Rock Site ("Site") is located approximately 17 miles northeast of Church Rock, McKinley County, New Mexico (see Figure 1). Figure 2 is a Site map that shows the location of the decommissioned and temporarily idled extraction wells, the performance monitoring wells, the evaporation ponds, and the reclaimed tailings areas. Figure 2 also shows the Remedial Action Target Area for each hydrostratigraphic unit, where the impacts of tailings seepage were originally identified and corrective action was implemented (EPA, 1988a). Additional background information on Site facilities and activities is available in the previous annual reviews (Canonie Environmental Services Corp. [Canonie], 1989, 1990, 1991, 1992, 1993 and 1995; Smith Technology Corporation, 1995 and 1996; Rust Environment and Infrastructure, 1997; Earth Tech, 1998, 1999, 2000, 2002a and 2002b; USFilter, 2004a; N.A. Water Systems, 2004, 2005, 2007, and 2008a; and Chester Engineers, 2009, 2010, 2011, and 2012).

## 1.2 Geologic Setting

### *1.2.1 Regional Geologic Setting*

The Site and additional area within the Flow Model boundaries (model domain) lie near the southern margin of the San Juan structural and hydrologic basin. The San Juan Basin extends north into Colorado where it encompasses the surface drainage basin of the San Juan River. The model domain is shown in relation to the San Juan Basin and the Gallup Sandstone in Figure 3 (after Kernodle, 1996). The Gallup Sandstone is of interest, because it comprises two of the

three transmissive hydrostratigraphic zones incorporated in the Flow Model (unconsolidated deposits comprise the third transmissive hydrostratigraphic zone incorporated in the Flow Model).

Figure 3 also shows the structural elevations on top of the Gallup Sandstone, as well as its extent and areas of outcrop. The model domain straddles a portion of the southernmost area of Gallup Sandstone outcrop. The top of the Gallup Sandstone descends over 5500 ft in elevation over approximately 60 miles north from the model domain to its northernmost extent, which corresponds to a regional dip (slope angle) of about 1 degree. Regional structures mapped in the vicinity of the model domain include the Zuni Uplift to the south and the Gallup Sag to the west (Science Applications and Bearpaw Geosciences, 1980; Canonie, 1987). These structures have local elements, which are described in Section 1.2.2.

The Gallup Sandstone is an important regional aquifer that has been the subject of several hydrogeologic studies (c.f. Stone, 1981; Kernodle et al., 1989). Broader regional studies have investigated the Gallup Sandstone in the context of the hydrogeology of the San Juan Basin (cf. Stone et al., 1983; Kernodle, 1996). Kernodle (1996) made a steady-state groundwater flow model of the San Juan Basin, including the Gallup Sandstone. Figure 3 shows the domain of the Flow Model relative to Kernodle's (1996) model estimate of regional piezometric elevations within the Gallup Sandstone. The model-predicted heads are consistent with well water-level observations reported in Kernodle et al. (1989) and Stone (1981). A northward (down dip) hydraulic gradient is predicted in the area of the Flow Model domain. Upward migration through several thousand feet of overlying rock strata is predicted in the north and northwest portions of the Gallup Sandstone. Eventually, much of this groundwater discharges to the San Juan River near the Four Corners (Stone, 1981).

Groundwater recharge to the Gallup Sandstone occurs predominantly where it outcrops at the western and southern margins of its regional extent (Stone, 1981; Kernodle, 1996). The model domain encompasses a portion of the southern area of outcrop where recharge of the Gallup Sandstone occurs (Figure 3). Kernodle (1996) reports that isotopic age dating of groundwater in the Gallup Sandstone is consistent with the theory that recharge rates in the past (pluvial climates of the Pleistocene Epoch) were greater than at present. Furthermore, Kernodle (1996) cites carbon-14 dating of water in the Morrison Formation (which occurs below the Gallup Sandstone) as evidence that groundwater had migrated less than 20 miles from outcrops in 40,000 years. It is reasonable to conclude that similarly slow rates of migration may prevail in the Gallup Sandstone. Kernodle (1996) presents maps showing modern (1931-1960) mean annual precipitation of 10 to 12 inches per year and mean annual evapotranspiration of 50 inches per year in the area of the model domain. Most recharge occurs during periodic runoff events where arroyo channels cross outcrop areas. Local recharge is addressed further in Section 2.

### *1.2.2 Local Geologic Setting*

Figure 4 is a geologic map and stratigraphic legend showing hydrostratigraphic units incorporated in the Flow Model. The map shows the portion of the model domain where these

units outcrop or subcrop (beneath unconsolidated materials). The area of unconsolidated materials (alluvium and tailings) shown in the map encompasses only the area included in the Flow Model, where transient saturation may have occurred in response to discharges of mine water and tailings fluids.

Four bedrock hydrostratigraphic units are directly represented in the Flow Model. From upper to lower these are the Dilco Coal (member of the Cravasse Canyon Formation), Zone 3 (comprising the Torrivo Sandstone of the Crevasse Canyon Formation and the uppermost sandstone of the Upper Gallup Sandstone), Zone 2 (a coal and shale unit of the Upper Gallup Sandstone), and Zone 1 (the lower sandstone of the Upper Gallup Sandstone). Beneath Zone 1 (and the base of the Flow Model) is the D-Cross Tongue of the Mancos Shale, which locally divides the Gallup Sandstone into upper and lower units or members.

The transmissive hydrostratigraphic units represented in the Flow Model are the unconsolidated materials (principally alluvium), Zone 3, and Zone 1. The Dilco Coal and Zone 2 are aquatards, as is the Mancos Shale. The top contact of the Mancos (equivalent to the bottom contact of Zone 1) forms the base of the model.

Two structures, the Pipeline Canyon lineament and the Pinedale monocline, are shown in Figure 4, based on mapping by Science Applications and Bearpaw Geosciences (1980). The Pinedale monocline is a second order fold on the northern margin of the Zuni Uplift. Science Applications and Bearpaw Geosciences (1980) interpret both structures as having resulted from passive draping or folding of younger sediments over rotational basement faults. The location of the Pipeline Canyon lineament at the Site is inferred, because of a lack of exposure. However, increases of fracture density (to one foot spacing) and small changes of dip angle (3-4 degrees) were reported to be associated with both structures.

Others have considered what influence fractures associated with the Pipeline Canyon lineament may have had on rates of infiltration of mine discharge water into hydrostratigraphic Zones 1 and 3 and on the migration rates of tailings-impacted groundwater. McLin and Tien (1982) note that when seen in outcrop the fractures are typically filled with secondary mineralization (gypsum or limonite) and they concluded that their influence on groundwater migration is secondary to the geometry of surface-water sources. In contrast, Raymondi and Conrad (1983) ascribe a significant role to lineament-related fractures facilitating infiltration of mine discharge water.

The remainder of this section describes the structural elevations and thicknesses of the transmissive hydrostratigraphic units represented in the Flow Model: the unconsolidated materials (alluvium and tailings), Zone 3, and Zone 1. Bases for these estimates include geologic logs of wells (see Figure 2 for locations), borings and geophysical surveys (see Figure B-2), historic topographic maps (see Appendix B, Figures B-2 and B-3), previous Site reports (Canonie, 1987; USFilter, 2004b), and regional reports (Stone, 1981; Kernodle, et al. 1989; Kernodle, 1996).

Figures 5 and 6 show the estimated extent, thickness and base elevation (top of rock) of unconsolidated material incorporated in the Flow Model. The figures also show locations of

wells and borings whose logs were the primary bases for the thickness and elevation estimates. The extent of unconsolidated material is based on mapping by Canonie (1987) with extrapolations based on interpretation of aerial photography. The extent shown in these figures is the same as shown in Figure 3, and represents only areas subject to transient saturation by mine discharge water or tailings fluids. For the purpose of modeling the unconsolidated material includes both alluvium and tailings. Tailings are confined to the area of the reclaimed tailings cells (Figure 2). With the exception of limited areas (the easternmost part of the North Cell and the two former borrow pits in the Central Cell), the tailings are underlain by alluvium (Canonie, 1987; USFilter, 2004b).

Figure 7 shows estimated structural elevations (structure contours) on the top of Zone 3 and its estimated vertical thickness (isopleths). The figure also shows locations of wells and borings whose logs were the primary bases for the thickness and elevation estimates. Included among these is the log for the NE CR mine shaft 1. These data were supplemented by regional information (see Figure 3) derived from Kernodle (1996). Structure contours in the area of greater data density rotate to a northeast orientation where they cross Pipeline Canyon. This change of strike and dip direction may be attributable to flexural folding associated with the Pipeline Canyon lineament (see Figure 3). The structure contours terminate along the margins of Pipeline Canyon and higher elevations in the southern portion of the model domain (outlined in purple). The loci of these termination points are the zero thickness isopleths, which were estimated by intersecting the estimated base of Zone 3 with surface topography. Areas where the vertical thickness is between 0 and approximately 30 feet correspond roughly to areas where Zone 3 outcrops at the surface or subcrops beneath unconsolidated material (see Figure 4 for a more precise delineation). Zone 3 is interpreted to have been removed by erosion to the south of these areas. The topographic surface used in this estimate and generally for the model was derived from a digital elevation model (DEM) acquired from the US Geological Survey (USGS) national map seamless server site.

Figure 8 shows estimated structural elevations (structure contours) on the base of Zone 1 and its estimated vertical thickness (isopleths). The base of Zone 1 also corresponds with the base of the Flow Model. The figure also shows locations of wells and borings (including the NE CR mine shaft 1) whose logs were the primary bases for the thickness and elevation estimates. As with the Zone 3, regional information (see Figure 3) supplemented geologic logs in the estimates shown in Figure 8. These estimates required additional calculations, because the regional data (Kernodle, 1996) are representative of the top of the Gallup Sandstone and not any of its subunits. Therefore, extrapolated Zone 3, Zone 2, and Zone 1 thickness data were subtracted from the estimated top of Zone 3 (Figure 7) to derive structure contours on the tops and bottoms of the lower hydrostratigraphic units. As with Zone 3, structure contours rotate to a northeast orientation where they cross Pipeline Canyon in the area of greatest data density. This change of strike and dip direction may be attributable to flexural folding associated with the Pipeline Canyon lineament (see Figure 3). Areas of Zone 1 outcrop, subcrop, and absence due to erosion (Figures 4 and 8) were estimated by methods analogous to that described above for Zone 3.

## 1.3 Conceptual Model of Groundwater Flow System

Additions of anthropogenic water to the groundwater flow system in the area of the model domain began with mine water discharge to Pipeline Arroyo in March 1968. Prior to then, wells drilled at the Site were dry, indicative of a general absence of saturation in the Upper Gallup Sandstone and overlying formations (Canonie, 1987). Evidence from the log of the NE CR mine shaft 1 (see Figures 7 and 8 for shaft location) indicates that the reason for this is that the pre-mining (natural) groundwater table is down-dip and north of the Site. Figure 9 is a reproduction of the log, which shows that shaft 1 first encountered measurable groundwater flow (30 gpm) at elevation 6692 (ft amsl) in rock logged as the Main (Upper) Gallup Sandstone. The original log has been annotated to show the relative positions of the Site bedrock hydrostratigraphic units: Zone 3 and Zone 1. Zone 2 is represented by the coal seam logged between Zones 3 and 1. Therefore, the log demonstrates that natural groundwater was first encountered approximately 10 feet above the base of Zone 3 at a location to the northwest and down-dip of the Site.

The regional groundwater flow system in the Gallup Sandstone is extensive relative to the area of the Site and the model domain (see Figure 3). It has also been subject to rates of groundwater migration that are very slow (see Section 1.2.1) relative to the migration rate of anthropogenic groundwater during the several decades following the introduction of mine discharge water in 1968. There is evidence from three of the most down-gradient Site monitor wells that supports the presence of the pre-mining, natural water table in Zone 1 at an elevation similar to that encountered near the base of Zone 3 by NE CR mine shaft 1. These wells, 0141, 0142, and 0143, are screened at the base of Zone 1, having screen top elevations ranging from 6683 to 6686 (ft amsl), less than 10 ft below the elevation of the pre-mining water table encountered in the NE CR mine shaft. Water sampled from these three wells has had concentrations of dissolved solids distinctively lower than that sampled from any other Site wells. For example, the October 2011 sample from Well 0142 had a field pH of 7.9, lab TDS of 1220 mg/L, bicarbonate of 245 mg/l, sulfate of 684 mg/L, and chloride of 17 mg/L (see Appendix C in Chester Engineers, 2012). Water of this quality has been characterized as pre-mining (natural) (United Nuclear Corporation, 2006).

Wells 0141, 0142, and 0143 are located at the northern limit of the Site near the Section 36 boundary (see Figure 2). The earliest water-level measurements from these wells, made in November 1980, indicate piezometric elevations ranging from 6749 to 6755 (ft amsl), or about 60 feet higher than the measured elevation of the pre-mining water table (6692 ft amsl in NE CR shaft 1). The likely reason for this is that, by 1980, piezometric heads in the portion of Zone 1 occupied by pre-mining groundwater had been elevated by contact with background groundwater introduced after March 1968. However, evidence from the sampling history of these wells indicates that contact between these two classes of groundwater (background and natural) had little if any apparent effect on the quality of the sampled groundwater, either before or subsequent to July 1989 (the date of initial routine sampling). The sampling history of Wells 0141, 0142, and 0143 indicates that the above cited October 2011 water quality parameters are

typical of samples collected from these three wells since the inception of the remedial sampling program in July 1989 (see Appendix C in Chester Engineers, 2012).

Figure 10 is a perspective view illustrating the topographic positions of the information sources described above (NE CR mine shaft 1 and Wells 0141, 0142, and 0143) relative to other Site features, including section lines. The perspective view is to the west and the topographic surface is rendered semi-transparent to better illustrate the relationship between the ground surface and the subsurface, northward-dipping Upper Gallup Sandstone. There is no vertical exaggeration, so this is a true perspective of the shallow (1-2 degree) dip of the Upper Gallup. Figure 10 also shows the locations of two cross sections, northwest trending A-A' and northeast trending B-B'.

Figure 11A is a northeast looking view of cross section A-A'. This cross section illustrates the position of the pre-mining water table encountered in the NE CR mine shaft 1 in 1968. The water table is extrapolated into Zone 1 on the basis of the monitoring well data described above and illustrated in cross section B-B' as shown in Figure 11B. Cross section B-B' shows the location of the pre-mining water table in Zone 1, inferred from the water quality of samples taken from monitoring wells 0141, 0142, and 0143. Note that unlike Figure 10, both cross sections employ vertical exaggeration to facilitate the view of features in the vertical dimension.

The conceptual model includes recognition that there was a pre-mining (natural) water table at about elevation 6692 ft. This water table had a broad geographical extent, consistent with the observations and interpretations presented above, as well as with regional models of piezometric elevations in the Gallup Sandstone (see Figure 3). The pre-mining water table and later interface (with anthropogenic background groundwater) was also persistent. This aspect of the conceptual model is consistent with data that demonstrate a very slow migration rate exhibited by the natural, regional groundwater flow system (see Section 1.2.1). It is also consistent with Site monitoring data, which demonstrates consistent water quality of the pre-mining groundwater despite post-mining contact with and surcharging (of head) by background groundwater.

The implication of the conceptual model for the Flow Model is that the pre-mining water table is an initial condition of known location. The evidence also indicates that while the pre-mining water table should not be treated as a boundary condition, it has not been substantially deflected by or mixed with the subsequently imposed background groundwater. To the extent either process has occurred, it has been demonstrably limited in Zone 1 to a relatively narrow geographical area up-dip of wells 0141, 0142, and 0143 (see Figure 11B).

# Section 2

## *Flow Model Grid and Boundary Conditions*

### 2.1 Flow Model Grid

MODFLOW utilizes a block-centered finite difference grid, which discretizes the domain of the Flow Model into rectangular cells. The cells are three-dimensional, having a horizontal arrangement as rows and columns and a vertical arrangement as layers. Each of the cells must be assigned material properties necessary for the solution of groundwater flow equations. These material properties should be specific to the geologic materials being simulated, which is a topic of Section 3. The block-centered methodology used by MODFLOW solves groundwater flow equations for values of head (piezometric surface elevation) at the center of each grid cell.

This section describes the geometry of the Flow Model grid, its external or boundary conditions and its internal sources and sinks that are used to simulate areas of recharge, areas of infiltration beneath arroyo channels, and wells that may extract or inject water. Figure 12 shows the horizontal arrangement (columns and rows) of cells that are active in the Flow Model grid. Notice that the active cells do not extend everywhere to the boundaries of the model domain (outlined in purple). Portions of the model grid outside areas, expected to accommodate groundwater flow, were rendered inactive. For example, Figure 12 shows the arrangement of cells active in layers 3 and 4 (increasing downward), representing Zone 3. The two areas where cells have been made inactive is south of the outcrop area of Zone 3 (compare to Figures 3 and 7), and north of a buffer zone down-dip of the pre-mining water table (elevation 6693 ft amsl, Section 1.3). This buffer was designed to allow for deflection of the interface between background and pre-mining groundwater. In layer 4 the buffer extends approximately 200 feet lower in elevation and 1 to 1.6 miles laterally in the down-gradient direction from the pre-mining water table. Inactive cells are removed as unneeded numerical overhead from calculations that must be made to solve the groundwater flow equations at the center of each active cell.

The horizontal configuration of cells in layer 5, representing Zone 2, and layer 6, representing Zone 1, differ only slightly from that of layers 3 and 4 (shown in Figure 12). For example, layers 5 and 6 have 13 more active cells than the 8480 cells active in layers 3 and 4, to accommodate the more southern extents of Zones 2 and 1. In contrast, there are many fewer cells active in layer 1 (1134 cells), representing unconsolidated materials, and in layer 2 (1341 cells), representing the Dilco Coal. The reason for this is that only the area of unconsolidated material (and underlying Dilco Coal) subject to transient saturation needed to be included in the model (see Figure 4). Broader active areas were needed in the deeper layers, which accommodated down-dip migration of the anthropogenic groundwater (background and seepage-impacted).

Variations of cell dimensions are made for two purposes. Horizontal dimensions are adjusted to account for variations of hydraulic gradients, as well as to increase precision in areas where more precise estimates are desired. Typically these objectives are related and satisfied by having smaller cell dimensions in areas near sources and sinks (see next subsection) and near material property contrasts (see Section 3), where hydraulic gradients are greater and more variable. It is

a constraint of the block-centered finite difference grid employed by MODFLOW that the horizontal cell dimensions are identical in each layer (i.e. each layer of the Flow Model has the same horizontal cell dimensions as shown in Figure 12). Those dimensions range from a minimum of 115 x 174 ft to a maximum of 240 x 341 ft.

A second purpose that may be served by variations of the vertical dimensions of cells is to make the cells correspond with distinct geologic materials, such as the hydrostratigraphic units described in Section 1.2.2. This approach was used in the Flow Model grid by employing a MODFLOW methodology (package) called layer-property flow (LPF). Use of LPF requires that surfaces representing the tops and bottoms of hydrostratigraphic units be mapped to each of the grid layers. This was done using the same types of digital information derived to produce Figures 5 through 8.

## 2.2 Boundary Conditions

The Flow Model employs a no-flow condition along most of its outer margins. As the name implies, this condition causes there to be a zero flux across such boundaries. As explained in Section 2.1 the extents of active cells were limited to the south to correspond with the extents of the modeled hydrostratigraphic units. The extents were limited to the north down-gradient of the pre-mining water table at a sufficient distance to allow for migration of the pre-mining groundwater in response to the surcharge of head imposed by eventual contact with background groundwater. Prior to this, migration rates of the pre-mining groundwater are expected to be sufficiently slow that they may be treated as static over the several decade time of the Flow Model simulations (Section 4). Additional no-flow boundaries correspond with the margins of the model domain (outlined in purple in Figure 12). These boundaries were placed at a distance from the initial contact area (between background and pre-mining groundwater) judged to be sufficient to allow for lateral spreading over the time-frame of the simulations.

The second type of boundary condition was set over a limited breadth of Pipeline Canyon to allow for drainage of groundwater out of the model domain via the alluvium. This drainage boundary condition was implemented with drain cells. The location of this boundary is shown in Figure A-1 (Appendix A). MODFLOW drain cells regulate discharge (out of the model) based on two parameters: drain elevation and conductance. The conductance parameter is input as a constant, while the drain elevation may be time-variable. The conductance parameter used in the flow model was derived from the horizontal hydraulic conductivity assigned to the alluvium (see Section 3), because the simulated drainage is primarily horizontal. The capability of assigning time-variable elevations to the drains is useful, because groundwater levels in the alluvium are known to have varied significantly in response to infiltration of mine water discharge between 1968 and 1986.

The water-level record from up-gradient alluvium Well 0627 (see Figure A-1 for location) was a valuable source on which to base drain elevation time series. Figure A-2 shows the relationship of the Well 0627 hydrograph to the derived elevations for one of the drain cells. Crucially, the well hydrograph spans the time (October 1989) when piezometric elevations in this area

transitioned from rising to falling. This facilitated a backward extrapolation of the drain elevations to the point of dryness when mine discharges began in 1968.

Time-variable inputs such as the drain elevations shown in Figure A-2 were mapped to simulation stress periods using automated routines available in GMS. MODFLOW allows for adjustments of time-variable inputs at user-defined intervals called stress periods.

## 2.3 Internal Sources and Sinks

The Flow Model uses several types of internal sources and sinks. MODFLOW river cells are used to simulate infiltration of mine discharge water via Pipeline Arroyo. Recharge cells are used to simulate two different sources: seepage-impacted water via the former tailings ponds, and natural water via Pipeline Arroyo and selected tributaries from periodic runoff events. Wells are used to simulate transient pumping and injection that occurred over the history of the Site. These sources and sinks are described further below.

### *2.3.1 River Cells*

Groundwater in the Southwest Alluvium in the vicinity of the tailings impoundments was created by the infiltration of pumped mine water that was discharged to the Pipeline Arroyo. Figure 13 is a time-series graph of the combined discharge from the NE CR and KM CR mines, from its start in 1968 to its end in 1986. This water infiltrated the alluvium and created temporary saturation in the vicinity of the tailings impoundments. Table 1 lists results of a 1981 study by Raymondi and Conrad (1983) of discharge losses to infiltration beneath the Pipeline Arroyo. Approximately ten percent of the flow was estimated to have infiltrated the alluvium between weirs located upstream and downstream of the tailings ponds (see Figure A-1 for locations).

The temporary saturation caused by discharged mine water is the recognized background groundwater (EPA, 1988a; 1988b; 1998; 2008b), which is post-mining and pre-tailings in age. The level of saturation began to decline in up-gradient areas when mine water discharge ceased in 1986 (transition to decline occurred later in down-gradient areas, see Section 2.2). As a result, the flanks of the alluvial valley and the northern property boundary alluvium have completely de-saturated and, by 2000, a 31 percent saturation loss had been observed further to the south (Earth Tech, 2000a).

MODFLOW river cells operate similarly to drain cells, with the important difference that they also allow for discharge of groundwater out of the model domain. River cells operate with three parameters: stream-bed elevation, stream-bed conductance, and stage elevation. Stream-bed elevations and conductance parameters are time-invariant, whereas stage elevations may be time-variable.

A methodology was devised to estimate the river cell parameters that served the objectives of being rational, self-consistent, and conducive to adjustment during model calibration. This approach made use of measures that could be reasonably estimated and relied upon to simplify assumptions for factors not readily measured. For example, discharge rates (primarily annual

averages) are known, as shown in Figure 13 and listed in Table 2. The path of the arroyo is known from maps and aerial photography (e.g. Figure A-1). The slope of the arroyo can be roughly estimated from the DEM. Other factors such as channel morphology and roughness are expected to have varied significantly with location and over time at most locations. Simplifying assumptions were made for these factors that are not subject to accurate measurement (except in a limited sense from aerial photography).

Manning's equation was used to calculate time-variant stages based on discharge, estimated channel slope, and a uniform trapezoidal cross section. The base width of the cross section was set at 4 ft (1 ft prior to November 1968), the side slope at 4 (run over rise), and Manning's roughness coefficient at 0.045 (to simulate a rough, natural channel). A wetted width was calculated from the stage estimate and the assumed channel geometry. This added the desired element of self-consistency to the method. This type of calculation is illustrated in Table 1 for the arroyo as a whole. In practice, these calculations were made separately for the arroyo segments shown in Figure A-1. The results of the stage calculations are listed in Table A-1 and the wetted-widths in Table A-2. The average wetted width was factored with vertical hydraulic conductivity (of the alluvium) to estimate the conductance parameter for each channel segment. Average wetted widths were used, because the conductance parameter, unlike stage, is time-invariant.

Calibration of the river cell parameters was facilitated by adjusting a single stage multiplier. The effect of this adjustment, made in a spreadsheet, carried through to the stage and conductance parameters for each arroyo segment. In the GMS modeling environment the parameters associated with the arroyo segments, including elevations, were mapped to individual river cells.

### *2.3.2 Recharge Areas*

#### *Tailings Ponds*

Recharge cells were used to simulate infiltration of seepage-impacted water from the former tailings ponds. Recharge is implemented as a uniform rate (e.g. feet per day) over the surface of a model cell. This rate may vary with time. Aerial photography was analyzed to estimate where and when recharge occurred from the various former tailings ponds. Figure B-1 shows estimated outlines of the tailings ponds at different stages of their history. The tailings ponds were mapped over time using the sequence of aerial photography shown in Figures B-4 through B-8. The topographic maps shown in Figures B-2 and B-3 were also used in these estimates.

The estimation of infiltration rates from the tailings ponds was less certain. Only one detailed study of pond infiltration was available for guidance. This was the study reported by Science Applications (1980), based on water-level measurements and water-balance calculations made for borrow pits 1 and 2 (see Figures 2 and B-1 for location), during non-operational periods in June and July 1980. The results of this study include estimates of infiltration (accounting for evapotranspiration) during a period of known water level in the two borrow pits (which were hydraulically connected). Figure 14 shows the recorded history of water levels in borrow pit 2.

Also shown are estimates of the infiltration rate over time, which were based on the reported 1980 rates scaled proportionally to the head of water above the bottom of the pit.

Information such as that available for the borrow pits was not available for the other former tailings ponds. However, calculations similar to those reported by Science Applications (1980) were made for the former south pond and north pond, albeit with less precise information. Both the south and the north tailings ponds ceased to be operational after a July 16, 1979 breach of the south pond, in which the water level and volume of the pond were significantly reduced (see south pond note in Table B-2). Both former tailings ponds subsequently dried up as demonstrated by aerial photography (Figures B-5 through B-8). By mapping the various stands of the two ponds to the post-breach topography shown in Figure B-3, rates of water-level decline (e.g. feet per day) were roughly estimated. Table B-1 shows infiltration rates for the two ponds estimated from average rates of water-level decline and recorded evapotranspiration (ET) rates (Science Applications, 1980).

A procedure similar to that described above employed a pre-breach aerial photograph (Figure B-3) and pre-breach topographic map (Figure B-1) to estimate the foot print and stage elevations during the period of tailings pond growth from June 1977 through July 1979.

Using an approach similar to that taken with the borrow pit 2 estimates, an assumption was made that infiltration rates were proportional to the head of water above the bottom of each pond. With this assumption the ET adjusted rates listed in Table B-1 were scaled using the estimated heads over time in each pond. The central pond, which is not represented in the Table B-1 calculations, was assumed to have the same base rate as the north pond.

Table B-2 also shows an estimated volumetric seepage rate and total seepage volume. These estimates were based on the wetted area and infiltration rate. The volumetric seepage rates were estimated to be reduced by a factor of 0.3 during periods after the water levels dropped below the surface of the tailings, assuming 30% porosity. The estimated dates, when seepage ended, were based on comparisons of the extrapolated rates of water-level decline with the elevation of the base of tailings.

*Natural Recharge*

Recharge cells are also used in the Flow Model to simulate the infiltration of natural water via Pipeline Arroyo and selected tributaries during periodic runoff events. This process was not initially included in the model, because it was thought to add negligibly to the flux of anthropogenic groundwater. It was added specifically to improve the fidelity of model-predicted heads in Zone 3 after the cessation of mine water discharge in 1986 and particularly in more recent times. The model-predicted rates of drainage out of the area of water-level measurements that surpassed those implied by the measurements. The mechanism of natural recharge was added to the Flow Model to compensate for this inaccuracy.

River cells were initially used to represent this recharge in a manner analogous to that used to simulate the infiltration of mine water discharge (see Section 2.3.1). This did not work, and the

reason is worth examining because it addresses compromises in the Flow Model design relative to the natural mechanisms it is simulating. The compromises were imposed by a limitation of MODFLOW in the technique it uses to rewet dry cells. This rewetting procedure, which is optional, is extensively used in the Flow Model. A corollary of the model's initial condition (the pre-mining water table) is that the geologic media up-gradient of that water table started out dry and only became saturated when flooded by anthropogenic groundwater. However, MODFLOW does not allow a cell to be rewetted from above (e.g. from a river, surface recharge, or an overlying cell), only from the cell below or an adjacent cell in the same layer. Therefore, the Flow Model does not mimic the rewetting process as it actually occurs from stream bed infiltration during periodic runoff events.

Several compromises were made to get around this limitation. One was that cells beneath the river cells, described in Section 2.3.1, were "seeded" with initial saturation so that infiltration via the arroyo could initiate. This approach did not succeed with the simulation of periodic natural recharge, because the long-term rate of recharge was insufficient to maintain saturation – the cells dried up early on and ceased to act as sources. The alternative approach taken was to represent runoff-derived recharge by recharge cells. This approach suffered the same fate as river cells when recharge was applied to the uppermost (layer 1) cells that represent the alluvium. This occurred because recharge also cannot rewet a dry cell. The second compromise taken was to use the option of applying recharge directly to the highest active (i.e. wet) cell beneath the designated recharge area. This permitted recharge to occur, though it commonly caused the recharge to bypass the alluvium and be applied directly to Zone 3 (layer 3 or 4). For the purposes of the Flow Model this may not be material, because in the areas it is being applied (see Figure B-1) recharge water probably resides only temporarily in the alluvium before infiltrating Zone 3.

A methodology similar to that described in Section 2.3.1 was used to estimate the rates used to simulate recharge from periodic runoff events. As with the estimation of river cell parameters, Manning's equation was used to estimate stages and wetted widths based on discharge and stream slope. Simplifying assumptions were made about channel geometry (trapezoidal), base width (4 ft for Pipeline Arroyo and 2 ft for tributaries), side slope (run/rise = 4), and Manning's roughness coefficient (0.045). Unlike the case with mine discharges, there are no available measurements of runoff discharges on which long-term estimates might be based.

Time invariant recharge was used to simulate the long-term effects of periodic recharge events. This was done because there are no available records of Site-specific runoff discharges or precipitation. Even if such data were available, the value of estimating runoff hydrographs for a long-term model simulation would be unlikely to justify the cost of such an effort.

The nearest available long-term (1960-2011) precipitation records are from stations in Gallup. These data were used to tabulate the average number of months per year having precipitation totals of 2 to 3 inches (0.97) and of 3 to 4 inches (0.37). There were no months in the period of record having more than 4 inches of precipitation. The purpose of this calculation was to estimate the average number of times per year when a runoff event is likely. Two inches of

precipitation in a single month was arbitrarily selected as a cut off for the purpose of the estimate. This was done to roughly account for the demands of ET and soil moisture deficits. No differentiation of winter months was made, because the timing of the runoff relative to the precipitation is not critical when the recharge is averaged over a year.

Catchment areas for each of the arroyo and tributary segments shown in Figure B-1 were estimated from the DEM. For each of these areas, the volume of water associated with 1 inch of precipitation was calculated. These estimates and the results of calculations described below are listed in Table B-3. A multiplier, subject to adjustment during model calibration, was applied to the precipitation volumes to calculate the fraction available to run off. The fraction available to run off, expressed as a discharge, was used in Manning's equation to calculate stages and wetted widths in each of the arroyo and tributary segments. These values were used (as explained in the table notes) to calculate a periodic recharge rate. The periodic recharge rate can be thought of as a rate applicable to the period of a single runoff event (involving an empirically derived fraction of 1 inch of precipitation). The next column of Table B-3 lists conversions of the periodic recharge rates to average rates, using a frequency factor based on the annual average numbers of months having 2-3 inches and more than 3 inches of precipitation. Finally, there is a conversion made for the purpose of model inputs to account for the difference between the idealized wetted areas of the stream channels and the areas of the recharge cells.

This approach may seem at once both complicated and, in several respects, simplistic. Simplifying assumptions were made to account for factors not readily subject to direct measurement or estimation by rigorous methods. The apparent complexity arises in large measure from translating what is in reality a process of periodic channel-bed infiltration to a model process of steady-state recharge. This compromise in the design of the Flow Model was necessitated by the limitations imposed by the MODFLOW cell rewetting process, as described at the beginning of this subsection.

### *2.3.3 Wells*

The Flow Model uses standard MODFLOW wells to simulate historic pumping by remedial action systems that operated in each of the hydrostratigraphic zones at the Site. Well locations and screen intervals were mapped precisely to the Flow Model cells using automated routines available in GMS. Similar routines mapped well pumping time-series to simulation stress periods. Well pumping time series are tabulated in Appendix C. Pumping time series prior to 2005 were derived from summaries of annual volumes reported in sources noted below (principally, Earth Tech, 2002b). Adjustments were made for seasonal pumping (typically off in winter months) if such information was known. Pumping time series, starting in 2005, are based on totalizer records (typically daily) and are, therefore, more accurate and precise.

Standard MODFLOW wells have limitations that affect their capacity to simulate the effects of well pumping. Well abstractions are treated as a source term, with the effect that their influence on head is distributed uniformly throughout the cell containing the well. If there are multiple wells in a cell, their abstractions are summed in the source term. If a cell becomes dry any well

in the cell ceases to abstract water. If a well is screened across more than one cell (vertically) the cessation of extraction from a dry cell will not affect the abstraction from a cell (typically below) that remains wetted. These limitations are reasonable compromises, but they do influence the capacity of the model to simulate heads in observation wells proximal to pumped wells, particularly if they share the same cell. Furthermore, the predicted head in the cell should not be compared to the water level in a pumped well, which can be expected to be much lower.

Summaries of remedial action system pumping are provided below for the three targeted hydrostratigraphic units. Locations of wells are presented in Section 3. Additional information is also provided in annual reports (e.g. Chester Engineers, 2012).

*Southwest Alluvium*

Active remediation of the Southwest Alluvium began with the pumping of three wells in October 1989. A fourth well was added in June 1991. The former extraction wells ceased being pumped in January 2001.

*Zone 3*

Historic corrective action in Zone 3 consisted of pumping three sets of extraction wells: (1) Northeast Pump-Back System, (2) Stage I Remedial Action System, and (3) Stage II Remedial Action System. The Northeast Pump-Back wells started operation in 1983; the Stage I and II wells were added later as part of the Remedial Action Plan (UNC, 1989) implemented in 1989.

The numbers of operating extraction wells were reduced as Zone 3 dewatering caused sustainable pumping rates to drop below 1 gpm. The number and pumped volumes of the former extraction wells, during the period of Zone 3 corrective action from 1989 through 2000, have been summarized in Earth Tech (2002b, Figure 3-2). Pumping from the last three Stage II wells ceased in 2000.

Extraction of impacted groundwater from a new array of wells in the northern part of Zone 3 was tested in April 2005 as part of the Phase I (i.e., post-pilot) hydrofracture program (MACTEC, 2006). Continuous pumping of these wells began in May 2005. Phase I ended in January 2006; however, the pumping of most of the Phase I wells has been continued and supplemented by the installation of additional extraction wells.

Based on UNC's hydrogeologic analysis and recommendations for the design of a new pumping system to intercept and recover impacted water (N.A. Water Systems, 2008b), five new extraction wells were installed during September 2008. Three of the wells started pumping during February 2009. In November 2009 the pumping regime was adjusted by substitution of pumping at a fourth well for one of the original three wells.

A pilot injection well (IW-A) began operation in April 2011. The purpose of this injection pilot test is to evaluate the potential for creating a hydraulic (or possibly an alkalinity) barrier, using one or more injection wells, to limit further northward advance of the seepage-impacted groundwater in the northern part of Section 36.

*Zone 1*

Zone 1 corrective action consisted of source remediation (neutralization and later dewatering of borrow pit 2) and pumping of a series of extraction wells from 1984 through 1999 (Earth Tech, 2002b). Well productivity in this hydrostratigraphic unit had always been very low. Earth Tech (2002b, Figure 4-1) summarized the pumping program for Zone 1, including the well systems pumped, the number of wells operating for each system, and the combined annual pumping rates. A maximum combined pumping rate of 14 gpm was achieved by the 17 East and North Cross-Dike Pump-Back wells. The productivity declined steadily over time, and by July 1999, when the system was decommissioned, the three remaining wells were yielding a combined annual average of 0.65 gpm. The three remaining Zone 1 wells were decommissioned at the end of July 1999.

# Section 3

## Flow Model Layers, Features, and Material Property Mapping

### 3.1 Layer 1

Layer 1 is uppermost in the Flow Model (layer numbers progress downward) and is mapped to simulate unconsolidated deposits, which include the alluvium and tailings. Over most of layer 1 its top represents the ground surface and its bottom represents the top of rock. An exception occurs where geologic units represented by deeper layers have been removed by erosion. In those areas the deeper layers represent alluvium, not bedrock. Sections 1.2.2 and 2.1 describe in detail the data sources and methods used to map such surfaces to the tops and bottoms of the model layers.

Tailings are limited to the area of the tailings cells (see Figure 2) and in most locations are underlain by alluvium. The role of tailings in the groundwater flow system is limited in time to the period of former tailings pond use and subsequent drainage (see Section 2.3.2 for a detailed account).

Most of the Flow Model sources (river cells and recharge cells) are specified in layer 1 as are the four sinks (pumping wells in the alluvium) and the drain cells. Detailed accounts of the purposes and implementations of these sources and sinks are provided in Section 2. Locations of these features and most of the lateral extent of layer 1 are shown in Figure 15A. The 1980 aerial photo inset is included to show the locations of features, such as the tailings ponds, which were reclaimed later.

Material properties are used as coefficients in the groundwater flow equations solved by the model. They are specific to the geologic materials being simulated and are typically estimated from well pumping tests or other hydrogeologic information such as groundwater fluxes and hydraulic gradients. Both types of analyses were used to estimate the hydraulic conductivities and porosities listed in Table 4. In addition to these properties or model parameters, the model uses storage coefficients to solve time-dependent (transient) simulations.

Material property estimates such as those shown in Table 4 are starting points for the material property zones mapped to each model layer. The material properties were refined and modified in an iterative process of calibration whereby the predictions of piezometric head made by successive versions of the model are compared with the history of heads measured in observation wells. Elements of this process are described in Sections 4 and 5, though the results are listed in Table 5 for comparison with the layer property zone maps presented in this section.

As shown in Table 5 the Flow Model employs three mutually perpendicular directional values of hydraulic conductivity: vertical, horizontal (row-wise), and horizontal (column-wise). These directions can be thought of as axes of the principal components (minimum, maximum, and intermediate) of the hydraulic conductivity tensor. However, MODFLOW does not allow for these axes to be rotated relative to the indicated three grid directions. Therefore, the orientation of the grid has implications for the mapping of material properties and is not arbitrary. This

concept is addressed further in the context of deeper layers, which represent rock units. Layer 1 has a single material property zone in which the horizontal hydraulic conductivity is isotropic (i.e. the same in all directions), but greater than the vertical hydraulic conductivity. The horizontal hydraulic conductivity of water-deposited sediments is commonly greater than the vertical component, because layers having higher concentrations of fines (clay or silt) tend to impede vertical flow.

Table 5 also lists two storage parameters: specific yield and specific storage. The specific yield is used in cases of pore water drainage (unconfined) and is always greater than the specific storage, which is used in cases of storage change under pressure (confined). Layer 1 is unconfined, because there is no confining layer within or above it. However, each of the lower layers in the Flow Model has the capacity to convert between unconfined and confined conditions.

## 3.2 Layer 2

Layer 2 represents the Dilco Coal, and alluvium where the Dilco Coal has been removed by erosion. Material zone mapping of layer 2 is shown in Figure 15B. The alluvium in layer 2 has the same material properties as in layer 1 (Table 5), as is the case wherever alluvium is mapped in the Flow Model layers. There are two material property zones mapped in the portion of layer 2 representing the Dilco Coal. The zone designated Dilco_M2 is aligned with the grid columns (northeast) in an area that is intended to represent the influence of the increased frequency of fractures associated with the Pipeline Canyon lineament (see Figures 4 and 10). This influence is manifested in two ways by the assigned values of hydraulic conductivity. Each of the directional components of hydraulic conductivity assigned to property zone Dilco_M2 are greater than those assigned to property zone Dilco_M1 (Table 5). The relatively low hydraulic conductivity component values assigned to zone Dilco_M1 reflect its characterization as an aquatard. The horizontal components of hydraulic conductivity also differ in zone Dilco_M2; the component in the grid column direction (northeast) is greater than that in the grid row direction (northwest). This anisotropy corresponds with that expected from a preferred northeastward alignment of fractures associated with the Pipeline Canyon lineament. This expectation is also the reason that the grid columns are aligned as they are.

## 3.3 Layers 3 and 4

Figure 15C shows material property zone mapping and the locations of pumped wells in layer 3 and Figure 15D shows the same for layer 4. Both layers represent portions of the alluvium and of Zone 3.

Unlike the case for the other rock hydrostratigraphic units, Zone 3 is represented by two model layers. This reflects the fact that Zone 3 is the focus of the Flow Model objectives. It is also the case that a division into two layers was made to account for the interpretation that the lower 15 to 20 feet of Zone 3 has generally a lesser hydraulic conductivity than the upper part (Larry Bush,

2011, personal communication). This interpretation was based on observations of wells when pumped or purged for sampling. The incorporation of this distinction in the Flow Model took on increasing significance as the piezometric surface in Zone 3 receded over time.

The division into two layers also improved the capacity of the Flow Model to account for a process that could not be explicitly simulated. That process is the progressive diminishment of hydraulic conductivity by geochemical reactions of minerals in the Zone 3 sandstone to the acids in the impacted groundwater. The effects and interpreted cause of this process were first made by the In-Situ Alkalinity Stabilization Pilot Study (ARCADIS BBL, 2007). Data obtained as part of the pilot study indicated that the mineral feldspar in the Zone 3 arkosic sandstone had been altered by the acidic tailings liquids, generating kaolinitic clay that significantly clogged pore spaces and reduced hydraulic conductivity. Quantitative estimates of hydraulic conductivity variations across three transects of the impact plume in Zone 3 made by USFilter (2004b) yielded estimates listed in Table 4. These estimates are consistent with interpreted progressive reductions of hydraulic conductivity in Zone 3 having been caused by exposure to impacted groundwater.

The mapping of material property zones in layers 3 and 4 (Figures 15C and 15D) was influenced by the considerations discussed above as well as by the interpreted influence of fractures associated with the Pipeline Canyon lineament (see Section 3.2 for further discussion). Adjustments of the material property zones were made in the process of model calibration. These adjustments improved the capacity of the model to simulate observed piezometric elevations (discussed further in Sections 4 and 5) and to simulate the migration of impacted groundwater by particle tracking (see Section 4.2).

## 3.4 Layer 5

Layer 5 represents the Zone 2 hydrostratigraphic unit, and alluvium in those areas where Zone 2 has been removed by erosion. Figure 15E shows the mapping of material property zones in layer 5. The portion of layer 5 representing Zone 2 is mapped into two material property zones: one property zone having lesser values of hydraulic conductivity components reflecting the aquatard character of Zone 2, and the other property zone representing the influence of fractures interpreted to be associated with the Pipeline Canyon lineament (see Section 3.2 for further discussion). Values associated with the property zones are listed in Table 5.

## 3.5 Layer 6

Layer 6 represents the Zone 1 hydrostratigraphic unit, and alluvium in those areas where Zone 1 has been removed by erosion. Figure 15F shows the locations of pumped wells and the mapping of material property zones in layer 6. The portion of layer 6 representing Zone 1 is mapped into two material property zones: one property zone having lesser values of hydraulic conductivity components typical of Zone 1 sandstone, and the other property zone representing the influence

of fractures interpreted to be associated with the Pipeline Canyon lineament (see Section 3.2 for further discussion). Values associated with the property zones are listed in Table 5.

# Section 4

## *Simulations*

### 4.1 Groundwater Flow and History Matching

As explained in the introduction (Section 1), a premise of the Flow Model development was that the model's time scope needed to begin with the start of mine water discharge in 1968. This premise derived from the understanding that simulation of the disposition of background groundwater from the past through the future is a requisite for predicting the future disposition of seepage-impacted groundwater. A corollary of the objective of predicting future events is that the time-scope of the model must also extend to the present.

As explained in Section 2, MODFLOW divides the time-scope of transient simulations into user-defined stress periods. Those stress periods are further divided into time steps, whose durations may be adjusted to improve the numerical stability of the iterative solution process or to acquire a solution at a particular time. The history matching simulation through 2011 used 142 stress periods, which were subdivided into a total of 514 time steps, each of roughly one-month duration. The simulation predicts the state of the groundwater flow system (heads and fluxes in each model cell) at each time step.

Output from two particular time steps of the continuous simulation from 1968 through 2011 was selected for presentation in this section. The earlier of these, January 1987, is at a time when Site-wide observations of well water levels and piezometric elevation maps were starting to be made (Canonie, 1987). The later time step, October 2011, coincides with Site-wide well water levels used to produce the most recent piezometric elevation maps (Chester Engineers, 2012).

The presentations made in this section include examples of the Flow Model error characteristics. These examples are provided here, because it is useful to view the relationships of simulation errors (predicted versus observed heads) in a geographic context, relative to the predicted piezometric surface as a whole as well as to sources and sinks. A comprehensive examination of Flow Model error characteristics, relative to all observations (the calibration target data set), is provided in Section 5.

#### *4.1.1 Simulation to January 1987*

Contours of model-predicted piezometric heads and simulation errors are shown for model layers associated with Zone 3, Zone 1 and the alluvium in Figures 16A through 16C. The figures also show the locations of wells actively being pumped at the time. The model-predicted piezometric surface elevations may be compared to maps reported by Canonie (1987), which are reproduced in a reduced format in Figures D-1 (alluvium), D-2 (Zone 3 and alluvium), and D-3 (Zone 1 and alluvium).

*Zone 3*

Figure 16A shows contours of model-predicted heads and actively pumped wells for January 1987 in Layer 4, representing the lower part of Zone 3 and the alluvium. At this time, the extent of impacted groundwater was restricted to an area within the southern half of the monitor well network (Canonie, 1987). Groundwater elsewhere in the map area is predominantly of background quality (except in the northwest map corner where the groundwater is interpreted to have been pre-mining quality). Therefore, the elongate mounding of the piezometric surface along and north of Pipeline Arroyo illustrates the predicted extent to which background groundwater had infiltrated Zone 3 by this time.

Root mean squared errors (RMS) are posted at the locations of observation wells. This statistic is a measure of the absolute error (observed heads minus model-predicted heads) averaged over 12 months of observations. A symbol color scale is used to indicate average error, ranging from cooler colors (dark blue) where the model predictions are high to warmer colors (dark red) where the model predictions are low.

The average errors are spatially correlated, with higher values located nearer to source areas (the arroyo and the tailings ponds) and lower values located near the eastern margin of continuous saturation. At this margin there is also a steep hydraulic gradient evidenced by the compact spacing of northeast trending contour lines. The head drop across this wetting front from west to east is 30 to 40 ft over a distance of 200 ft or less. There is an area of discontinuous saturation to the east of the model-predicted wetting front. This is also an area where model predictions underestimate observed heads, resulting in higher-valued average errors.

Despite the local occurrence of average errors ranging from -19 to 50 feet, the overall shape and elevations of the model-predicted head contours bear many similarities to the observation-based contour map shown in Figure D-2 (Canonie, 1987). These similarities extend to the general shapes and elevations associated with contours in the vicinity of the tailings ponds, beneath the arroyo to the west and northwest and in the alluvium to the southwest. In particular, model-predicted mounding of the piezometric surface beneath the tailings ponds and the arroyo is very similar to that observed. The area of greatest divergence is in the northeast where the model fails to fully predict the measured eastward progress of the wetting front. The front is also steeper in the model prediction than was observed. This is attributable to the approximation involved in using the iterative cell rewetting procedure in MODFLOW to simulate the progression of an unconfined wetting front through unsaturated media. The question of whether the model objectives might be intolerably compromised by such errors will be answered by examining the degree to which error characteristics improve as the simulation progresses to the present time.

*Zone 1*

Figure 16B shows contours of model-predicted heads and actively pumped wells for January 1987 in Layer 6, representing the Zone 1 and the alluvium. Root mean squared errors (RMS) are posted at the locations of observation wells.

The average errors are spatially correlated, with lower values clustered near actively pumped wells. In many cases, these errors are associated with observations made in monitor wells occupying the same cell as one or more pumped wells. As explained in Section 2.3.3, this is a circumstance that is expected to result in less accurate predictions of piezometric surface elevations. In other locations the errors are smaller. This is particularly so at down-gradient wells near the Section 36 boundary and at up-gradient wells near the former north tailings pond and along Pipeline Arroyo. In these locations RMS errors are less than the contour interval of 10 ft. Between these locations average errors range from 9 to 15 ft, indicating higher than observed piezometric elevations. The overall shape and elevations of the model-predicted head contours are very similar to the observation-based contour map shown in Figure D-3 (Canonie, 1987). The model-predicted piezometric surface (Figure 16B) also indicates an area of background groundwater infiltration to the west of Pipeline Arroyo, that is not evident in Zone 3 (compare Figure 16A).

*Alluvium*

Figure 16C shows contours of model-predicted heads for January 1987 in Layer 1, representing unconsolidated materials (alluvium and tailings). Root mean squared errors (RMS) are posted at the locations of observation wells. The predicted piezometric surface is restricted for the most part to the area beneath Pipeline Arroyo (and its tributary leading from the mine discharge points, see Figure 15A) and areas beneath the former tailings ponds. The predicted hydraulic gradient follows the southwest slope of Pipeline Arroyo, except in the areas of the former tailings ponds where mounding is evident. In these respects, the predicted piezometric surface is similar to the observation-based contour map shown in Figure D-3 (Canonie, 1987).

Fidelity to measured piezometric elevations is also reflected in the posted RMS errors, which are commonly close to or less than the contour interval of 10 ft. In exception to this are average errors ranging from -17 to 23 ft at wells clustered near the former tailings ponds. Another area of difference between model-predicted and observed piezometric elevations is north of the former tailings ponds where the model fails to predict the observed extent of saturation to the east of Pipeline Arroyo. Efforts made to overcome this inaccuracy were mostly unsuccessful. However, this area later dried up and is underlain by the Dilco Coal, an aquatard. Therefore, the significance of this transient area of saturation, if any, to the flux of groundwater in Zone 3 was probably minor.

### *4.1.2 Simulation to October 2011*

*Zone 3*

Figure 17A shows contours of model-predicted heads and actively pumped wells for October 2011 in Layer 4, representing the lower part of Zone 3 and the alluvium. The amplitude of the predicted mound in the piezometric surface, representing background groundwater, is much diminished relative to January 1987 (compare to Figure 16A). However, it covers a large area and is in full contact with pre-mining groundwater in the area shown northwest of the NE CR mine shaft 1.

Zone 3 is predicted to be dry under most of the area of the tailings cells and its piezometric surface has dropped in elevation by approximately 50 ft at the southernmost observation wells and by approximately 20 ft near the down-gradient limit of observations in 1987. The eastern margin of saturation, which by 2011 had been in westward recession for several decades, no longer exhibits the steep hydraulic gradient of the earlier wetting front.

RMS errors posted at observation well locations are near to or less than the contour interval of ten feet. Average errors are balanced over a range from -10.3 to 11.1 ft. While some spatial correlation of average errors remains, it is less apparent than in the January 1987 simulation. In all these respects the error characteristics of the Flow Model are improved in the simulation of current conditions. This adds confidence to the predictions of future conditions.

*Zone 1*

Figure 17B shows contours of model-predicted heads for October 2011 in Layer 6, representing Zone 1 and the alluvium. As in Zone 3, piezometric surface elevations are much diminished in the October 2011 simulation relative to January 1987 (Figure 16B), having decreased by approximately 30 ft near the southern most observation wells (east of the tailings cells) and by approximately 40 ft near the northernmost observation wells (near the Section 36 boundary).

Root mean squared errors (RMS) are posted at the locations of observation wells. Average errors range from -6.6 to 5.7 ft at the more up-gradient and down-gradient observation wells. In between is a cluster of observation wells where the average error is spatially correlated from -21.6 to -9.7 ft. In the calibration of the model accuracy in this area of Zone 1 was sacrificed to improve the accuracy of the simulation in the same area of Zone 3. This was done because simulation of groundwater in Zone 3 is the focus of the modeling objectives.

A degree of inverse correlation of error in Layers 6 and 4 is interpreted to result from Zone 2 (simulated by layer 5) being less effective an aquatard in the Flow Model as it is in reality. Vertical flow from one layer to another is calculated according to the harmonic (geometric) mean of the vertical conductances of the upper and lower cells. Zone 2 is represented by a single layer. Therefore, its vertical hydraulic conductivity does not fully constrain vertical flow across the layer. Attempts to reduce the vertical hydraulic conductivity of Zone 2 (from the values listed in Table 5) tended to cause localized instances of numerical instability. It was decided that local areas of greater error could be tolerated outside of Zone 3 to improve the accuracy within Zone 3. The presentation below of predicted layer 1 piezometric elevations provides another example of this.

*Alluvium*

Figure 17C shows contours of model-predicted heads for October 2011 in Layer 1, representing unconsolidated materials (alluvium and tailings). The extent of saturation and elevations of the piezometric surface are similar to the observation-based contour map presented in the most recent annual report (Chester Engineers, 2012). This is apparent in the range of RMS errors

posted at observation well locations. With one exception, they are less than the contour interval of 10 ft.

The exception is a -21.3 ft error at up-gradient Well 0509D (see also Figure 2). This well is located in a portion of the alluvium saturation that is interpreted to have become stranded as the water table receded below the rim of a localized basin in the bedrock surface (Chester Engineers, 2012). This depression is mimicked in the model, though only at the precision of cell discretization. The model simulation appears to have reproduced the interpreted stranding of alluvium groundwater, though at a higher than observed head at Well 0509D. Another contributing factor is the application of natural recharge at locations shown in Figure B-1 (see also Section 2.3.2). Recharge rates at cells located in the arroyo were calibrated mostly to improve the error characteristics of the simulation in Zone 3. Similar recharge cells originally placed in the model further downstream in Pipeline Arroyo were removed, because they caused alluvium water levels to be overestimated. The remaining overestimate at Well 0509D was judged to be tolerable, because of its isolation and the beneficial effect of the simulated recharge on the Zone 3 estimates.

## 4.2 Convective Transport by Particle Tracking

Particle tracking is the method chosen to simulate purely convective transport of impacted groundwater. MODPATH (Pollock, 1994) was used to make the particle tracking analyses. The particle tracking technique makes full use of the three-dimensional solution for transient heads and cell-to-cell fluxes calculated by the MODFLOW simulation. The technique also provides for particle tracking forward or backward in time. The simulation presented in this section used backward particle tracking to determine the likely sources of groundwater in the general area of seepage-impacted groundwater in Zone 3.

Figure 18 shows the outer margin of the impact plume delineated in yellow and contours of field pH from October 2011 data reported in the latest annual report (Chester Engineers, 2012). The field of colored dots shown in Figure 18 occupies layer 4 cells (base of Zone 3) selected for particle tracking backward in time. MODPATH tracks particles backward until they reach a source, which in practice is the first water table encountered along the backward tracked path of the particle. Particles were classified by manually investigating each backward traced termination point (or source). The clearly identifiable sources are classified as either north pond, borrow pits 1 or 2, or nontailings (typically an arroyo recharge or river cell). Some particle tracks stopped short of these three sources and are unclassified as to source. Typically these are particles that encountered a transient water table within a Zone 3 cell. This is possible, because each of the model layers is capable of converting from confined to unconfined (water table) conditions. The concentrations of unclassified particles are greater near the eastern margin of saturation, where the thickness of saturation is less, and down-gradient, where the travel distances are greater. Nevertheless, they also occupy areas of seepage-impacted groundwater whose sources can reasonably be construed to be the former tailings ponds.

Taken together, the field of red and orange particles that can clearly be identified as tailings-sourced, and those yellow particles that reasonably can be construed to have a tailings source, conservatively map the extent of seepage impact based on October 2011 sample data. The model was calibrated to achieve this outcome. Those calibration steps included modifications of material property zones, particularly in layers 3 and 4. Recharge rates in the north pond were also increased by a factor of 50% from those calculated in Table B-2.

Having demonstrated the capacity of the model to simulate convective transport of seepage impacted groundwater to the present time, the next steps are to make predictive analyses of future migration under simulated conditions. The next section presents such a simulation.

## 4.3 Predictive Simulation to 2026

This section presents a 15-year forward predictive simulation to 2026 based on hypothetical pumping from existing extraction wells in Zone 3. The only water source in the simulation is the steady-state, natural recharge used in the simulation through October 2011. Forward particle tracking was made from layer 3 and 4 cells inside the delineation (yellow line) of seepage impact shown in Figure 18.

The predictive simulation assumes that existing Zone 3 extraction wells will continue to operate with empirically estimated pumping rate decline curves. Figure 19 shows the estimated pumping rate curves, which were fit to log-time functions. This approach accounts for the effects of gradually declining saturated thickness, but not other processes such as siltation. Therefore, the projected pumping rates are optimistic.

Figure 20 shows contours of the predicted piezometric surface elevations in layer 4 (base of Zone 3). The field of view is expanded to show more of the area predicted to be occupied by background groundwater. The area of seepage-impacted groundwater is that occupied by the red forward particle tracks. In this simulation the particle tracks do not extend north of the northern line of extraction wells, many of which operate through the entire simulation.

It is instructive to view the extent of seepage-impacted groundwater in relationship to the much larger mound of background groundwater. The background groundwater occupies a large area of Zone 3 between the down-gradient pre-mining water and the seepage-impacted groundwater. The seepage-impacted groundwater is marginalized between the eastern edge of saturation and the hydraulic mound created by the background groundwater. It is not difficult to predict that this relationship will continue indefinitely into the future even as the background groundwater continues to spread laterally to the east and west.

Figure 21 shows contour lines of saturated thickness calculated by subtracting the pre-mining water table elevation of approximately 6700 ft amsl from the piezometric surface elevations shown in Figure 20. The resulting thicknesses represent approximately the mound of impression in Zone 3 created by background groundwater.

It is worthwhile to test the model prediction of the extent of background groundwater to information about its source: mine water discharge. To do so, the predicted piezometric surface mound must be converted into a comparable volume of water. The Zone 3 mound of impression was compared to the estimated upper and lower surfaces of Zone 3 (see Figure 7) to calculate the aquifer volume estimated to be occupied by background groundwater. This step was required, because some of the piezometric mound shown in Figure 21 represents pressure head above the physical top of Zone 3. An analogous calculation was made using predicted piezometric surface elevations in Zone 1 (not shown). The resulting aquifer volumes are listed in Table 6 and, by accounting for porosity, expressed as water volumes. The combined volumes of estimated background groundwater in Zones 1 and 3 are roughly 10% of the total reported volume of mine discharge water. This ratio compares favorably with the estimated percentage of mine water discharge lost to infiltration based on weir measurements (see Table 1, Section 2.3).

# Section 5

## *Error Characteristics*

### 5.1 Comparison of Predicted and Observed Heads

Comparisons of model-predicted heads and observed heads are shown in Figures 22A through 22C for Zone 3 wells, Zone 1 wells, and alluvium wells. Each of the graphs plot model-predicted heads on the y-axis and observed heads on the x-axis. The axes are drawn with identical data ranges, so that a perfect correspondence of simulated and observed heads would result in a lower-left to upper-right line of points. Deviations from such a line represent simulation errors. Such plots are a useful way to display the total dynamic (time-dependent) range of observed heads as well as tendencies for simulation error to correlate with the observed heads.

Figure 22A shows the comparison for Zone 3. The total range of predicted heads and observed heads is similar, about 160 ft. There is not a dominant pattern of correlation of simulation errors with observed head, except for a clustering of lower than observed heads in the mid-range of observed heads, between 6860 and 6900 ft. These simulation errors are mostly associated with the model tendency to underestimate observed heads along the eastern margin of saturation, particularly in early time steps (relative to the 1980 start of observations; see Figure 16A, Section 4.1.1).

Figure 22B shows similar information for Zone 1. The total range of observed heads is approximately 200 ft. There is less simulation error overall than in Figure 22A. However, there is a downward curvature of the data at lower elevations and higher elevations indicating a tendency of the model to underestimate observed heads at down-gradient and up-gradient observation wells.

Figure 22C compares predicted and observed heads in the alluvium. The total dynamic range of observed heads is 130 ft. Simulation error generally is relatively low. However, there are several sets of data points that track well below the rest. These are associated with wells in the northern area of the alluvium where the model underestimated both the extent and depth of saturation. This area of transient saturation and its minor significance to the modeling objectives is described in Section 4.1.1.

### 5.2 Comparison of Residuals and Observed Heads

Figures 23A through 23C show the same information as in Figures 22A through 22C, but in a way that detrends the plots to show relative error as a function of the observed heads. Residuals are calculated by subtracting the model-predicted head from the observed head. Therefore, a positive residual indicates an underestimate and a negative residual indicates an overestimate. Also shown are the mean residual and the root mean squared residual for the entire calibration data set (all observations).

Figure 23A shows model residuals for Zone 3. The root mean squared residual for the entire simulation is 15.9 ft, a measure of the average absolute error. The mean error for the entire

simulation is 7.8 ft, indicating an average tendency to underestimate observed heads. This average is manifested primarily by relatively high positive errors in the mid-range of observed heads, from 6860 to 6900 ft. As explained in the previous section, these errors are primarily associated with the model tendency to underestimate observed heads along the eastern margin of saturation, particularly in early time steps (relative to the 1980 start of observations; see Figure 16A, Section 4.1.1).

Figure 23B shows model residuals for Zone 1. The root mean squared residual for the entire simulation is 14.1 ft and the mean residual is -0.01 ft. While these statistics are relatively good, there is a marked curvature to the data plot at lower and upper extremes of observed heads. The underestimates of head at the upper extreme of observed heads are associated with numerous observation wells that were proximal to active pumping wells in the vicinity of the former borrow pits (see Figure 16B). As explained in Section 4.1.1, proximity to pumped wells is an expected source of error in finite difference simulations. There is a marked improvement of the simulation in this area of Zone 1 after pumping ceased (see Figure 17B and further discussion below).

Figure 23C shows model residuals for the alluvium. The root mean squared residual for the entire simulation is 9.7 ft. The mean residual for the entire simulation is -3.98 ft, indicating a tendency to overestimate observed heads. There is also a cluster of positive residuals of approximately 50 ft associated with underestimated heads at a few wells that were described in the previous section.

## 5.3 Residuals Versus Time

Figures 24A through 24C are plots of model residuals versus simulation time for Zone 3, Zone 1, and the alluvium. These plots are useful indicators of the accuracy of the simulation as a function of time.

Figure 24A shows residuals versus time for Zone 3 observations. It is apparent that simulation error, particularly underestimations, were greater during earlier time steps. The January 1987 simulation shown in Figure 16A is representative of this earlier period. The groundwater flow system in Zone 3 was very dynamic in this period, because of the outward migration of the wetting front, substantial infiltration sources in Pipeline Arroyo and the tailings ponds, and well pumping. This dynamism and associated simulation error diminished as the effects of these sources receded. By the present time (2011) the range of residuals is reduced to about plus or minus 10 ft.

Figure 24B shows residuals versus time for Zone 1 observations. From about 1993 on, the range of residuals is substantially less than at prior time steps. The range of residuals by 2011 is about 25 ft, though there is a bias toward negative residuals, indicating overestimation of heads. This bias was explained in Section 4.1.2 as a compromise made to improve the error characteristics of the simulation in Zone 3.

Figure 24C shows residuals versus time for observations in alluvium wells. As with the previous plots there is a significant reduction of the range of residuals in later years of the simulation. From 1997 forward, the main body of residuals falls between plus or minus 10 ft. However, there is a line of residuals at -20 ft over this same time period. These residuals are associated with Well 0509D. An explanation for the simulation error at this well is presented in Section 4.1.2.

# Section 6

## *Conclusions*

The Flow Model described by this report has met the functionality goals outlined in the Introduction. These capabilities are to predict the future disposition of three genetic classes of groundwater. Two of these classes are anthropogenic and have been defined in the ROD (EPA, 1988b) and subsequent Site documents: post-mining/pre-tailings (background) and groundwater affected by tailings seepage (seepage-impacted). The third class of groundwater is derived from natural recharge and is described by the ROD as pre-mining/pre-tailings (natural). The model was used to predict current (October 2011) and future (October 2027) dispositions of the three genetic classes of groundwater, within and outside the area of the monitor well network. This was done after verifying the capacity of the model to simulate, with sufficient accuracy, the historic development of the anthropogenic part of the groundwater system recorded by monitor well observations (water levels) and samples (presence or absence of seepage impacts). These steps demonstrate attainment of the functionality goals set for the model.

With this report the task of developing the tool is complete. The main objective of utilizing the Flow Model is to support decision-making for future Zone 3 ACL applications.

# Section 7

## *References*


ARCADIS BBL, 2007, In-Situ Alkalinity Stabilization Pilot Study, UNC Church Rock Site, Gallup, New Mexico. June.

Canonie Environmental Services Corp., 1995, EPA Remedial Action and NRC Ground Water Corrective Action, Five-Year Review (1989-1994). January.

Canonie Environmental Services Corp., 1993, Ground Water Corrective Action, Annual Review 1993, Church Rock Site, Gallup, New Mexico. December.

Canonie Environmental Services Corp., 1992, Ground Water Corrective Action, Annual Review 1992, Church Rock Site, Gallup, New Mexico. December.

Canonie Environmental Services Corp., 1991, Ground Water Corrective Action, Annual Review 1991, Church Rock Site, Gallup, New Mexico. December.

Canonie Environmental Services Corp., 1990, Ground Water Corrective Action, Annual Review 1990, Church Rock Site, Gallup, New Mexico. December.

Canonie Environmental Services Corp., 1989, Ground Water Corrective Action, Annual Review 1989, Church Rock Site, Gallup, New Mexico. December.

Canonie Environmental Services Corp., 1987, Geohydrologic Report, Church Rock Site, Gallup, New Mexico. May.

Chester Engineers, 2012, Annual Review Report – 2011 – Groundwater Corrective Action, Church Rock Site, Church Rock, New Mexico. January 28, 2012.

Chester Engineers, 2011, Annual Review Report – 2010 – Groundwater Corrective Action, Church Rock Site, Church Rock, New Mexico. January 28, 2011.

Chester Engineers, 2010, Annual Review Report – 2009 – Groundwater Corrective Action, Church Rock Site, Church Rock, New Mexico. January 28, 2010.

Chester Engineers, 2009, Annual Review Report – 2008 – Groundwater Corrective Action, Church Rock Site, Church Rock, New Mexico. January 28, 2009.

Earth Tech, Inc., 2002a, Ground Water Corrective Action, Annual Review - 2001, Church Rock Site, Gallup, New Mexico. January.

Earth Tech, 2002b, Annual Review Report – 2002 – Groundwater Corrective Action, Church Rock Site, Gallup, New Mexico. December.

Earth Tech, Inc., 2000, Ground Water Corrective Action, Annual Review - 2000, Church Rock Site, Gallup, New Mexico. December.

Earth Tech, Inc., 1999, Ground Water Corrective Action, Annual Review - 1999, Church Rock Site, Gallup, New Mexico. December.

Earth Tech, Inc., 1998, Ground Water Corrective Action, Annual Review - 1998, Church Rock Site, Gallup, New Mexico. December.

Harbaugh, A.W., Banta, E.R., Hill, M.C., and McDonald, M.G., 2000, MODFLOW-2000, the U.S. Geological Survey modular ground-water model -- User guide to modularization concepts and the Ground-Water Flow Process: U.S. Geological Survey Open-File Report 00-92, 121 p.

Kernodle, J.M., Levings, G.W., Craigg, S.D., and W.L. Dam, 1989, Hydrogeology of the Gallup Sandstone in the San Juan structural basin, New Mexico, Colorado, Arizona, and Utah, U.S. Geological Survey Hydrologic Investigations Atlas HA-720-H, 2 sheets.

Kernodle, John M., 1996, Hydrogeology and steady-state simulation of ground-water flow in the San Juan Basin, New Mexico, Colorado, Arizona, and Utah, U.S Geological Survey Water-Resources Investigations Report 95-4187, 117p.

MACTEC Engineering and Consulting, Inc., 2006, Phase I Full Scale Hydraulic Fracturing Final Report, United Nuclear Church Rock Facility, New Mexico. June.

McLin, S.G., and P.L. Tien, 1982, Hydrogeologic characterization of seepage from uranium mill tailings impoundment in New Mexico, in Proceedings of the Second Ann. Symp. on aquifer restoration and groundwater monitoring, Columbus OH, Nat. Water Well Assoc., pp. 343-358. May.

N.A. Water Systems, 2008a, Annual Review Report 2007 – Groundwater Corrective Action, Church Rock Site, Church Rock, New Mexico. January 29, 2008.

N.A. Water Systems, 2008b, Recommendations and Summary of Hydrogeologic Analysis – Evaluation of Groundwater Flow in Zone 3 for the Design of a Pumping System to Intercept and Recover Impacted Groundwater, UNC Church Rock Tailings Site, Gallup, New Mexico. April 25, 2008.

N.A. Water Systems, 2007, Annual Review Report 2006 – Groundwater Corrective Action, Church Rock Site, Church Rock, New Mexico. January 9, 2007.

N.A. Water Systems, 2005, Annual Review Report 2005 – Groundwater Corrective Action, Church Rock Site, Church Rock, New Mexico. December 28, 2004.

N.A. Water Systems, 2004, Annual Review Report 2004 – Groundwater Corrective Action, Church Rock Site, Church Rock, New Mexico. December 30, 2004.

Pollock, D.W., 1994, User's Guide for MODPATH/MODPATH-PLOT, Version 3: A particle tracking post-processing package for MODFLOW, the U.S. Geological Survey finite-difference ground-water flow model: U.S. Geological Survey Open-File Report 94-464, Chapter 6.

Raymondi, R.R., and R.C. Conrad, 1983, Hydrogeology of Pipeline Canyon, Groundwater, V.21, N.2, pp. 188-198.

Rust Environment and Infrastructure, 1997, Ground Water Corrective Action, Annual Review - 1997, Church Rock Site, Gallup, New Mexico. December.

Science Applications, Inc. and Bearpaw Geosciences, 1980, Geology of the Church Rock Area, New Mexico, UNC Mining and Milling Division, Albuquerque, New Mexico. July.

Science Applications, Inc., 1980, Seepage Study, UNC Church Rock Operations, volume IV, water balance calculations. August.

Science Applications, Inc., November 1981, Status Report – Geology of the United Nuclear Corporation's N.E. Church Rock Tailings Area, United Nuclear Corporation, Mining and Milling Division, Albuquerque, New Mexico.

Sergent, Hauskins & Beckwith, May 1976, Geotechnical Investigation Report, Tailings Dam and Ponds, Church Rock Uranium Mill, United Nuclear Corporation, Church Rock, New Mexico.

Sergent, Hauskins & Beckwith, July 1976, Seismic Refraction Investigations Report, Tailings Dam and Ponds, Church Rock Uranium Mill, United Nuclear Corporation, Church Rock, New Mexico.

Sergent, Hauskins & Beckwith, October 1978, Engineering Analysis Report, Tailings Disposal Systems Analysis, Church Rock Uranium Mill, United Nuclear Corporation, Church Rock, New Mexico.

Smith Technology Corporation, 1996, Ground Water Corrective Action, Annual Review - 1996, Church Rock Site, Gallup, New Mexico. December.

Smith Technology Corporation (Smith Environmental Technologies Corporation), 1995, Ground Water Corrective Action, Annual Review - 1995, Church Rock Site, Gallup, New Mexico. December.

Stone, William J., 1981, Hydrogeology of the Gallup Sandstone, San Juan Basin, Northwest New Mexico, Groundwater, v.19, n. 1, pp. 4-11.

Stone, W.J., Lyford, F.P., Frenzel, P.F., Mizell, N.H. and E.T. Padgett, 1983, Hydrogeology and water resources of the San Juan Basin, New Mexico, Socorro, New Mexico Bureau of Mines and Mineral Resources Hydrologic Report 6, 70 p.

United Nuclear Corporation, 2006, Letter Submittal to Gary Janosko (NRC), "Revised License Amendment Request for Changing Ground Water Protection Standard for Radium in Source Materials License SUA-1475 (TAC LU0092) Groundwater Corrective Action Program." April 7, 2006 (Revision of February 22, 2006 Submittal).

United Nuclear Corporation, 1989, Remedial Action Plan, Church Rock Uranium Mill Tailings Facility. April.

U.S. Environmental Protection Agency (EPA), 2008b, Third Five-Year Review Report for the United Nuclear Corporation Ground Water Operable Unit, Church Rock, McKinley County, New Mexico. September 2008.

U.S. Environmental Protection Agency (EPA), 2006, Letter on "Supplemental Feasibility Study, UNC Superfund Site, Church Rock, NM, Administrative Order (Docket No. CERCLA 6-11-89)." June 23, 2006.

U.S. Environmental Protection Agency (EPA), 1998, Five-Year Review Report. September.

U.S. Environmental Protection Agency (EPA), 1988a, Remedial Investigation, United Nuclear Corporation Church Rock Site. August.

U.S. Environmental Protection Agency (EPA), 1988b, Record of Decision, United Nuclear Corporation, Ground Water Operable Unit, McKinley County, New Mexico. U.S. Environmental Protection Agency, Region VI, Dallas, Texas, September.

USFilter, 2004a, Annual Review Report 2003 – Groundwater Corrective Action, Church Rock Site, Church Rock, New Mexico; January 14, 2004.

USFilter, 2004b, Rationale and Field Investigation Work Plan to Evaluate Recharge and Potential Cell Sourcing to the Zone 3 Plume, Church Rock Site, Gallup, New Mexico. January 19, 2004.

# Tables

Table 1

Monthly Average Streamflow in Pipeline Canyon[1] - 1981

| Month[2] | North Weir ($ft^3/d$) | South Weir ($ft^3/d$) | Flow Difference ($ft^3/d$) |
|---|---|---|---|
| March | 509,760 | 466,560 | 43,200 |
| April | 535,680 | 483,840 | 51,840 |
| May | 509,760 | 466,560 | 43,200 |
| June | 483,840 | 440,640 | 43,200 |
| Average | 509,760 | 464,435 | 45,325 |

Notes

1. Data source: Raymondi, Richard R. and Ronald C. Conrad (1983)
2. Average of daily measurements
3. Weir locations shown in Figure A-1

Table 2
Estimated Average Flow Depths and Widths in Pipeline Arroyo, based on Discharges from the Northeast Church Rock (NECR) and Kerr McGee Church Rock (KM CR) Mines, 1968 - 1986

| Date[1] | Combined Rate[2] | | | Estimated Flow Depth[3] | Estimated Wetted Width |
|---|---|---|---|---|---|
| | (gpm) | ($ft^3$/d) | ($ft^3$/s) | (ft) | (ft) |
| Mar-68 | 30 | 5,775 | 0.07 | 0.08 | 1.6 |
| Jul-68 | 30 | 5,775 | 0.07 | 0.08 | 1.6 |
| Nov-68 | 1500 | 288,770 | 3.34 | 0.35 | 6.8 |
| Jul-69 | 2100 | 404,278 | 4.68 | 0.42 | 7.4 |
| 1970 | 2000 | 385,027 | 4.46 | 0.41 | 7.3 |
| 1971 | 2200 | 423,529 | 4.90 | 0.44 | 7.5 |
| 1972 | 2500 | 481,283 | 5.57 | 0.47 | 7.8 |
| 1973 | 3600 | 693,048 | 8.02 | 0.56 | 8.5 |
| 1974 | 3000 | 577,540 | 6.68 | 0.51 | 8.1 |
| 1975 | 3300 | 635,294 | 7.35 | 0.54 | 8.3 |
| 1976 | 4050 | 779,679 | 9.02 | 0.6 | 8.8 |
| 1977 | 4650 | 895,187 | 10.36 | 0.64 | 9.1 |
| 1978 | 4900 | 943,316 | 10.92 | 0.66 | 9.3 |
| 1979 | 4600 | 885,561 | 10.25 | 0.64 | 9.1 |
| 1980 | 4200 | 808,556 | 9.36 | 0.61 | 8.9 |
| 1981 | 3550 | 683,422 | 7.91 | 0.56 | 8.5 |
| 1982 | 3550 | 683,422 | 7.91 | 0.56 | 8.5 |
| 1983 | 2800 | 539,037 | 6.24 | 0.49 | 7.9 |
| 1984 | 2800 | 539,037 | 6.24 | 0.49 | 7.9 |
| 1985 | 3050 | 587,166 | 6.80 | 0.51 | 8.1 |
| 1986 | 3250 | 625,668 | 7.24 | 0.53 | 8.2 |

Notes
1. Listed dates prior to 1970 correspond to incremental flow rate increases noted on the NECR mine shaft log as shown in the adjacent column. Dates from 1970-1986 correspond to yearly average rates shown in the adjacent column.
2. Dicharges from the NECR mine began when the shaft encountered water in the Upper Gallup sandstone in Mar. 1968 and ended in Feb. 1983. Discharges from the KM CR mine began in Nov. 1971 and ended Feb. 1986.
3. Flow depths and widths calculated using Manning's equation for a trapezoidal channel shape and an average slope of 0.016. Flow depths and widths for channel segments estimated separately based on segment slopes.
4. Channel geometry and roughness assumed to be uniform: Manning's coef. 0.045, side slopes 4ft/ft, bottom width 1 ft prior to Nov. 1968, 4 ft afterward.

Table 3
Estimated Annual Average Recharge in Arroyo Chanels from Periodic Runnoff Events

| Stream Arc | Watershed Area ($ft^2$) | Vol. per inch precip. per day ($ft^3/d$) | Runoff Rate at Fraction **0.037** ($ft^3/s$) | ($ft^3/s$) | Channel Slope | Channel Bottom Width (ft) | Side Slope | Manning's Coef. | Calculated Stage (ft) | Calculated Wetted Width (ft) | Conductance per Unit Length ($ft^2/d$ per ft) | Recharge Rate per Unit Length ($ft^3/d$ per ft) | Annualized Recharge Rate per Unit Length ($ft^3/d$ per ft) |
|---|---|---|---|---|---|---|---|---|---|---|---|---|---|
| **18** | 162,920,386 | 13,576,699 | 339,417 | 3.93 | 0.0110 | 4 | 4 | 0.045 | 0.52 | 8.16 | 19.38 | 3.16 | 0.0258 |
| **3** | 261,430,623 | 21,785,885 | 544,647 | 6.30 | 0.0112 | 4 | 4 | 0.045 | 0.67 | 9.36 | 22.23 | 4.48 | 0.0365 |
| **11** | 7,075,202 | 589,600 | 14,740 | 0.17 | 0.0309 | 2 | 4 | 0.045 | 0.1 | 2.8 | 6.65 | 0.24 | 0.0020 |
| **17** | 431,426,211 | 35,952,184 | 898,805 | 10.40 | 0.0002 | 4 | 4 | 0.045 | 2.2 | 21.6 | 51.30 | 28.16 | 0.2295 |
| **10** | 4,315,510 | 359,626 | 8,991 | 0.10 | 0.0037 | 2 | 4 | 0.045 | 0.14 | 3.12 | 7.41 | 0.36 | 0.0029 |
| **6** | 4,315,510 | 359,626 | 8,991 | 0.10 | 0.0391 | 2 | 4 | 0.045 | 0.07 | 2.56 | 6.08 | 0.16 | 0.0013 |
| **22** | 4,315,510 | 359,626 | 8,991 | 0.10 | 0.0053 | 2 | 4 | 0.045 | 0.12 | 2.96 | 7.03 | 0.30 | 0.0024 |
| **4** | 12,605,662 | 1,050,472 | 26,262 | 0.30 | 0.0330 | 2 | 4 | 0.045 | 0.13 | 3.04 | 7.22 | 0.33 | 0.0027 |
| **12** | 25,552,191 | 2,129,349 | 53,234 | 0.62 | 0.0007 | 2 | 4 | 0.045 | 0.52 | 6.16 | 14.63 | 2.12 | 0.0173 |

**Table 4**
**Summary of Hydraulic Conductivity and Porosity Estimates**

| Hydrostratigraphic Unit | Hydraulic Conductivity | | | | Porosity | |
|---|---|---|---|---|---|---|
| | Vertical | | Horizontal | | | Source |
| | cm/s | ft/d | cm/s | ft/d | | |
| Southwest Alluvium | 2.70E-05 | 0.076535 | 2.00E-03 | 5.669 | 30% | 1 |
| Zone 1 | | | 1.00E-04 | 0.283 | 7-9% | 2 |
| Zone 3 (impacted) | | | 5.00E-05 | 0.142 | | 3 |
| Zone 3 (unimpacted) | | | 2.95E-04 | 0.836 | 6-8% | 4 |
| Zone 3 (partially impacted) | | | 2.16E-04 | 0.612 | 6-8% | 4 |

1 (Canonie, 1987; US Filter, 2004b; Sergent, Hauskins & Beckworth, May 1976)

2 (Canonie, 1987)

3 (Arcadis BBL, June 2007)

4 (NA water Systems, April 2008)

Table 5

Summary of Model Parameters for Material Property Zones

| | Units | Layer 1 | Layer 2 (Dilco Coal) | | Layers 3 and 4 (Zone 3) | | | | | | Layer 5 (Zone 2) | | Layer 6 (Zone 1) | |
|---|---|---|---|---|---|---|---|---|---|---|---|---|---|---|
| | | Alluvium | Dilco_M1 | Dilco_M2 | Z3_M1 | Z3_M2 | Z3_M3 | Z3_M4 | Z3_M5 | Z3_M6 | Z2_M1 | Z2_M2 | Z1_M1 | Z1_M2 |
| **Kh(max)**[1] | (ft/d) | 7.125 | 0.01 | 0.1 | 0.836 | 2.38 | 0.418 | 1.19 | 0.377 | 0.142 | 0.01 | 0.015 | 0.425 | 0.637 |
| **Kh(min)** | (ft/d) | 7.125 | 0.01 | 0.067 | 0.836 | 1.19 | 0.418 | 0.797 | 0.377 | 0.142 | 0.01 | 0.010 | 0.425 | 0.427 |
| **Kv** | (ft/d) | 2.375 | 0.0005 | 0.01 | 0.042 | 0.238 | 0.021 | 0.119 | 0.0189 | 0.007 | 0.0005 | 0.00075 | 0.035 | 0.064 |
| **Ss**[2] | | 0.001 | 0.0008 | 0.0008 | 0.0008 | 0.0008 | 0.0008 | 0.0008 | 0.0008 | 0.0008 | 0.0008 | 0.0008 | 0.0016 | 0.0016 |
| **Sy** | | 0.25 | 0.18 | 0.18 | 0.12 | 0.12 | 0.06 | 0.12 | 0.06 | 0.06 | 0.12 | 0.12 | 0.06 | 0.06 |
| **Porosity** | | 0.25 | 0.18 | 0.18 | 0.12 | 0.1 | 0.06 | 0.08 | 0.06 | 0.06 | 0.06 | 0.06 | 0.1 | 0.1 |

Notes

1. Hydraulic conductivity is designated by three directional components: Kh(max) is column-wise (northeast), Kh(min) is row-wise (northwest), Kv is vertical.
2. Two storage parameters are designated: Ss is specific storage (for confined conditions) and Sy is specific yield (for unconfined conditions).
3. Porosity influences groundwater velocities used for particle tracking, but does not affect Flow Model estimates of head.
4. See Figures 15a through 15f for maps of material property zones

Table 6
Background Groundwater Volume Calculations

| Zone | Total Sat. Vol. ($ft^3$) | Porosity | Fluid Volume ($ft^3$) | Mine Discharge ($ft^3$) |
|---|---|---|---|---|
| 1 | 2.89E+09 | 0.1 | 2.89E+08 | |
| 3 | 1.56E+09 | 0.06 | 9.38E+07 | |
| total | 4.45E+09 | | 3.82E+08 | 3.67E+09 |

# Figures

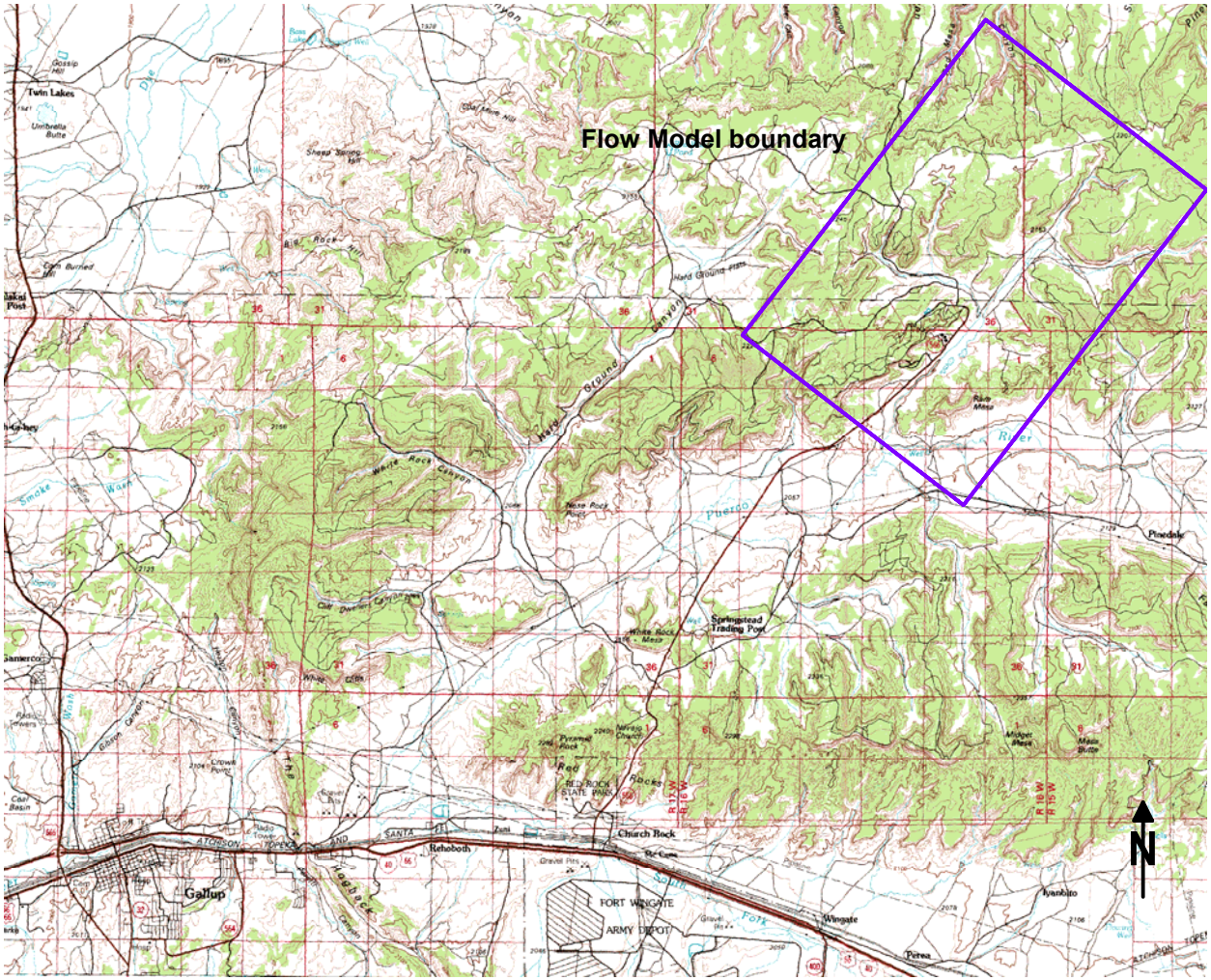


(map after USGS 30x60 minute, 1:100,000, Gallup, New Mexico Topographic Map, 1981)

**Scale**

0 3 6

(miles)

FIGURE 1
Location of Flow Model Domain

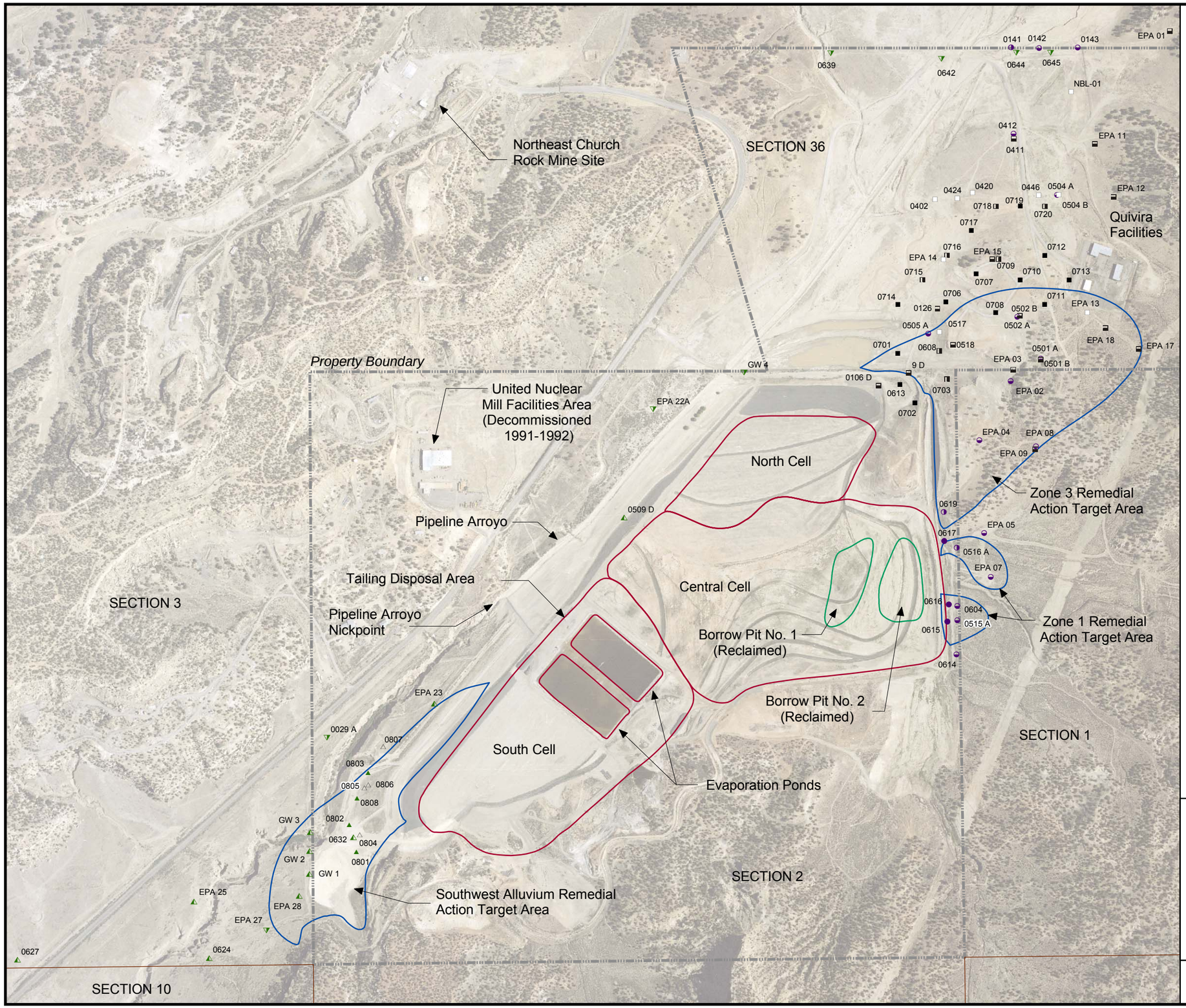


## Legend

**Southwest Alluvium**

- Idled Extraction Well
- Monitoring Well
- Water Level Monitoring Well
- Dry Monitoring Well

**Zone 3**

- Idled Extraction Well Used for Monitoring
- Decommissioned or Idle Extraction Well
- Monitoring Well
- Dry or Decommissioned Monitoring Well

**Zone 1**

- Decommissioned Extraction Well
- Decommissioned Monitoring Well
- Monitoring Well

0 400 800 1,600

Feet

**FIGURE 2**

Site Layout and Performance Monitoring Well Locations 2010 Operating Year

United Nuclear Corporation Church Rock Site, Church Rock, New Mexico

CHESTER ENGINEERS

Z:\databases\6209_GE_CR\GISDATA\arcmap_doc\2008_annual_report\f02_site_layout.mxd; January 13, 2009

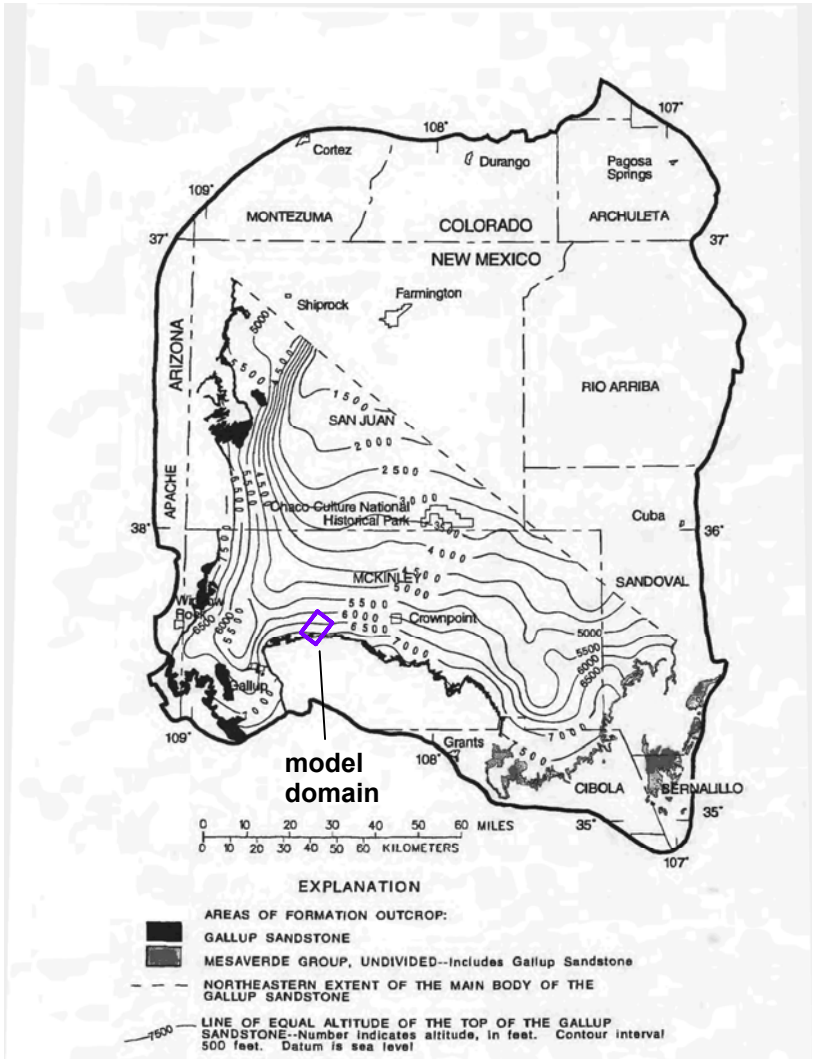


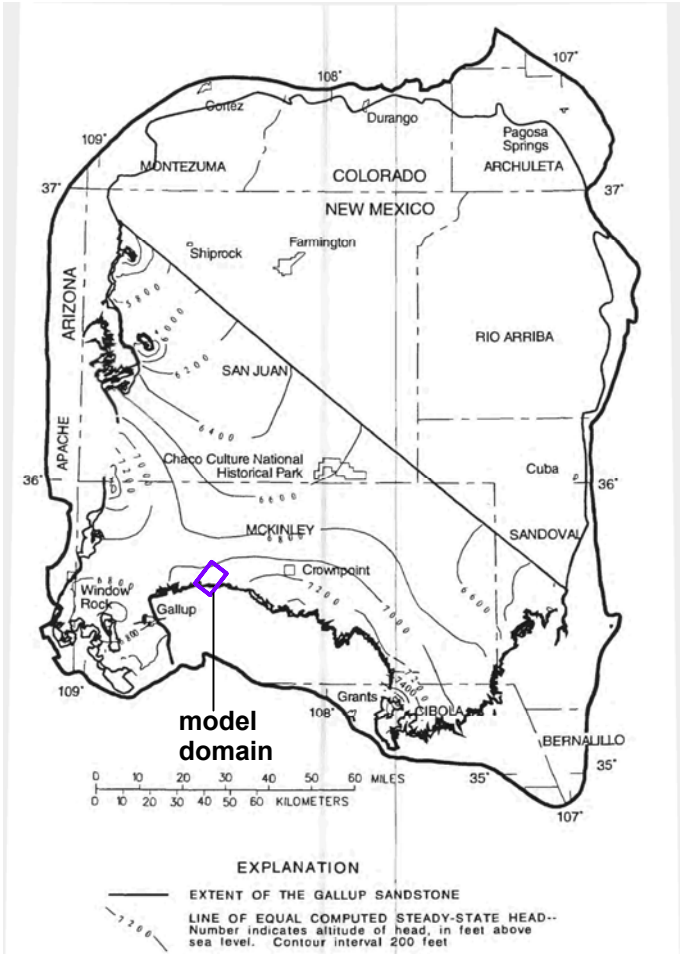


FIGURE 3
Regional setting of the Flow Model domain with respect to the structure (left) and simulated potentiometric surface (right) of the Gallup Standstone. Figures modified from Kernodle (1996).

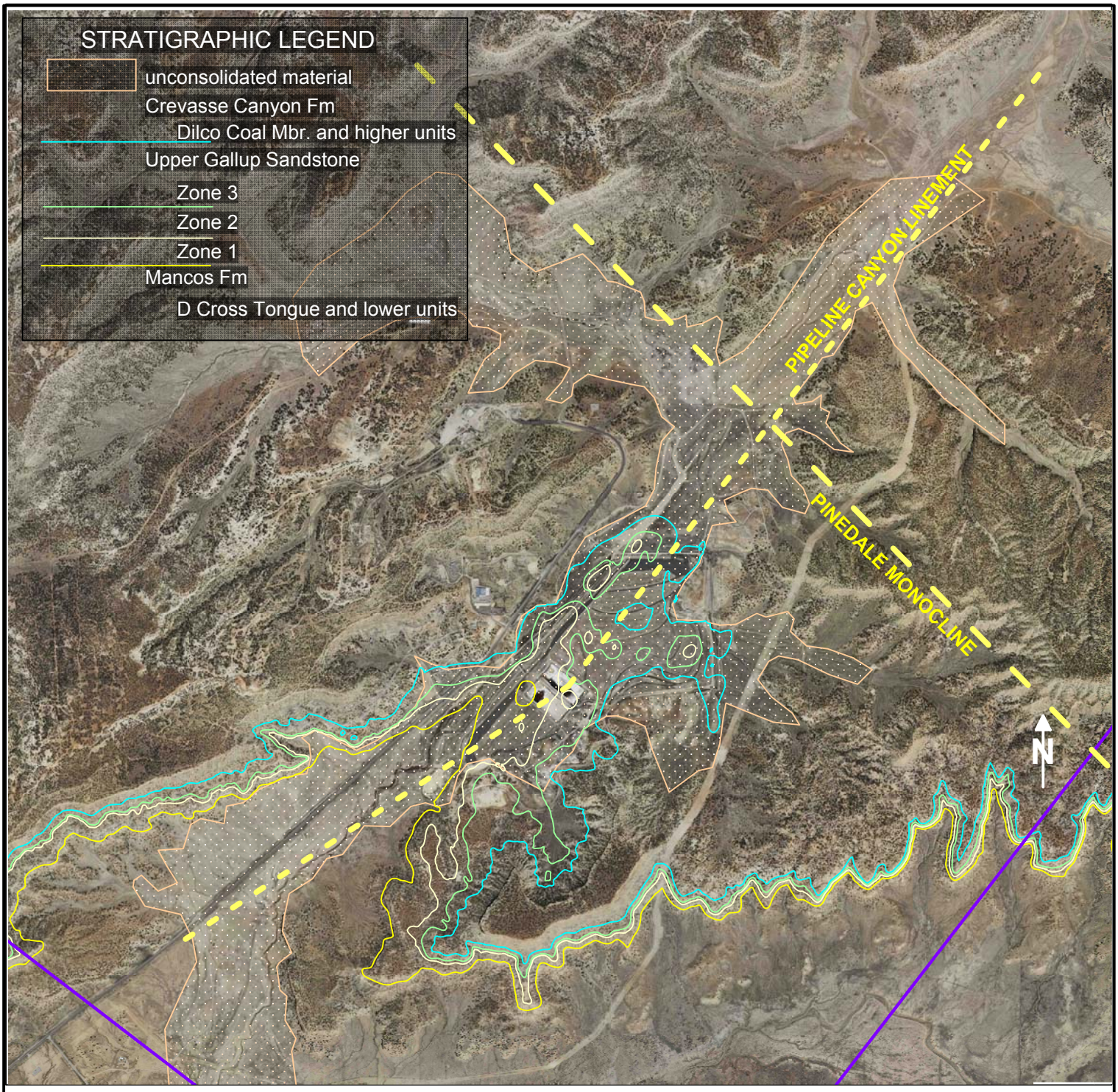


**FIGURE 4**
**Map of hydrostratigraphic units used for development of the Flow Model and local structures. Locations of Pipeline Canyon Lineament and Pinedale Monocline after Science Applications and Bearpaw Geosciences (1980). Note that the Zone 3 unit incorporates the Torrivo Sandstone Mbr. of the Crevasse Canyon Fm. as redefined by Canonie (1987).**

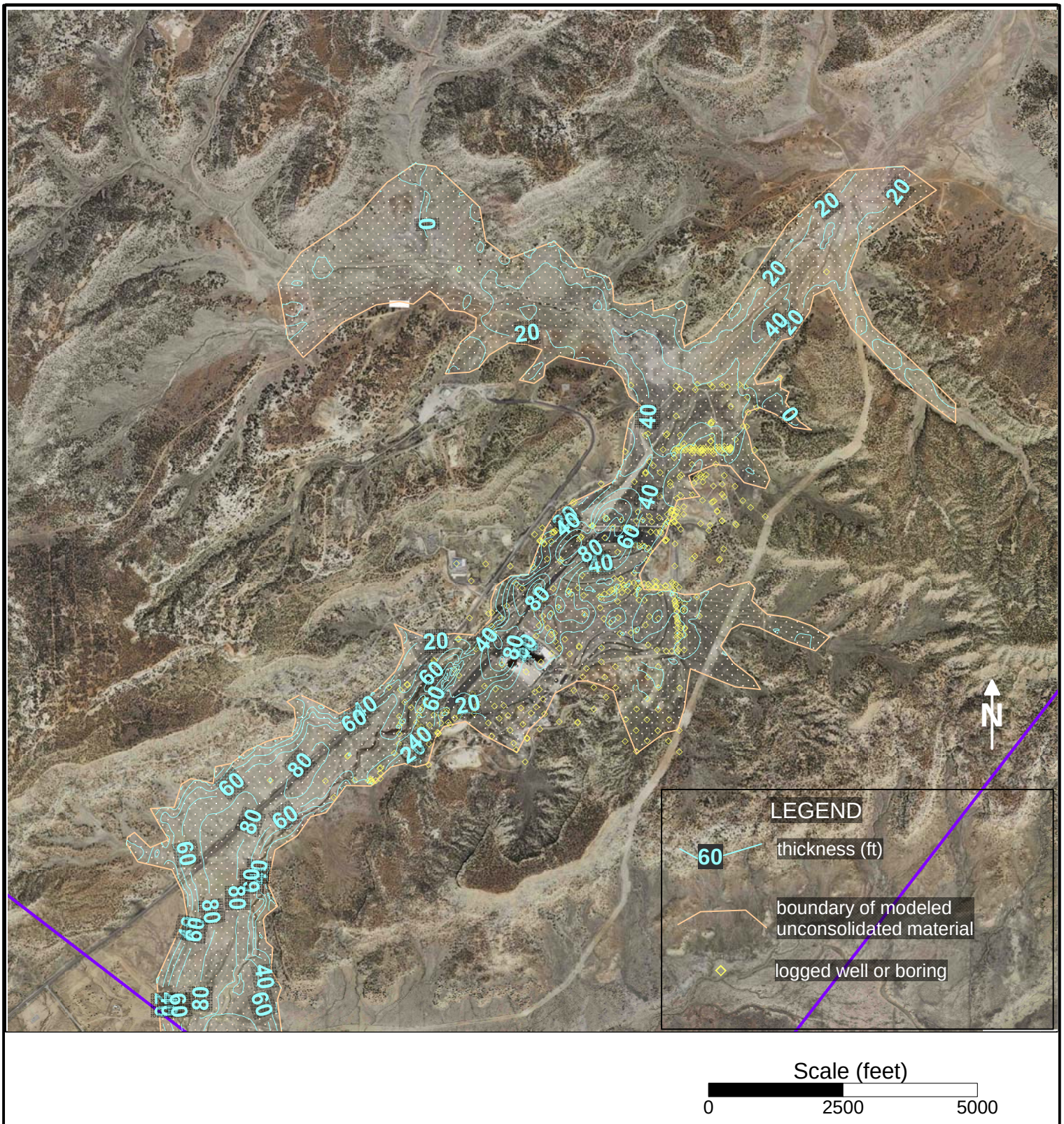


**FIGURE 5**
**Estimated extents and thickness of unconsolidated material (alluvium and tailings) incorporated in Flow Model**


**FIGURE 6**
**Estimated elevation of the top of rock within the modeled extent of unconsolidated material**

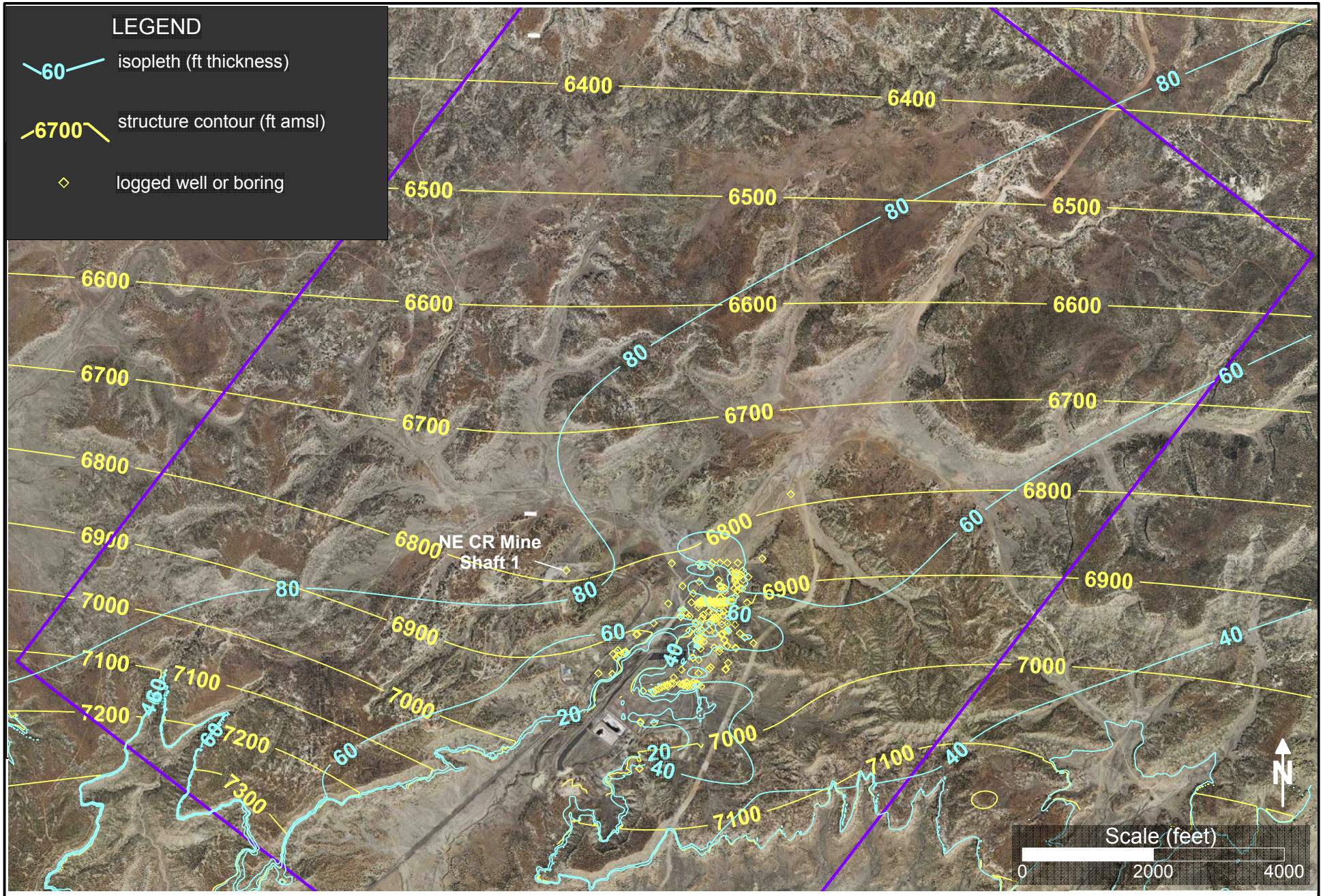


**FIGURE 7**
**Estimated top structure contours (elevations) and isopleths (vertical thickness) for Zone 3, boring logs supplemented with regional data (see Figure 3)**

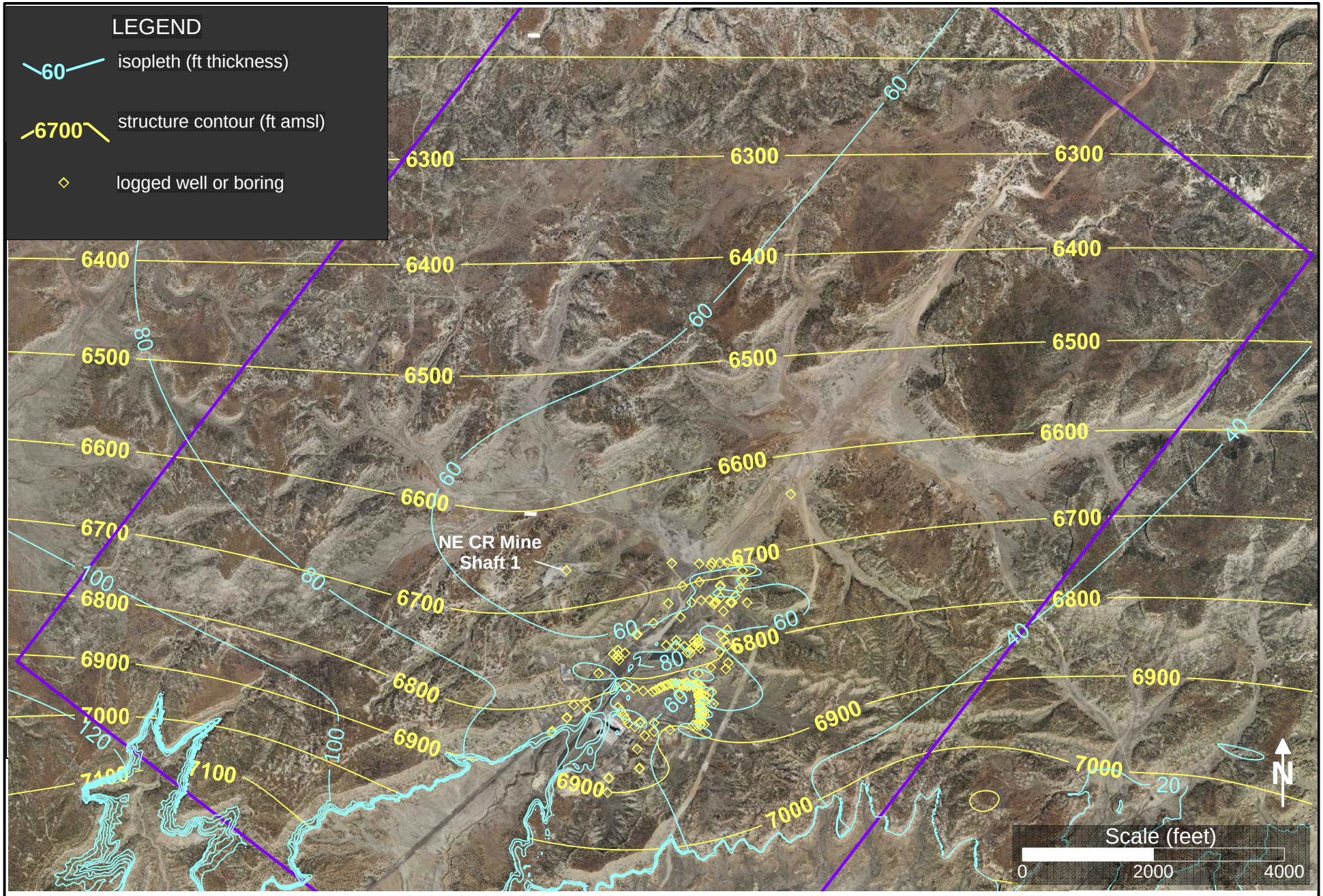


**FIGURE 8**
**Estimated bottom structure contours (elevations) and isopleths (vertical thickness) for Zone 1, boring logs supplemented with regional data (see Figure 3)**

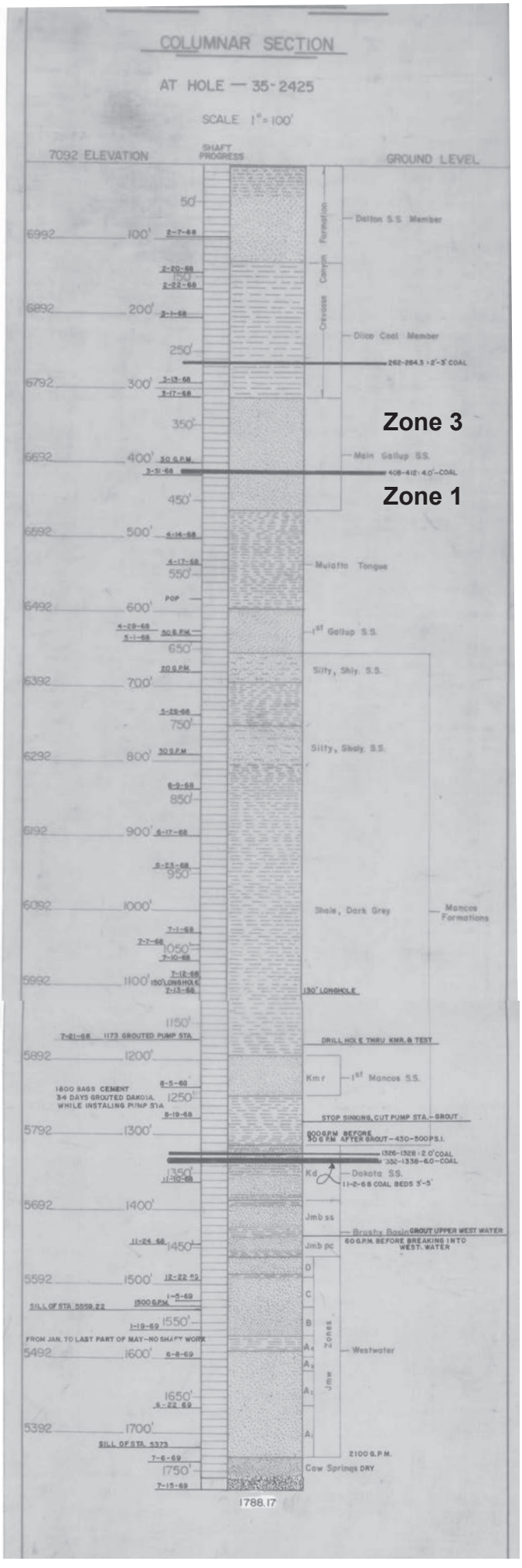


**FIGURE 9**
Northeast Church Rock Mine shaft 1 geologic section

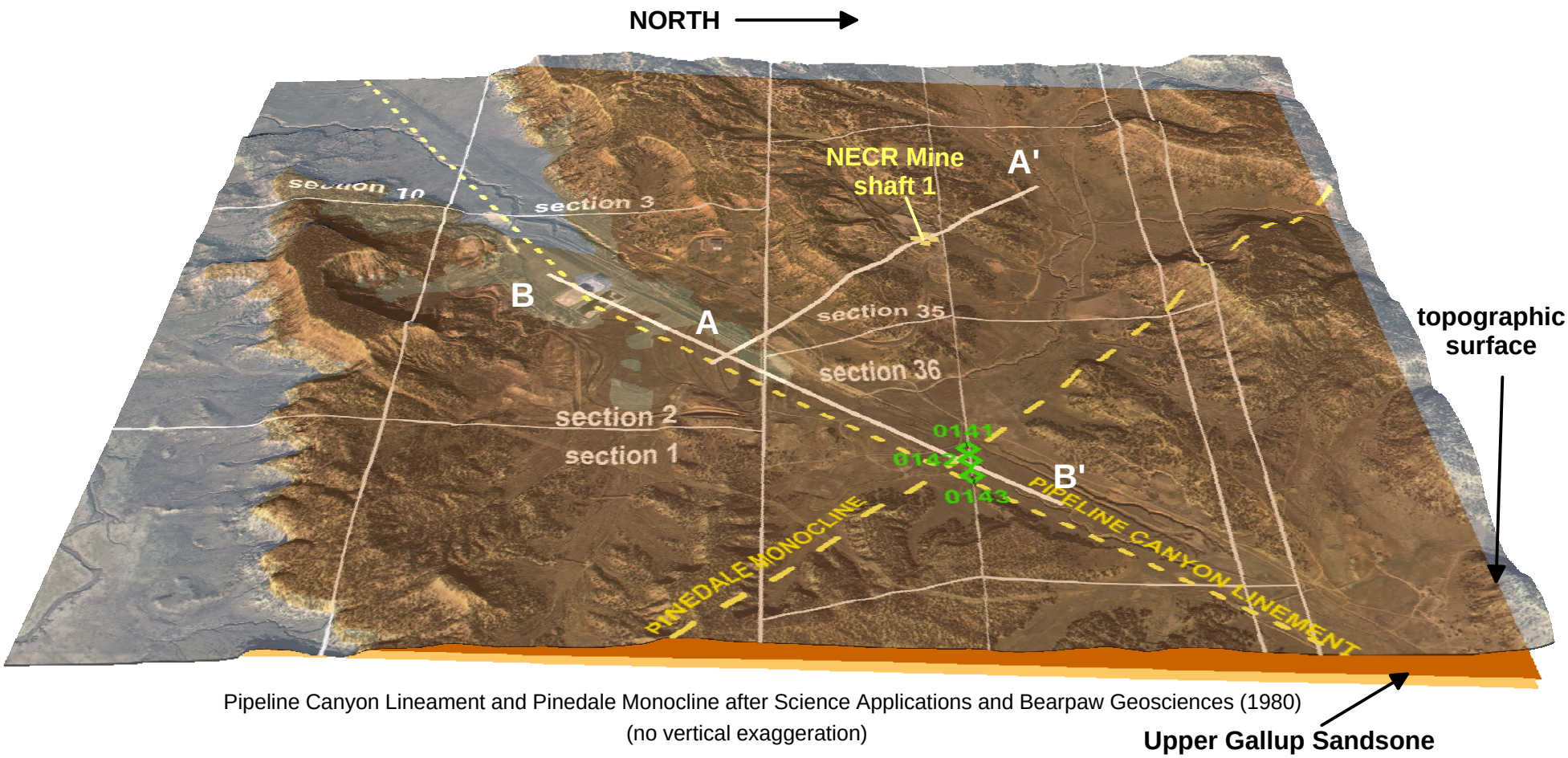


Pipeline Canyon Lineament and Pinedale Monocline after Science Applications and Bearpaw Geosciences (1980)
(no vertical exaggeration)

FIGURE 10
West-looking perspective view of topographic surface and north-dipping Upper Gallup Sandstone, showing locations of Pipeline Canyon Lineament, Pinedale Monocline, cross sections A-A', B-B' and associated features. Surface imagery (NAIP 2009 orthophoto) rendered semi-transparent to show underlying Upper Gallup Sandstone.

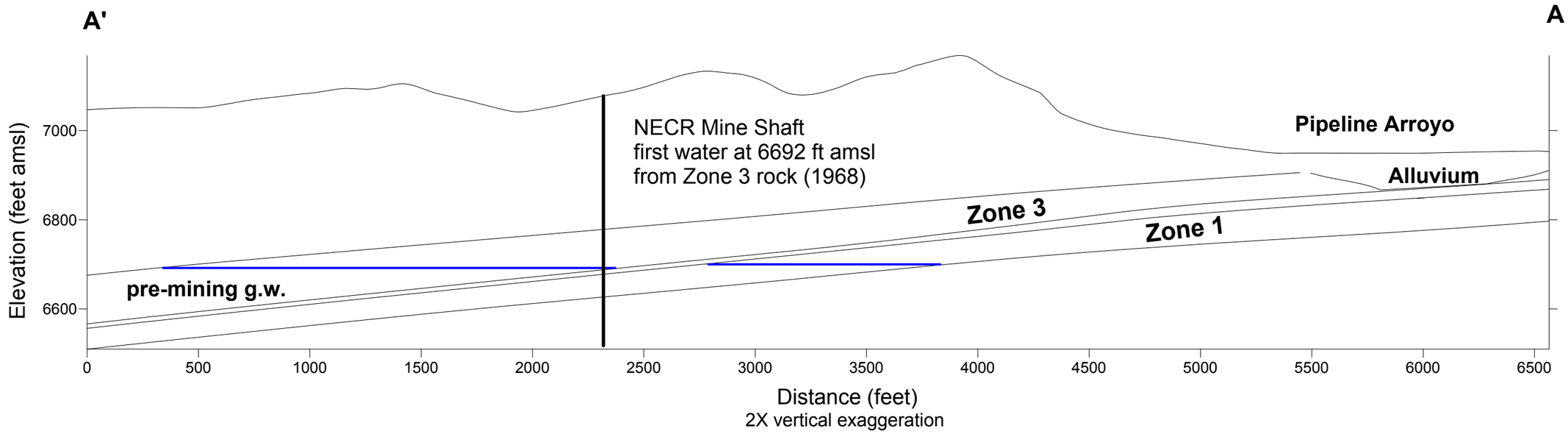


**FIGURE 11A**
**Northeast-looking view of cross section A-A' (see Figure 10 for location)**

Pre-mining water table shown in Zone 3 where encountered in NECR mine shaft in 1968 (at elevation 6692 ft amsl). Elevation of pre-mining water table shown in Zone 1 is interpreted by analogy, but is also consistent with sample data from Zone 1 monitoring wells.

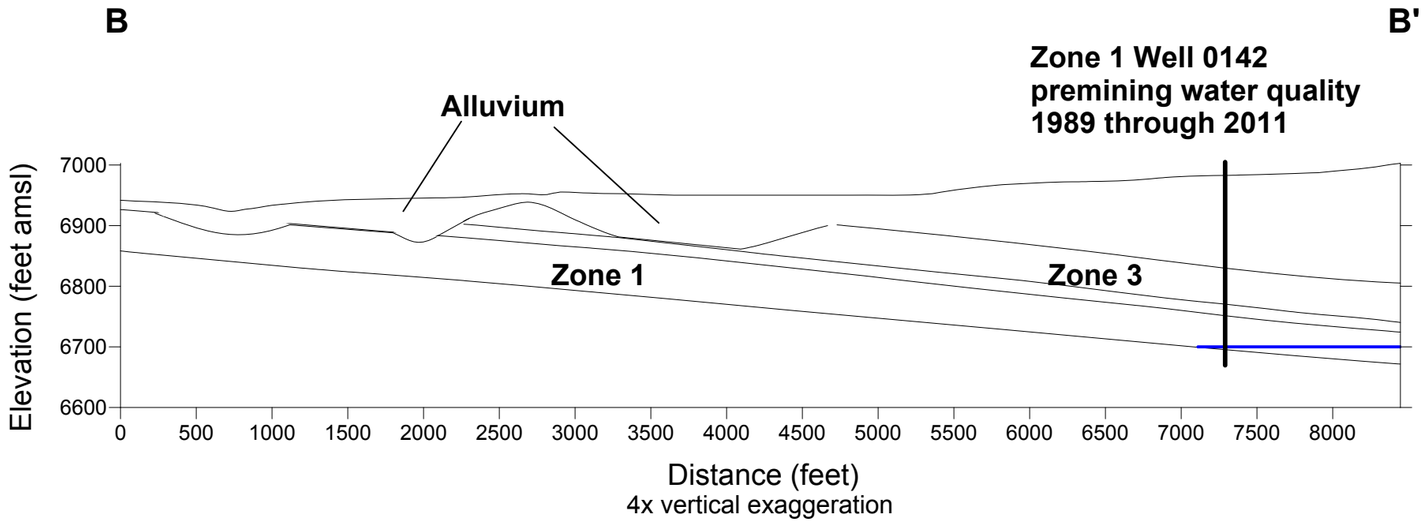


**FIGURE 11B**
**Northwest-looking view of cross section B-B' (see Figure 10 for location)**

Zone 1 pre-mining water table depicted by blue line is consistent with early sample data from Zone 1 monitoring wells 0141, 0142, and 0143. These wells are screened at the base of Zone 1. The persistence of pre-mining water quality in these wells (through 2011 in 0142) demonstates little or no displacement of pre-miningroundwater by background groundwater.

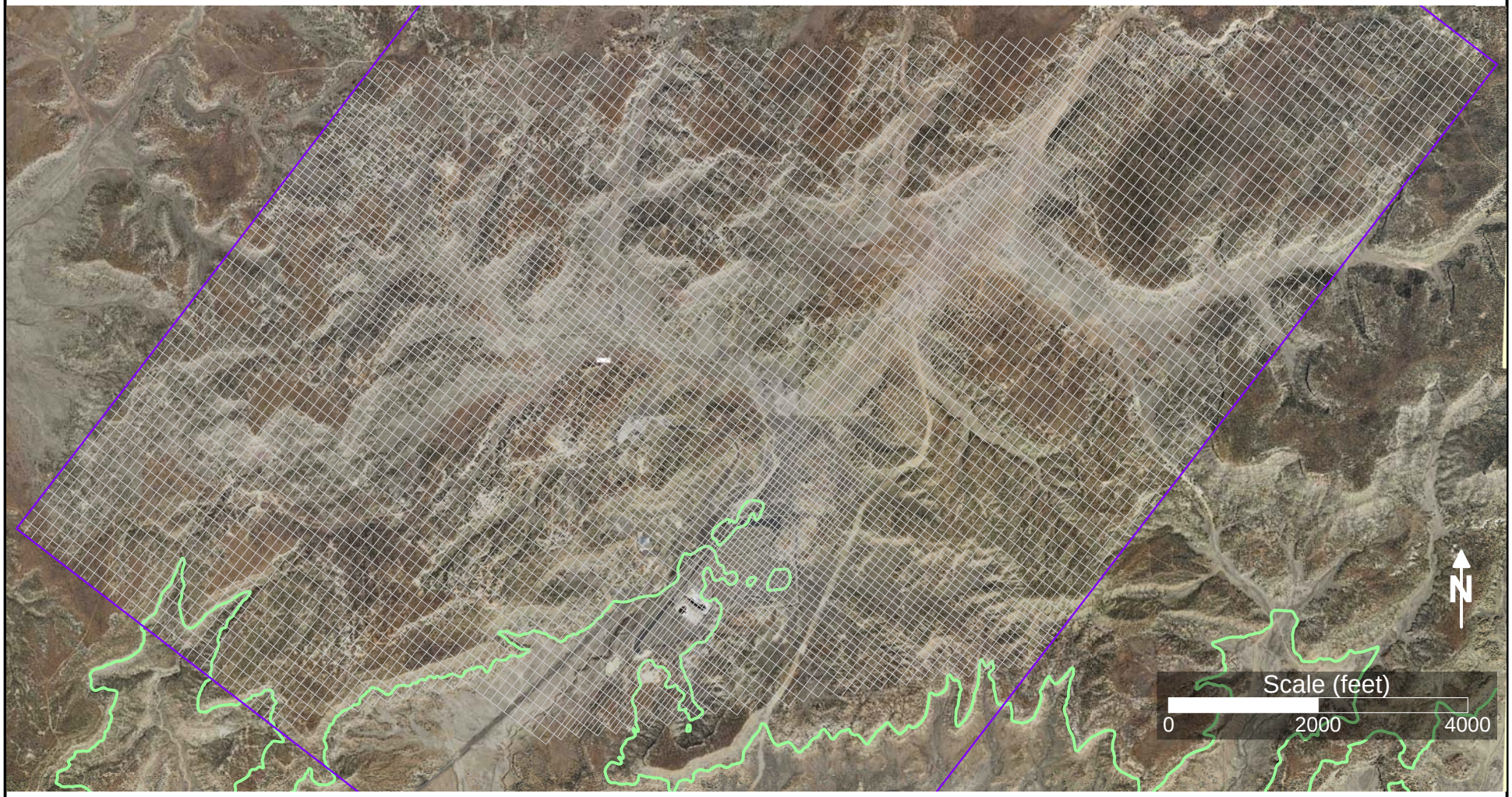


**FIGURE 12**
**Extent of Flow Model active grid cells,**
**estimated southern extent of Zone 3 outlined in green for reference**

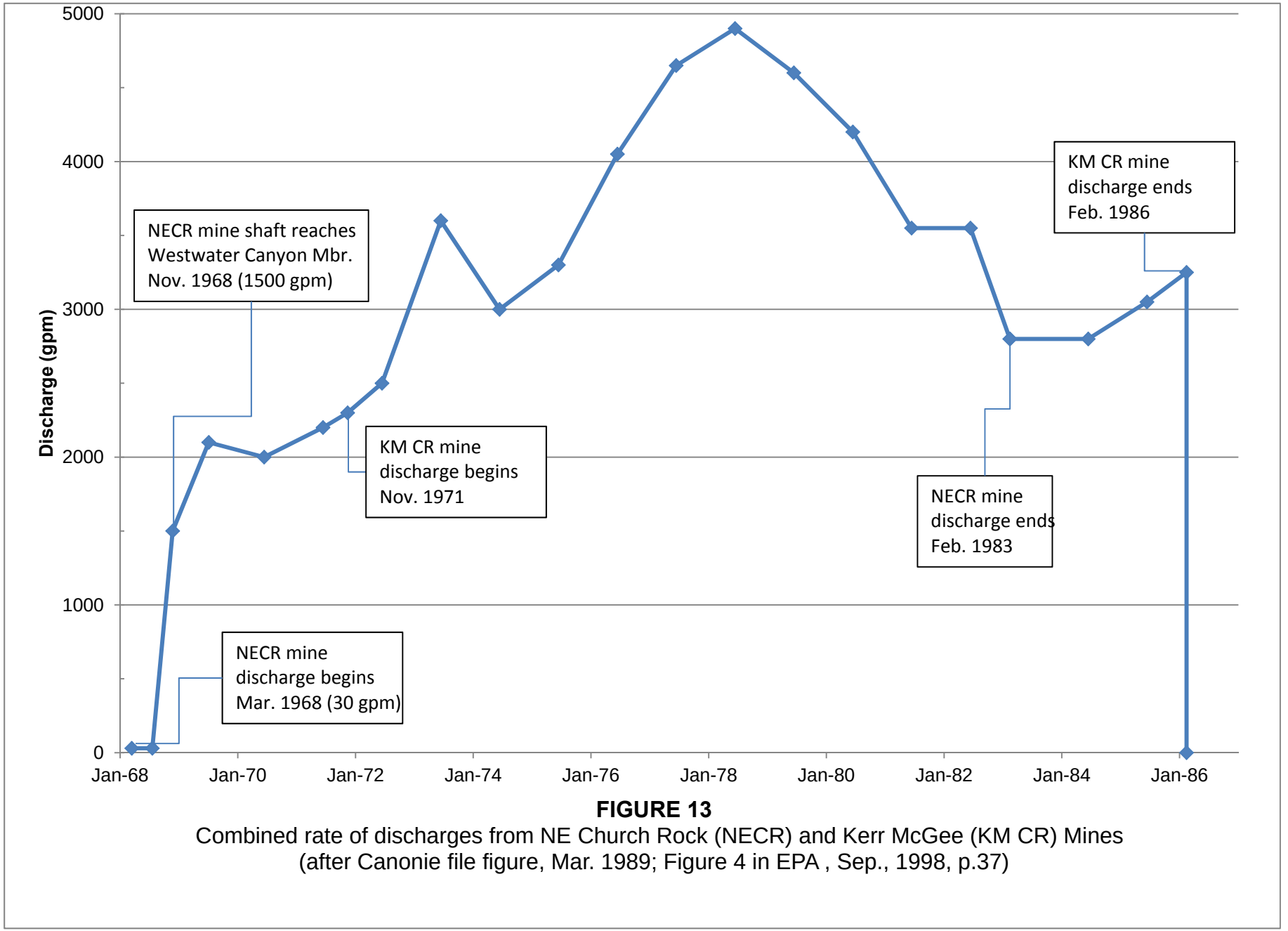


**FIGURE 13**

Combined rate of discharges from NE Church Rock (NECR) and Kerr McGee (KM CR) Mines
(after Canonie file figure, Mar. 1989; Figure 4 in EPA , Sep., 1998, p.37)

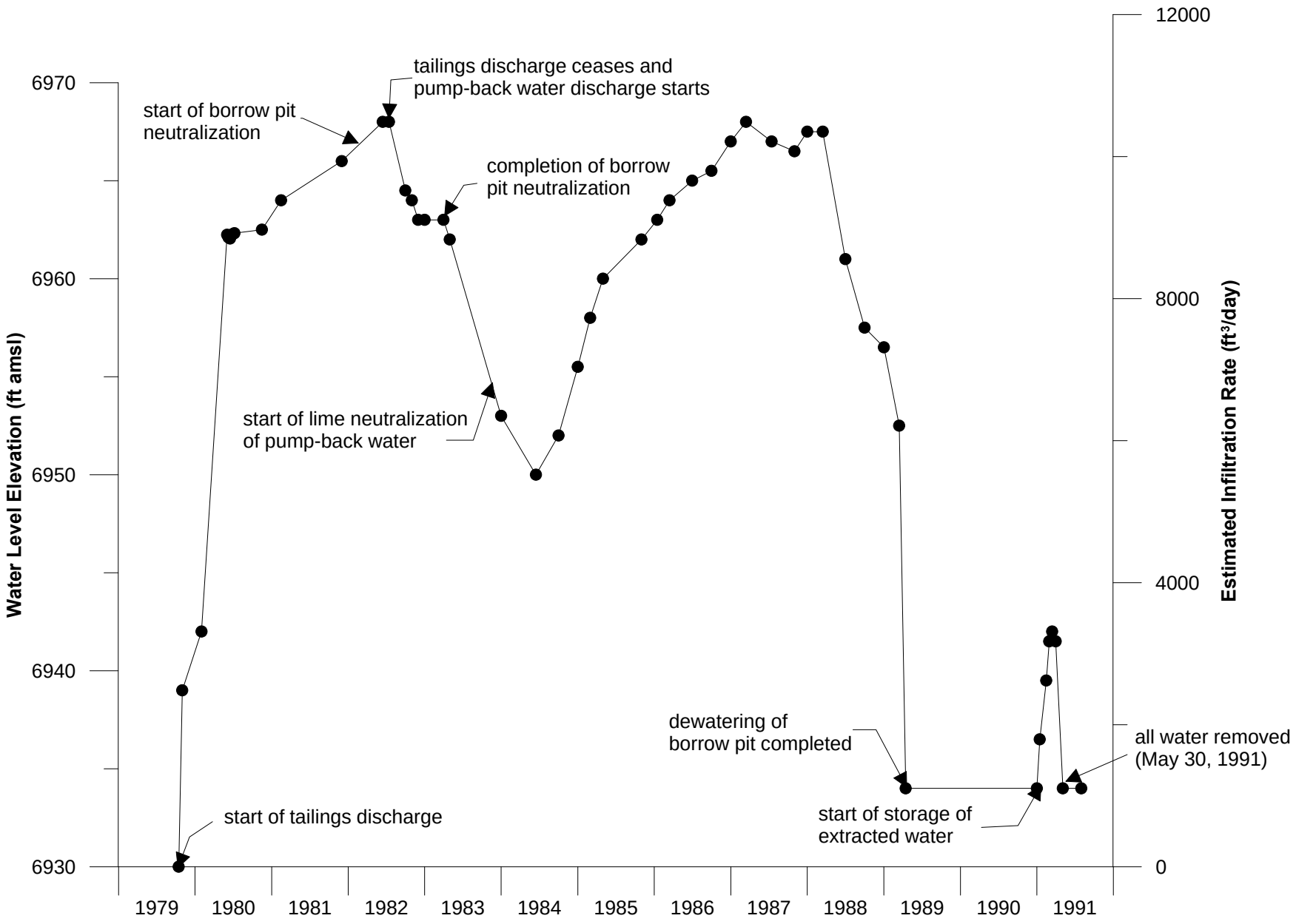


FIGURE 14

Borrow Pit 2 stage and estimated infiltration rate (after Canonie file drawing, June 1995).
Infiltration estimates based on June-July 1980 seepage study (Science Applications, August 1980).

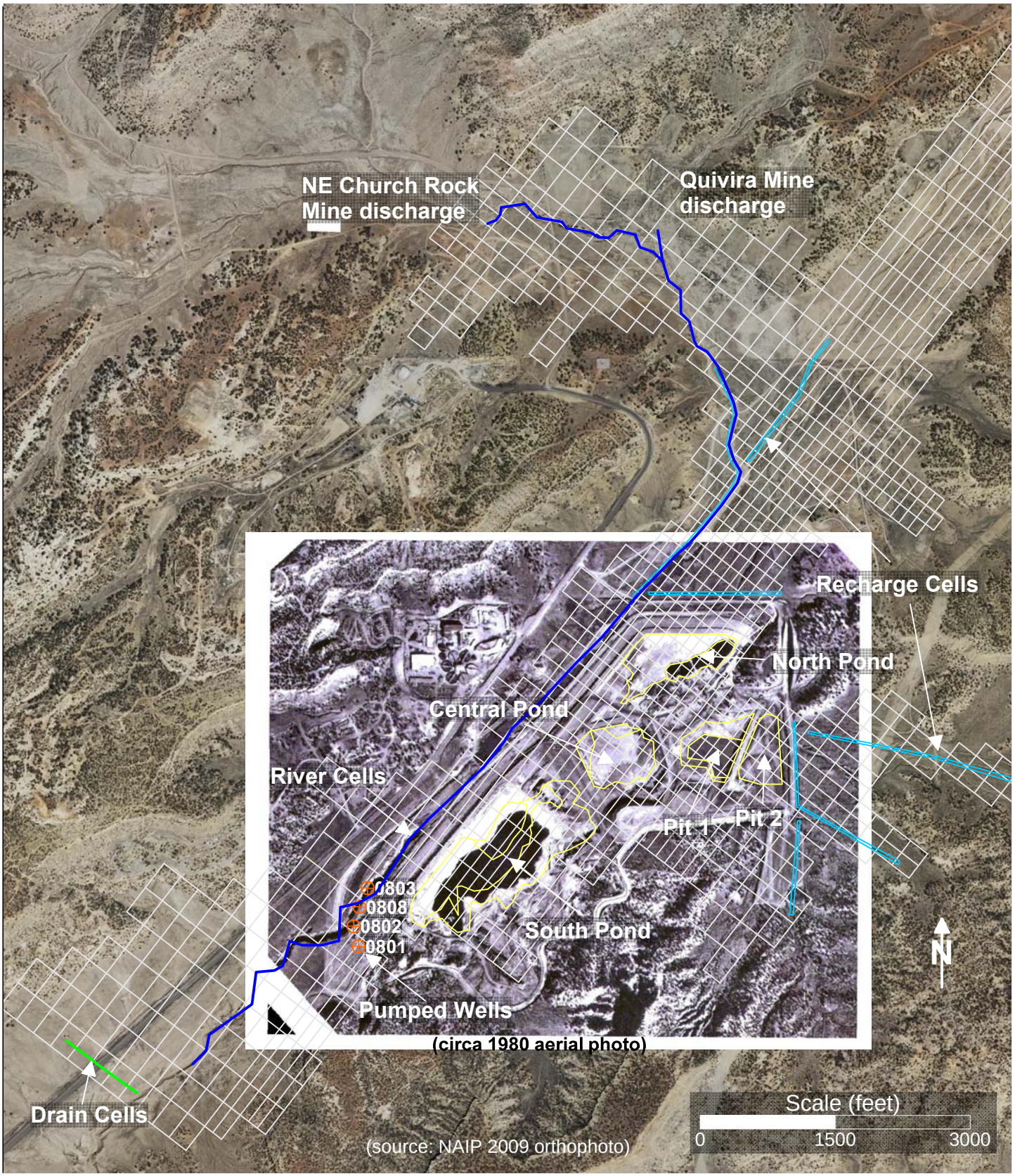


**FIGURE 15A**
**View of model layer 1 grid, representing alluvium, showing river cells (mine water discharge), recharge cells (arroyo recharge), pond areas (tailings seepage), drain cells (alluvium boundary drainage), and pumped wells**

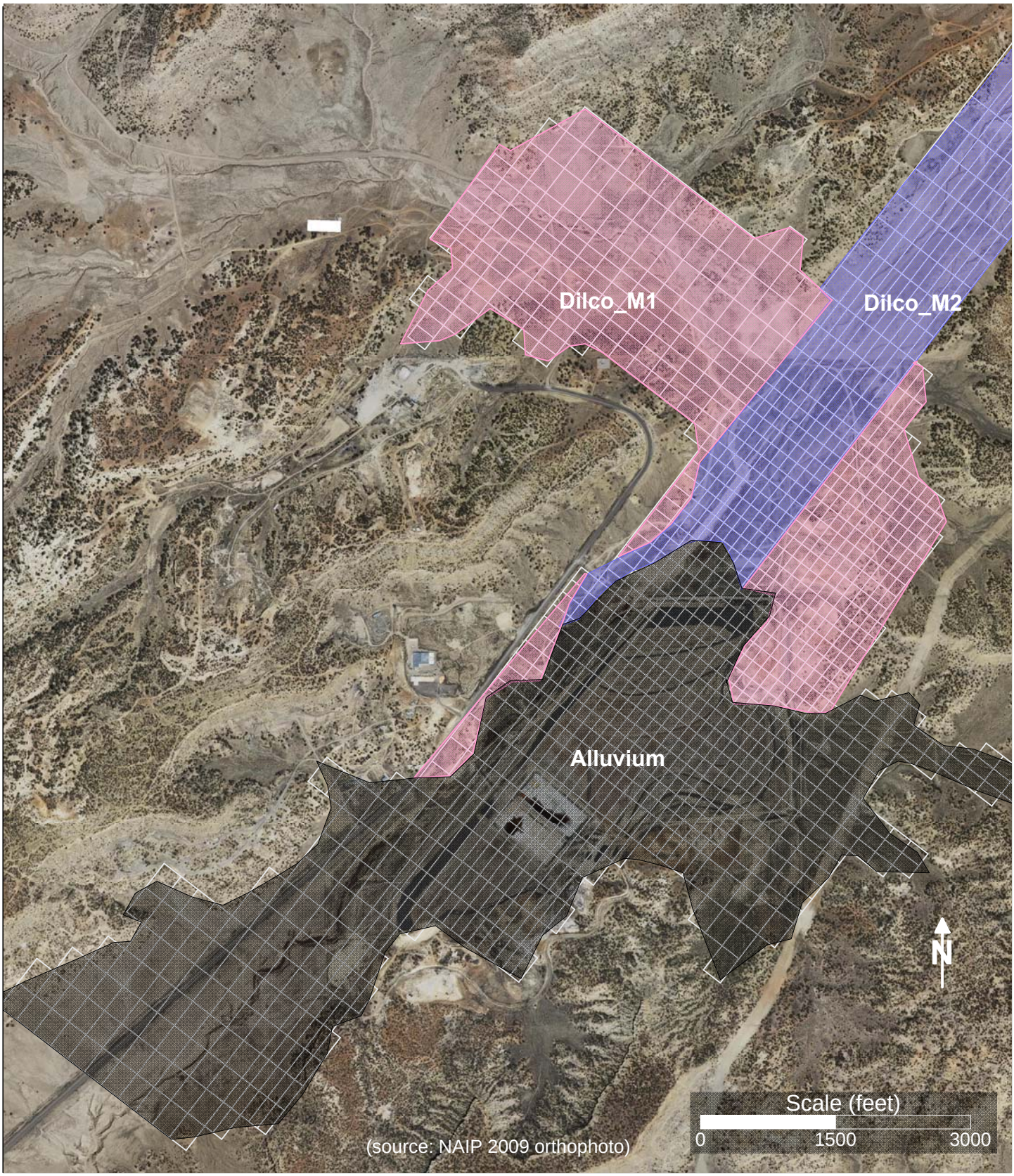


FIGURE 15B
View of model layer 2 grid, representing Dilco Coal and alluvium,
showing material property zones


FIGURE 15C
View of model layer 3 grid, representing Zone 3 (upper 5-60 ft) and alluvium, showing material property zones and pumped wells

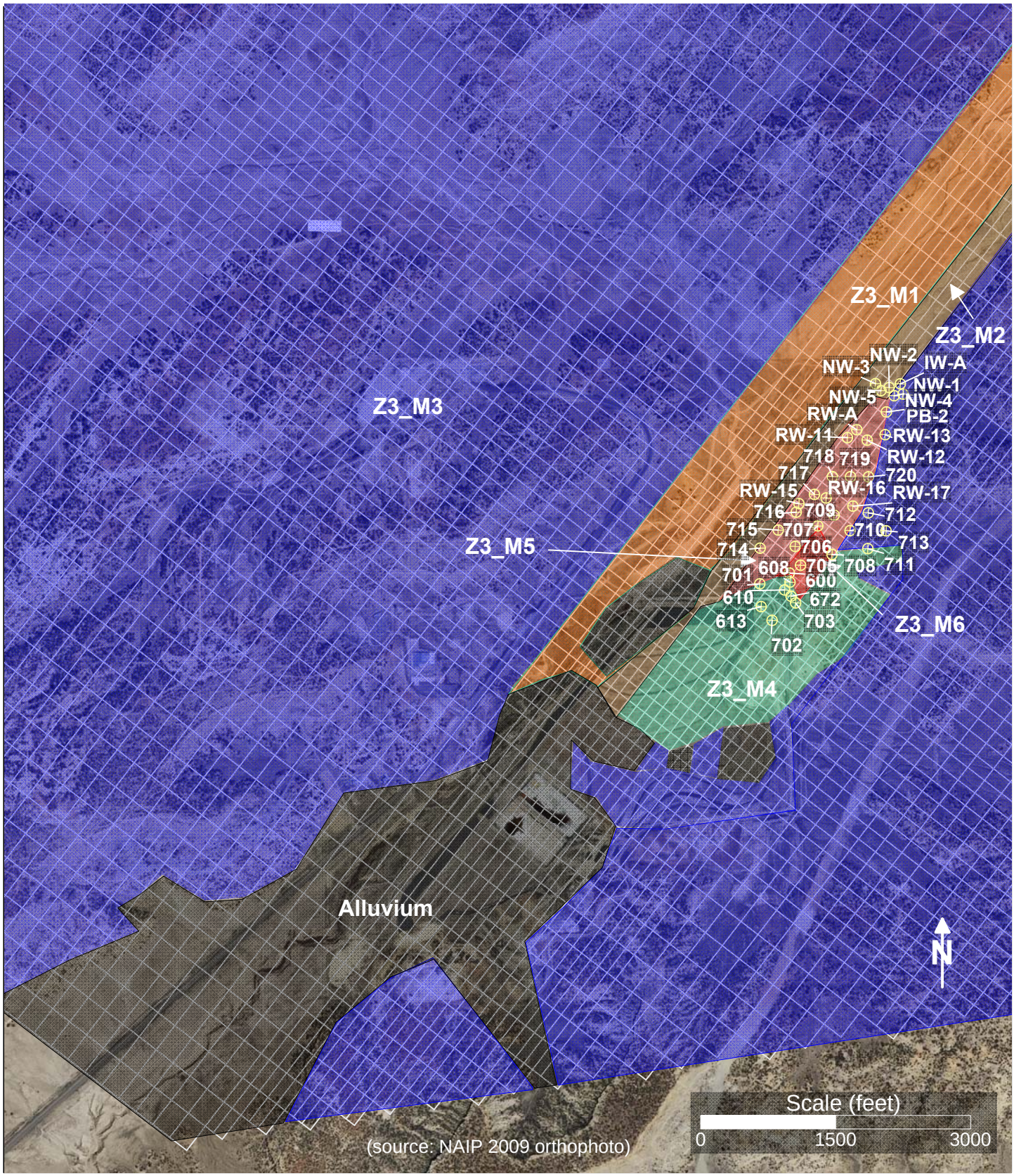


FIGURE 15D
View of model layer 4 grid, representing Zone 3 (lower 5-20 ft) and alluvium, showing material property zones and pumped wells

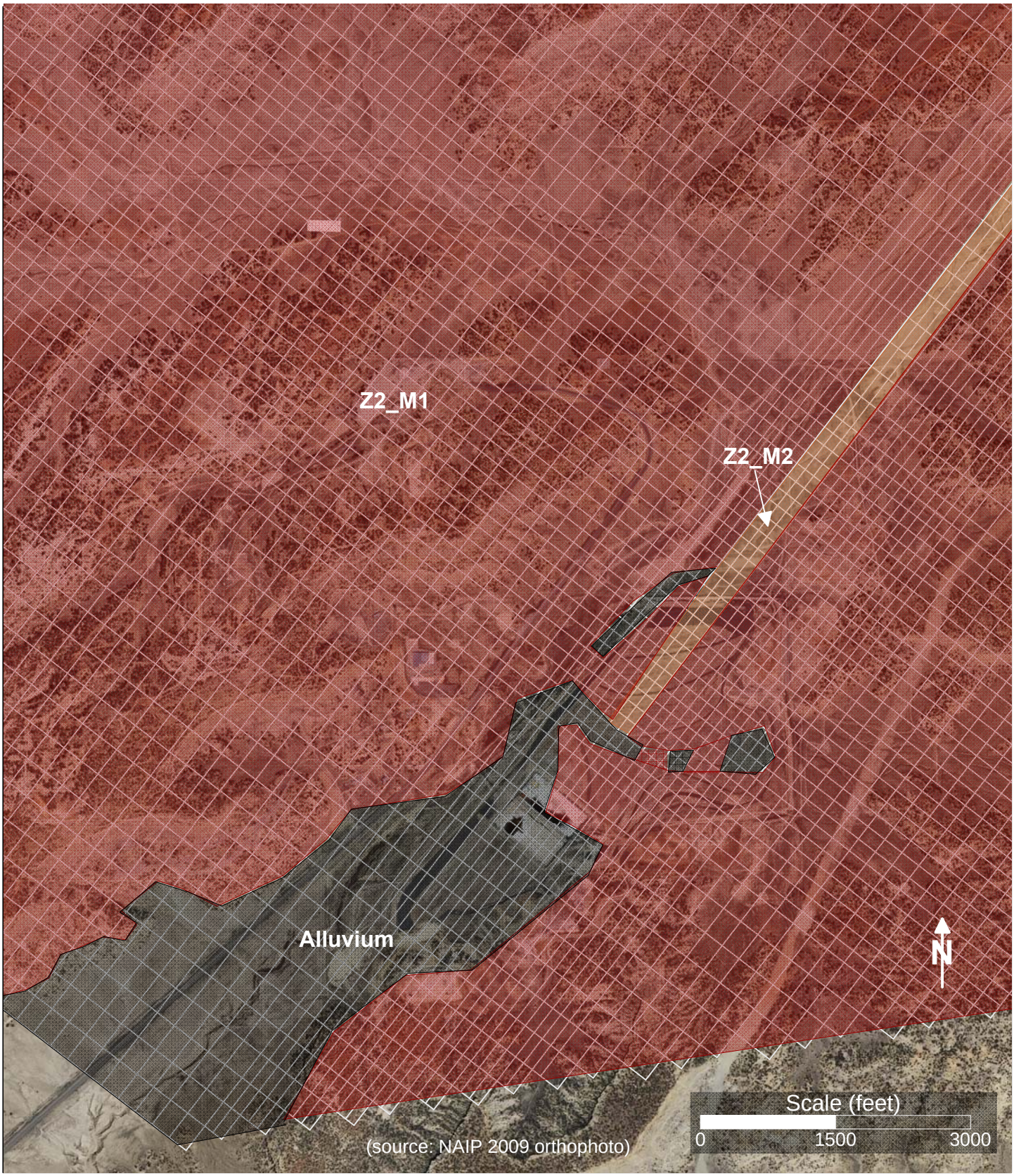


FIGURE 15E
View of model layer 5 grid, representing Zone 2 and alluvium,
showing material property zones

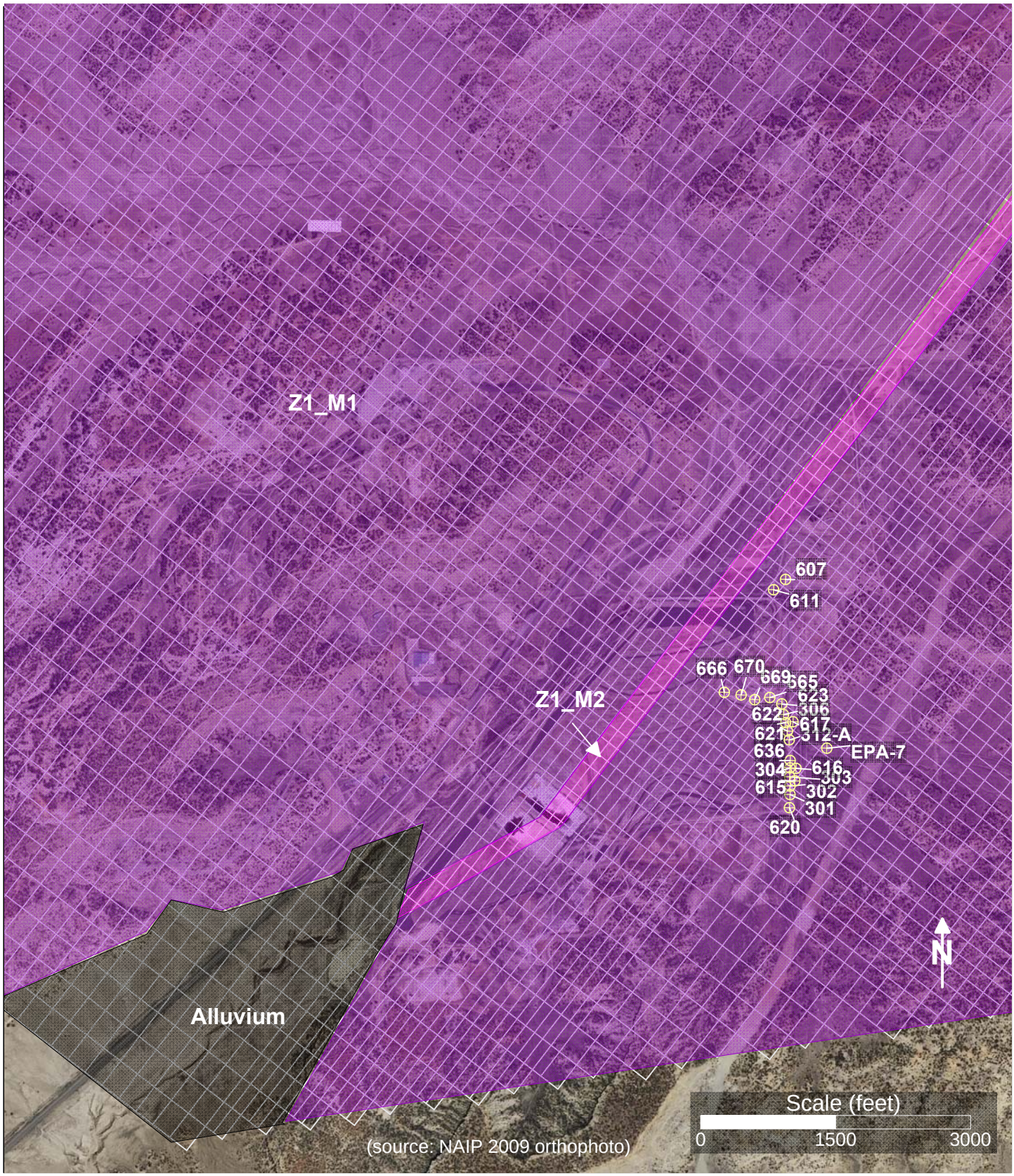


FIGURE 15F
View of model layer 6 grid, representing Zone 1 and alluvium,
showing material property zones and pumped wells

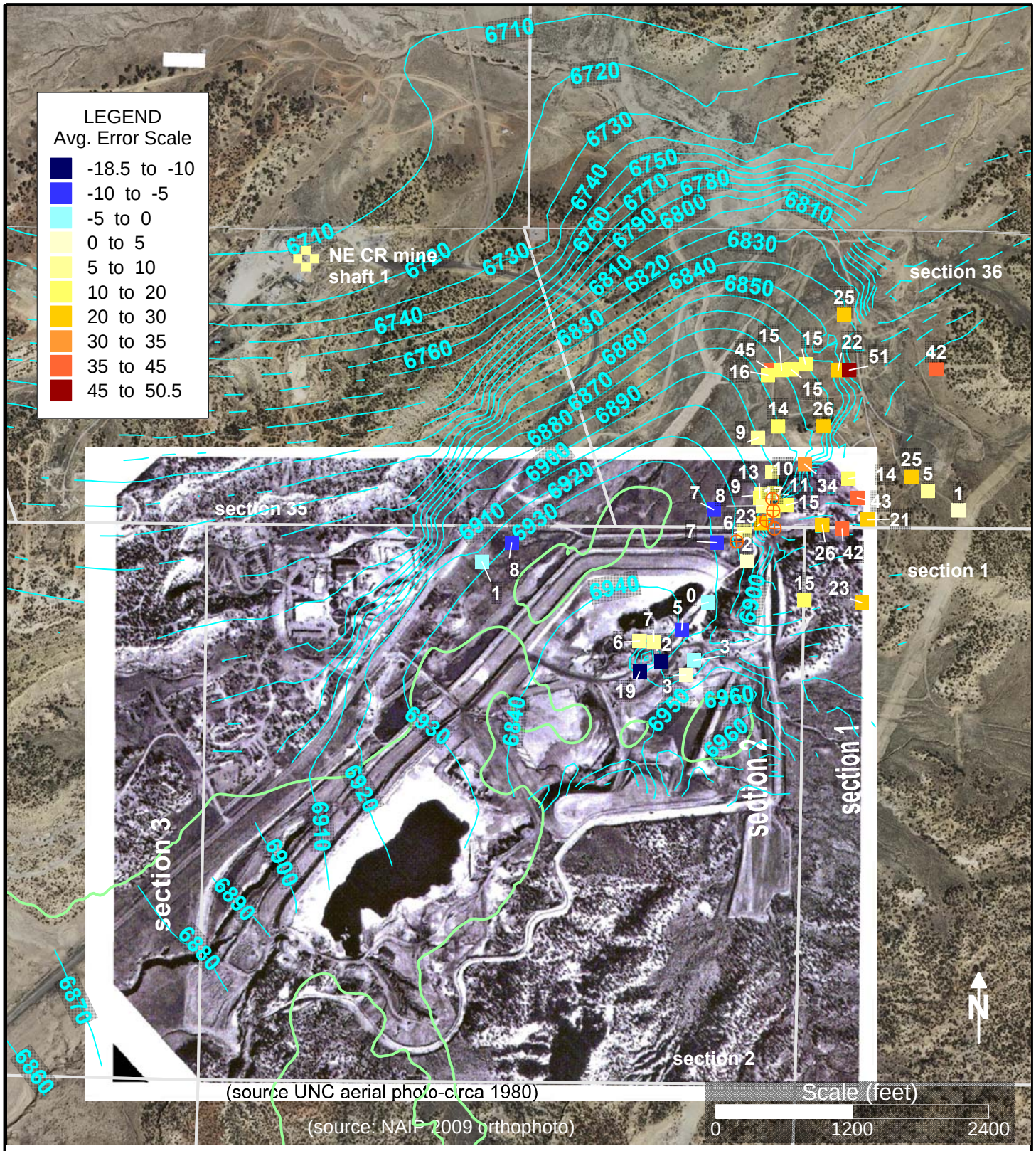


**FIGURE 16A**
**Model layer 4 piezometric elevation contours for January 1987, representing the base of Zone 3 and alluvium (within areas delimited in green) Average and RMS errors (observation-model) shown for Oct. 86 - Oct. 87. Active wells shown with orange crosshair symbols**

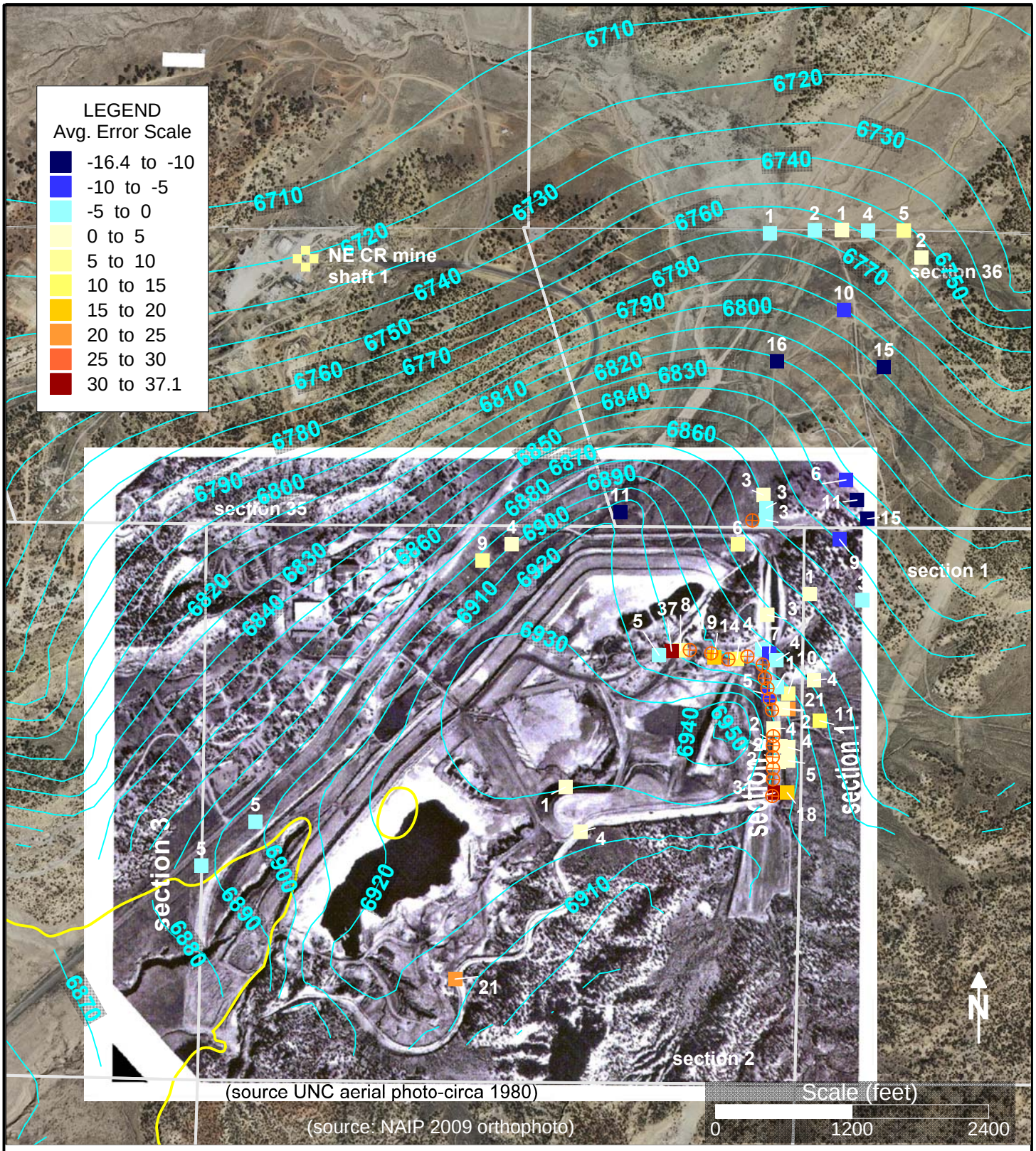


**FIGURE 16B**
**Model layer 6 piezometric elevation contours for January 1987, representing Zone 1 and alluvium (within areas delimited in yellow) Average and RMS errors (observation-model) shown for Oct. 86 - Oct. 87. Active wells shown with orange crosshair symbols**

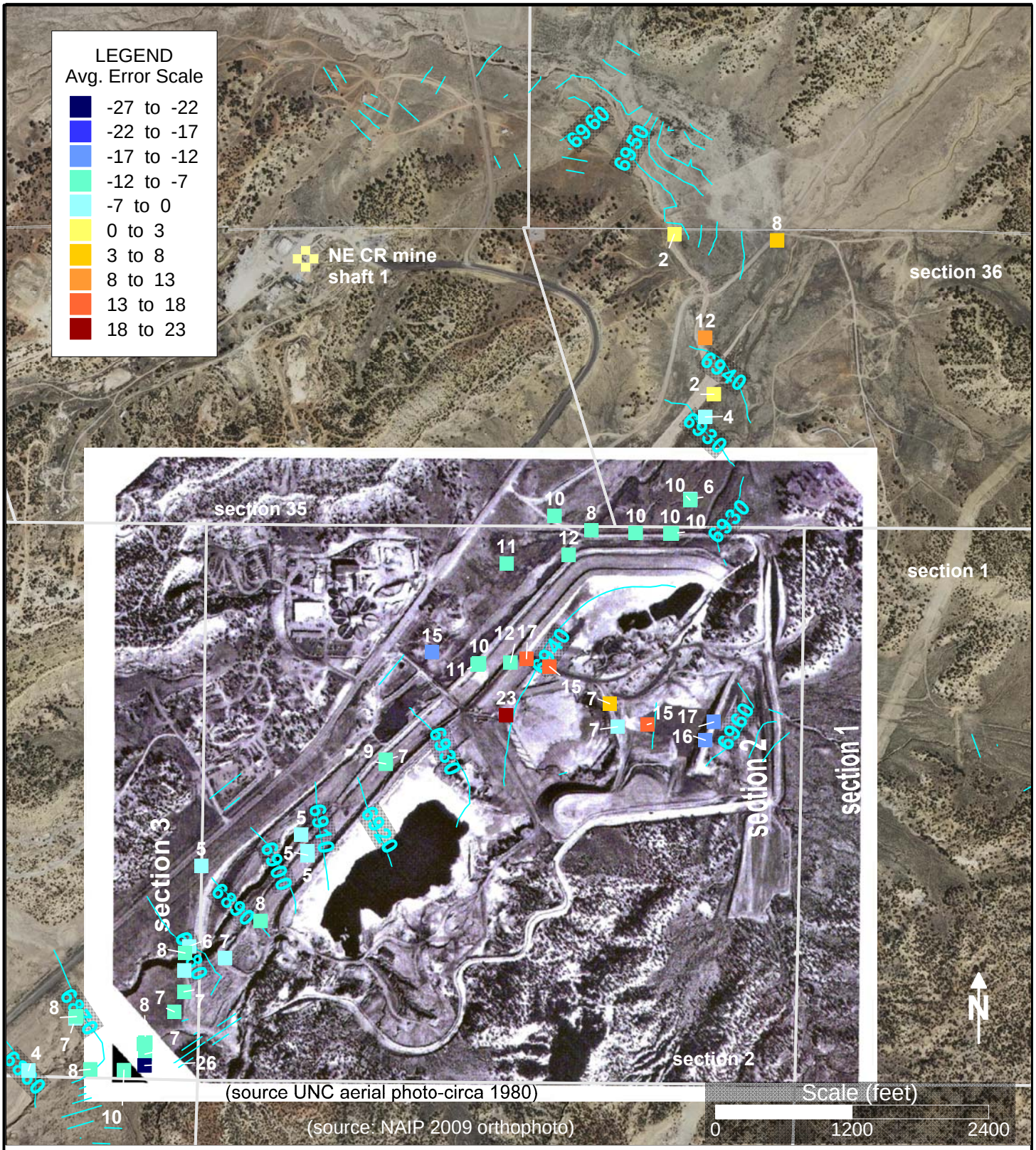


**FIGURE 16C**
**Model layer 1 grid and piezometric elevation contours for January 1987, representing the alluvium,**
**Average and RMS errors (observation-model) shown for Oct. 1986 - Oct. 1987.**

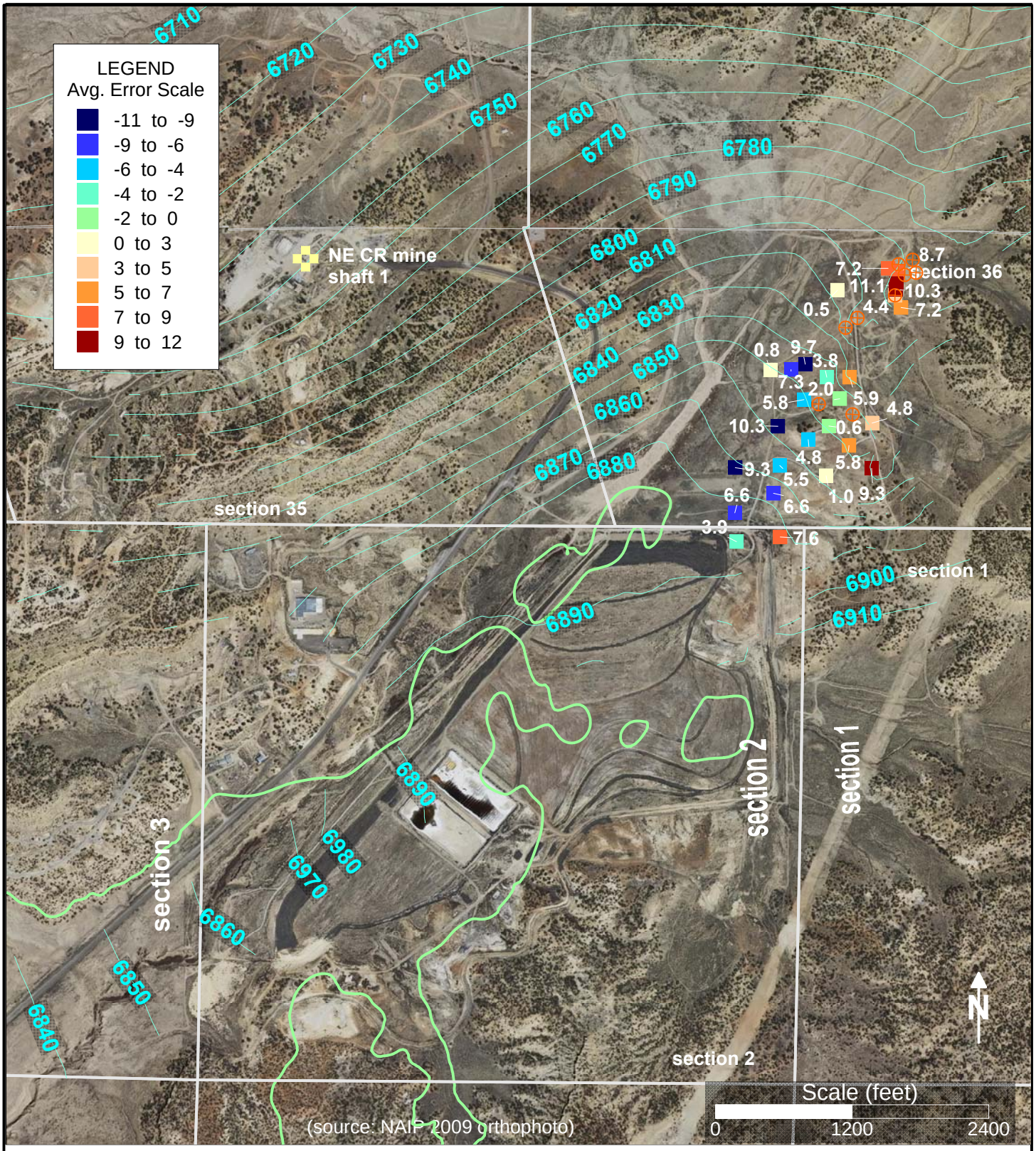


**FIGURE 17A**
**Model layer 4 piezometric elevation contours for October 2011, representing the base of Zone 3 and alluvium (within areas delimited in green Average and RMS errors (observation-model) shown for Oct. 2009 - Oct. 2010. Active wells shown with orange crosshair symbols**

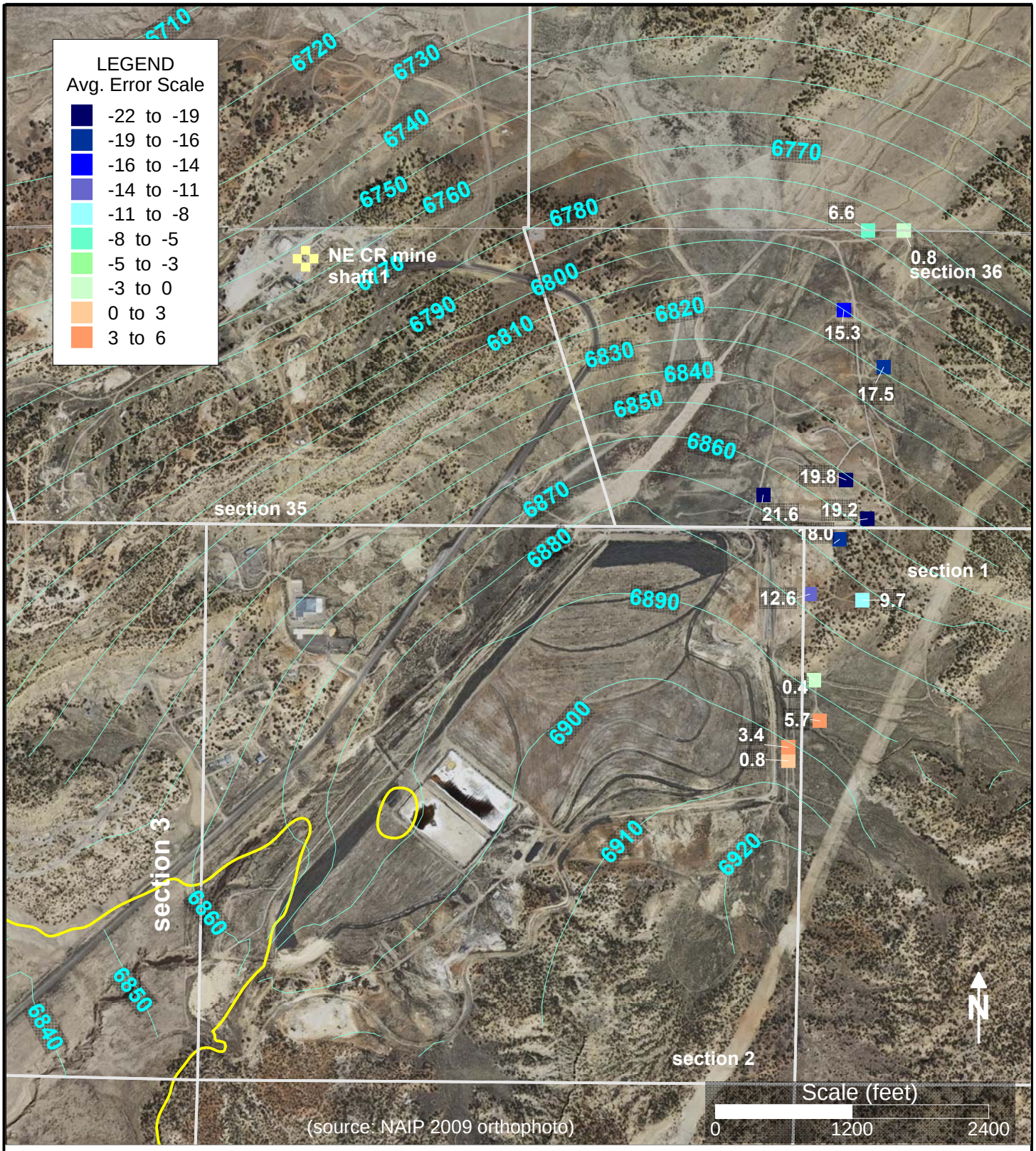


**FIGURE 17B**
**Model layer 6 piezometric elevation contours for October 2011, representing Zone 1 and alluvium (within areas delimited in yellow) Average and RMS errors (observation-model) shown for Oct. 2009 - Oct. 2010.**

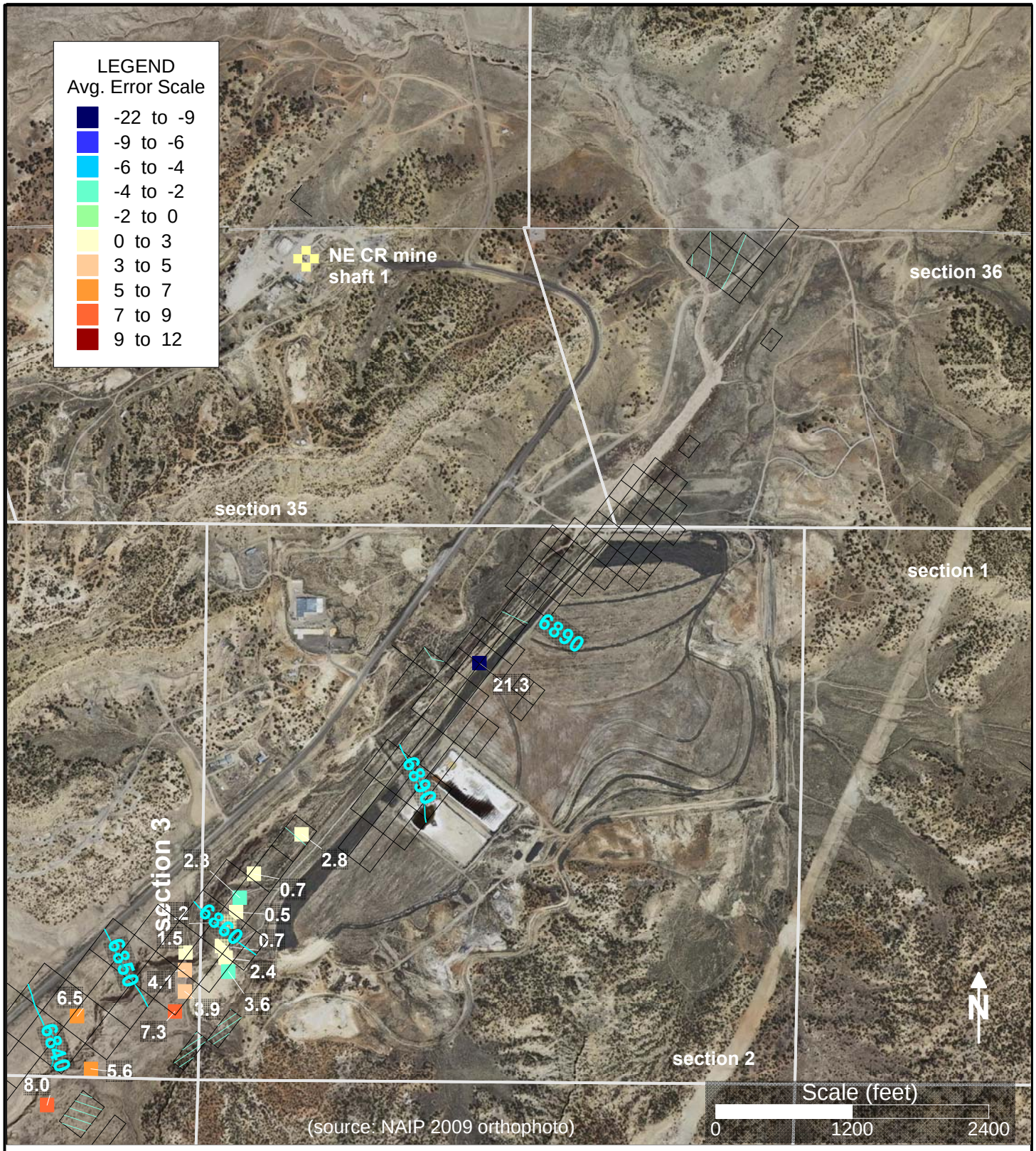


**FIGURE 17C**
**Model layer 1 grid and piezometric elevation contours for October 2011, representing the alluvium**
**Average and RMS errors (observation-model) shown for Oct. 2009 - Oct. 2010.**

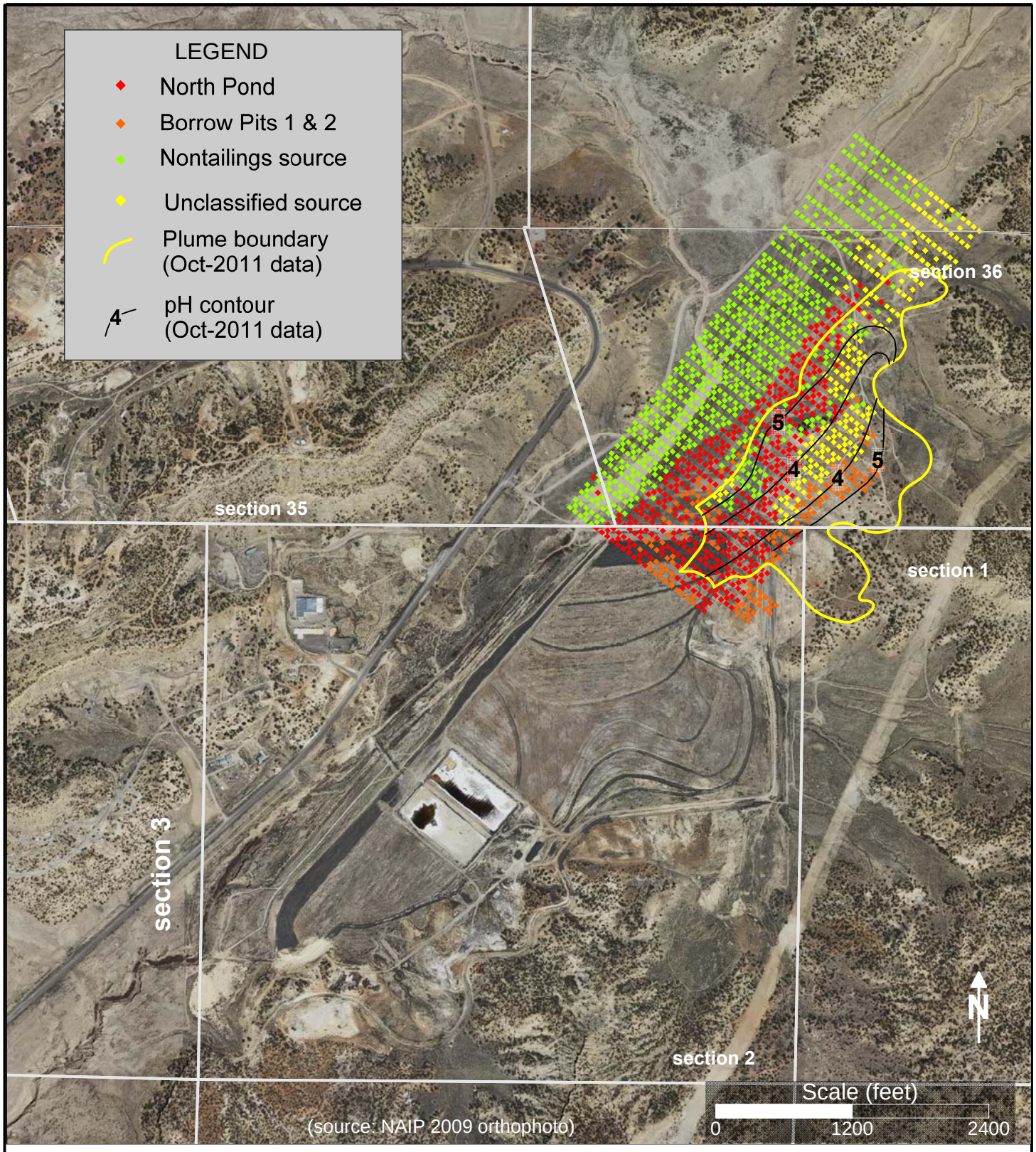


**FIGURE 18**
**Particle track end points for simulation date October 15, 2011,**
**Classified by source locations analyzed by backward tracking,**
**Tracks stopped short of sources are unclassified,**
**Base of Zone 3, model layer 4,**
**Seepage impact plume and pH contours based on Oct 2011 data**

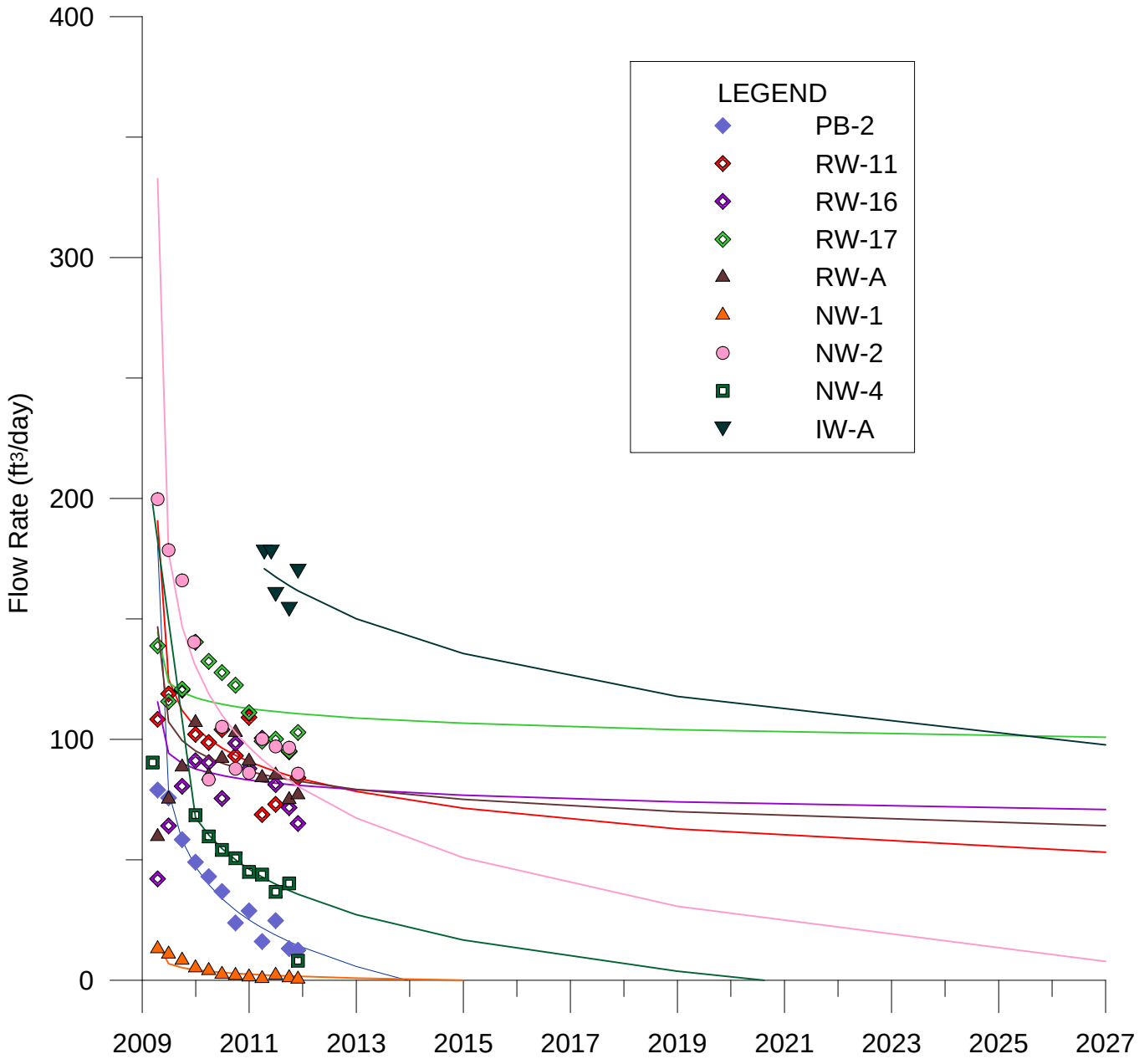


FIGURE 19
Projected flow rates of Zone 3 pumping wells and injection well (IW-A)
used in predictive model scenario,
projections based on log-time regressions

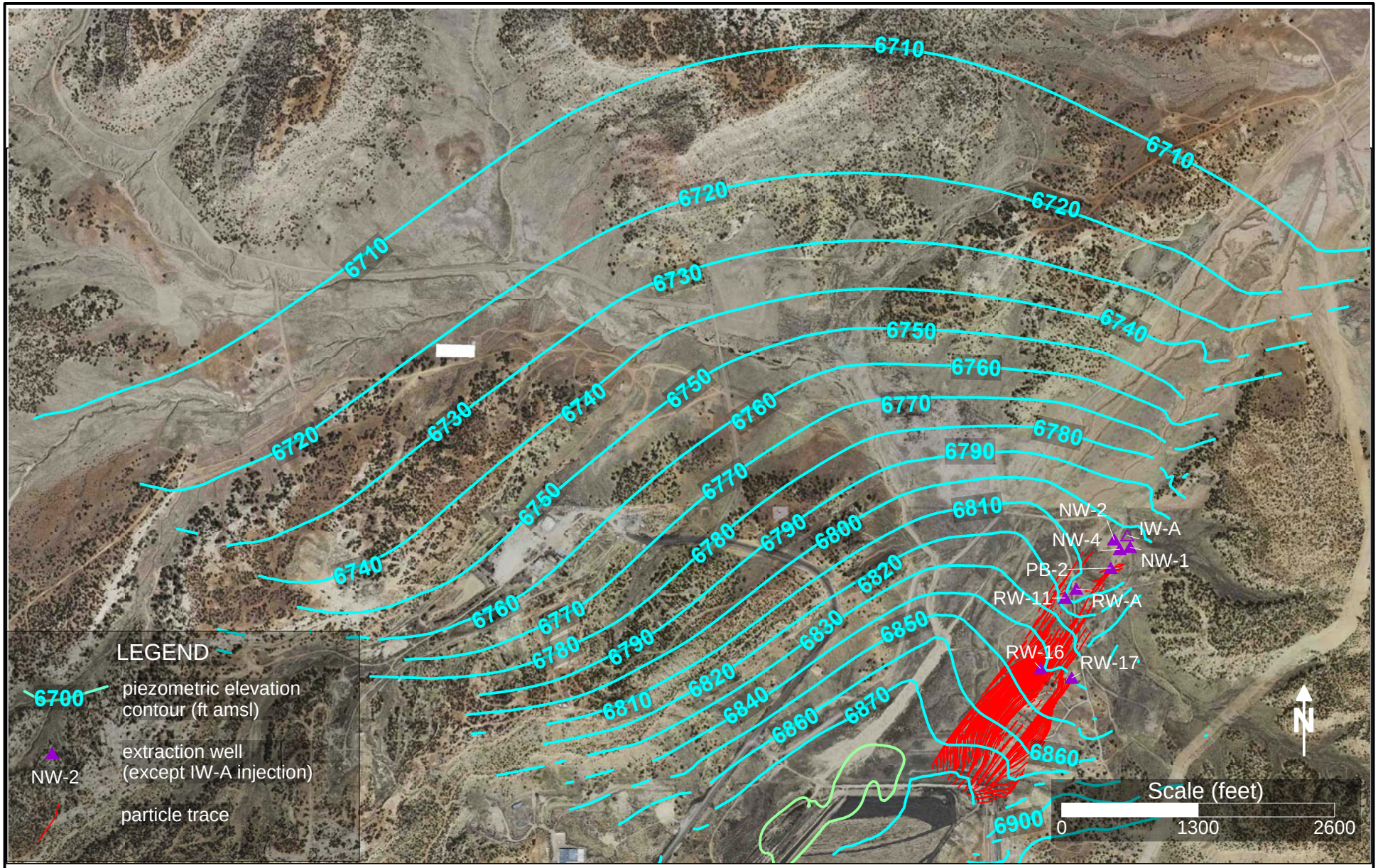


**FIGURE 20**
**2011-2026 particle traces (red) from area of tailings seepage impact, Model layer 4 piezometric elevation contours for October 2026, representing base of Zone 3 and alluvium (within areas delimited in green)**

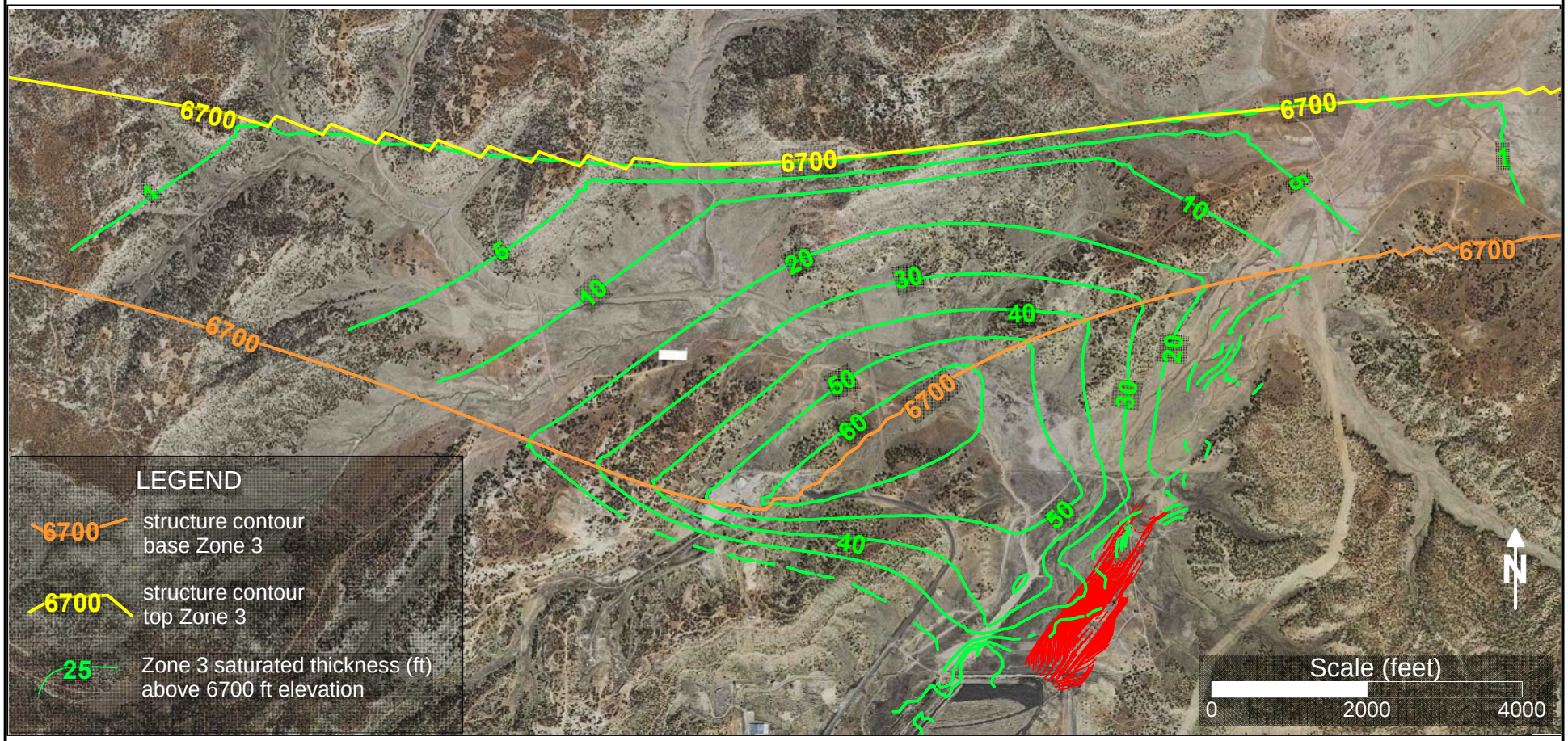


**FIGURE 21**
**Saturated thickness in Zone 3 above 6700 ft elev., model simulation of October 2026, 2011-2026 particle traces from area of tailings seepage impact shown in red.**

**FIGURE 22A**
**Model Heads versus Observed Heads Zone 3**

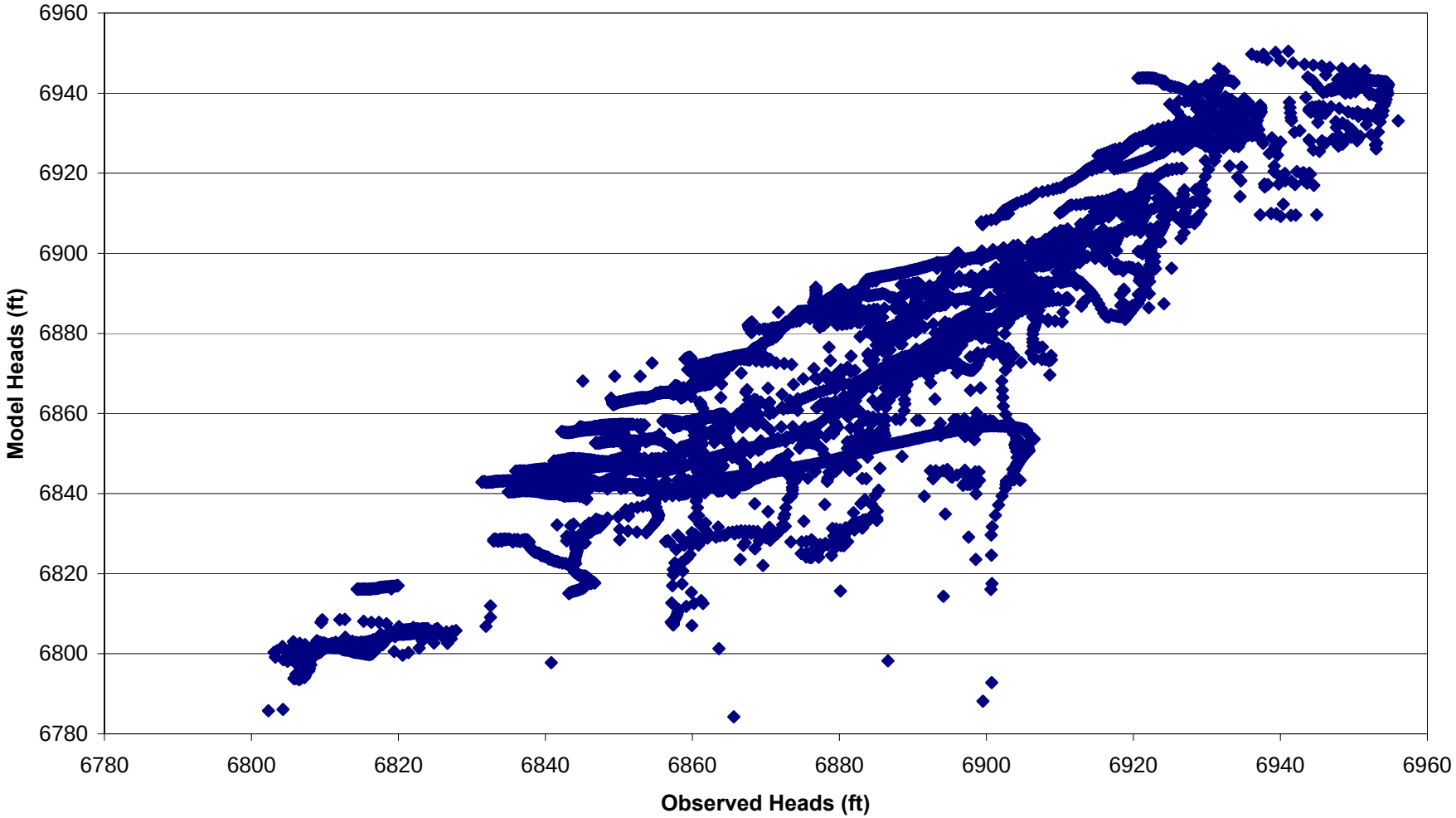

**FIGURE 22B**
**Model Heads versus Observed Heads Zone 1**

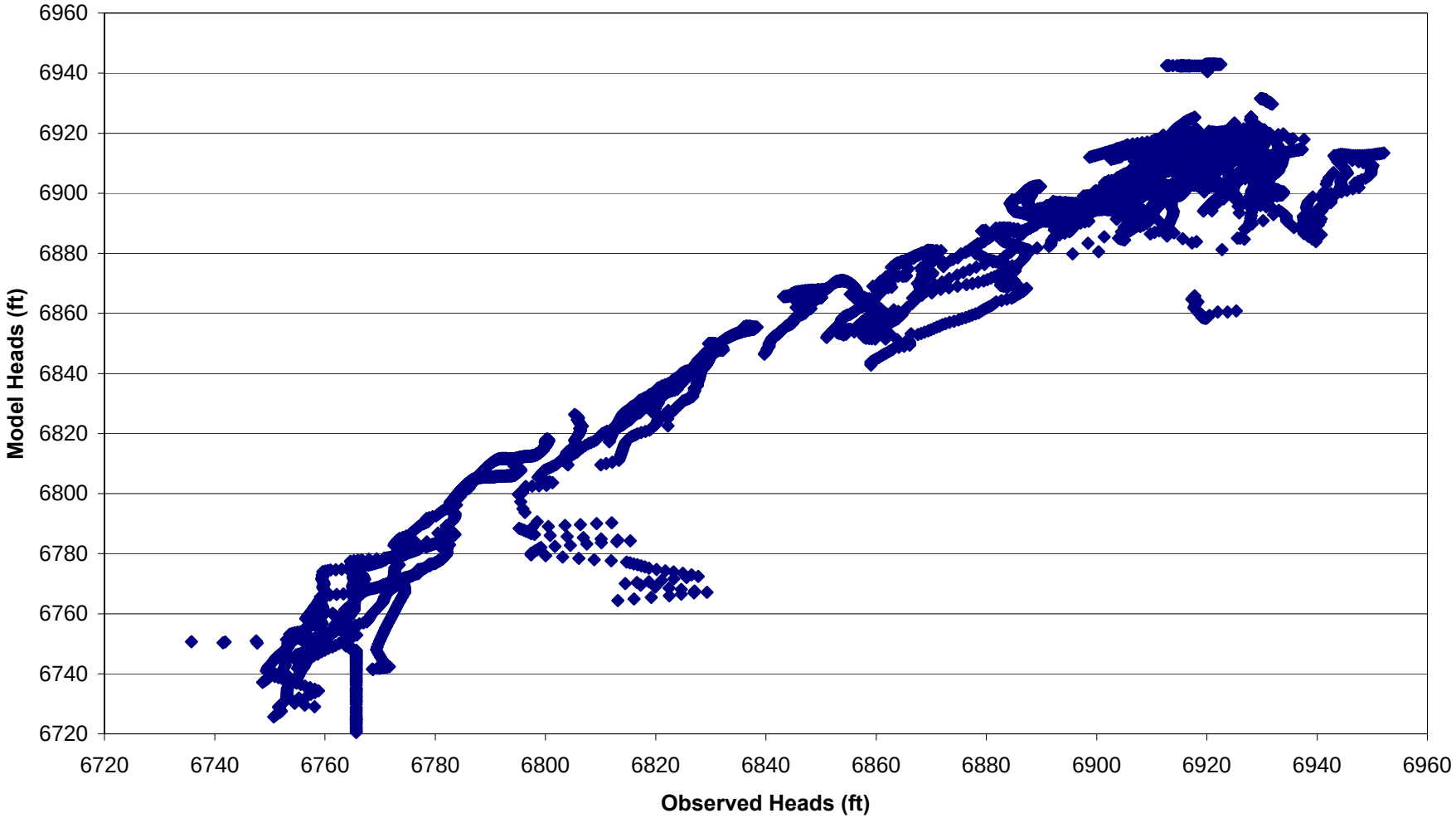

**FIGURE 22C**
**Model Heads versus Observed Heads Southwest Alluvium**

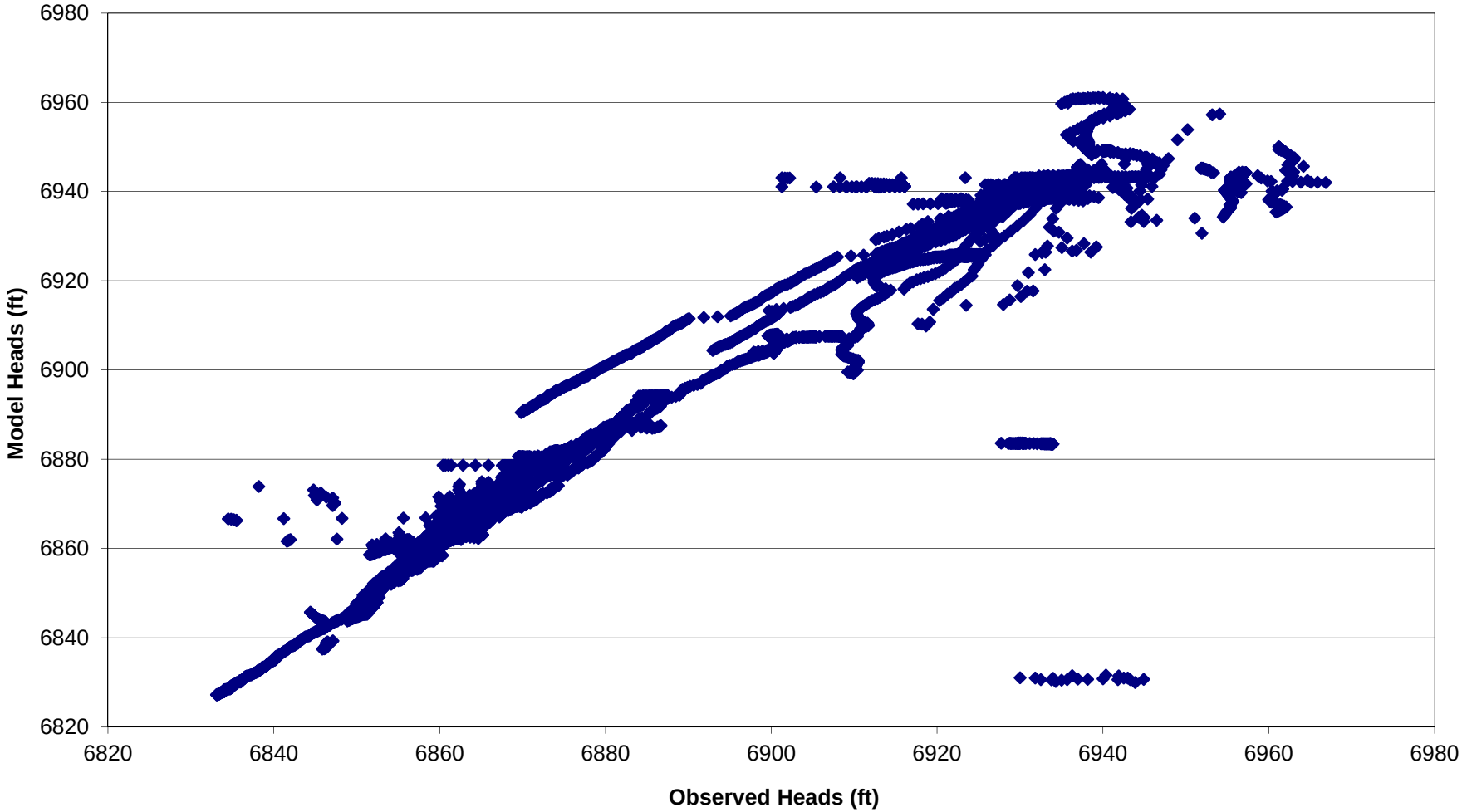

**FIGURE 23A**
**Residuals versus Observed Transient Heads in Zone 3**
**(residual = observed - model)**

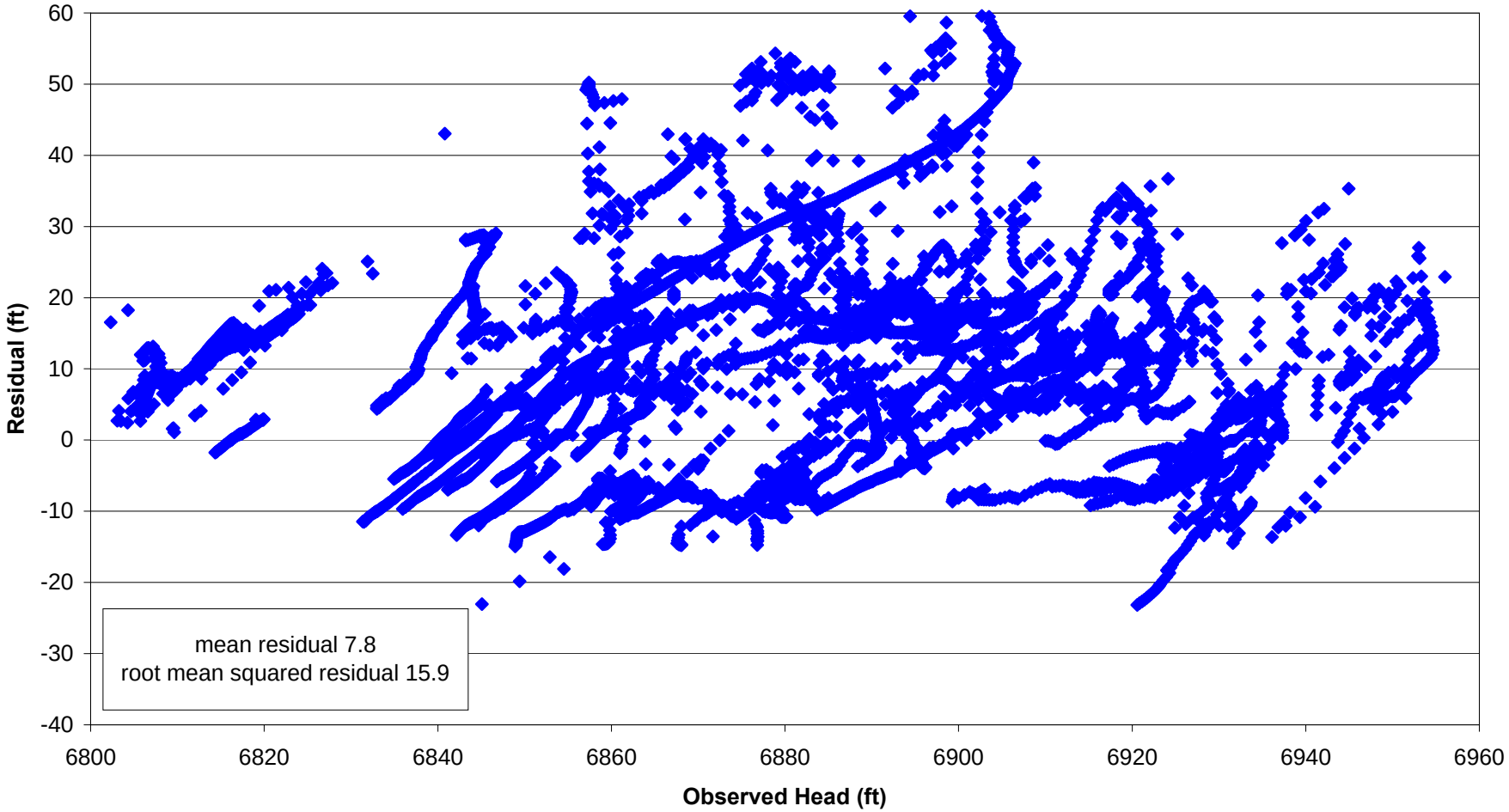

**FIGURE 23B**
**Residuals versus Observed Transient Heads in Zone 1**
**(residual = observed - model)**

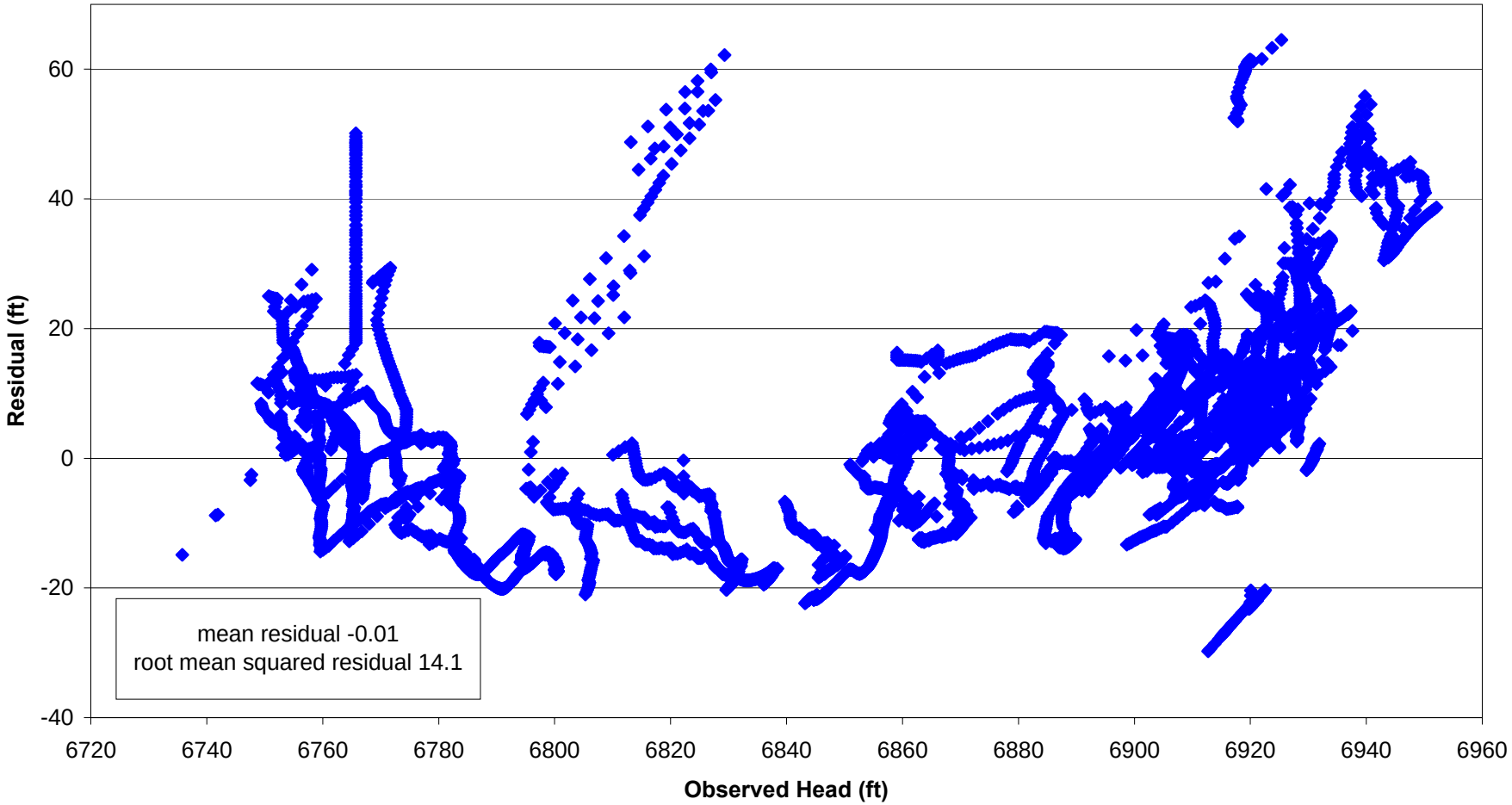

**FIGURE 23C**
**Residuals versus Observed Transient Heads in Southwest Alluvium**
**(residual = observed - model)**

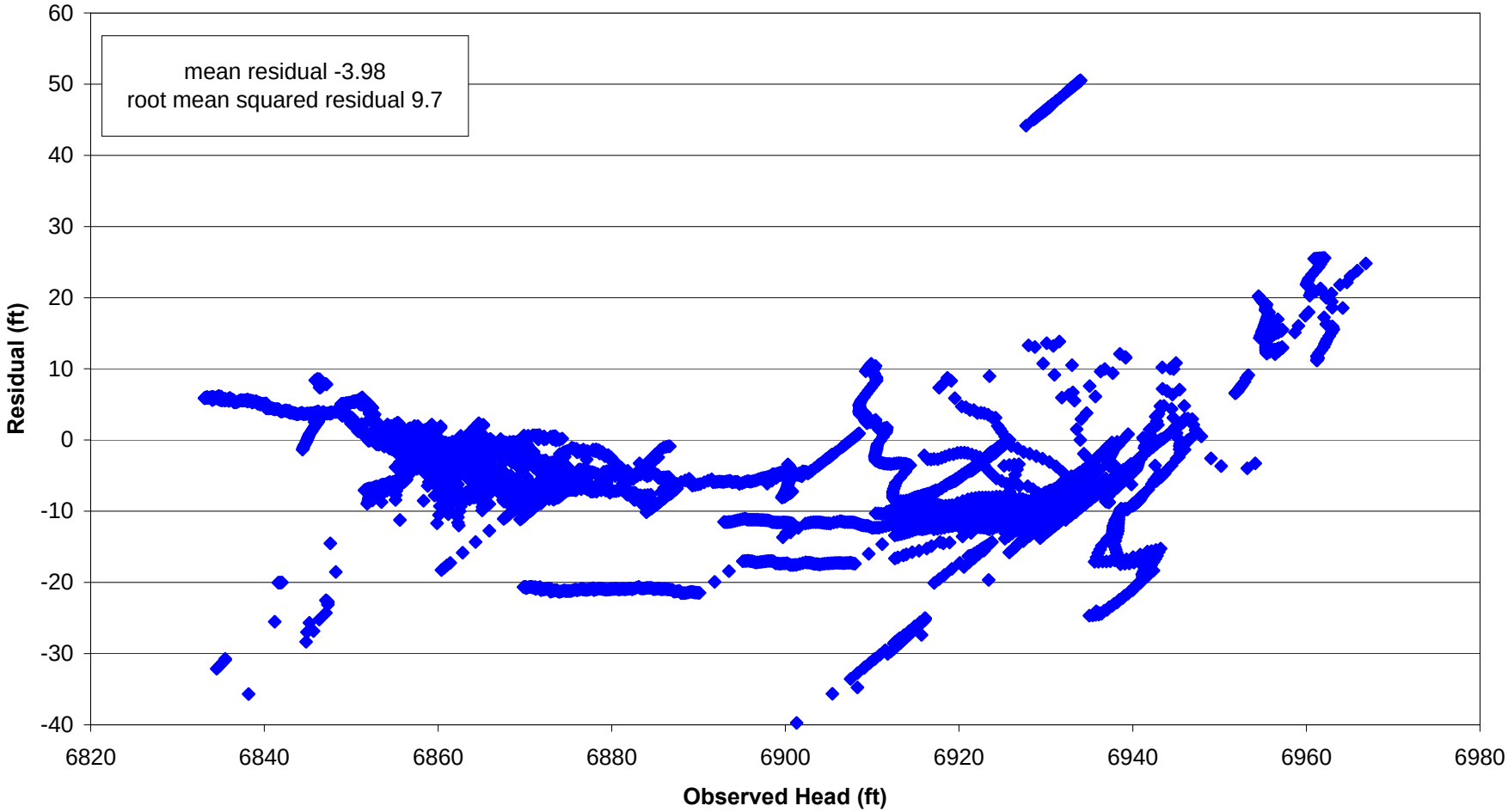

**FIGURE 24A**
**Zone 3 Residuals vs Time**

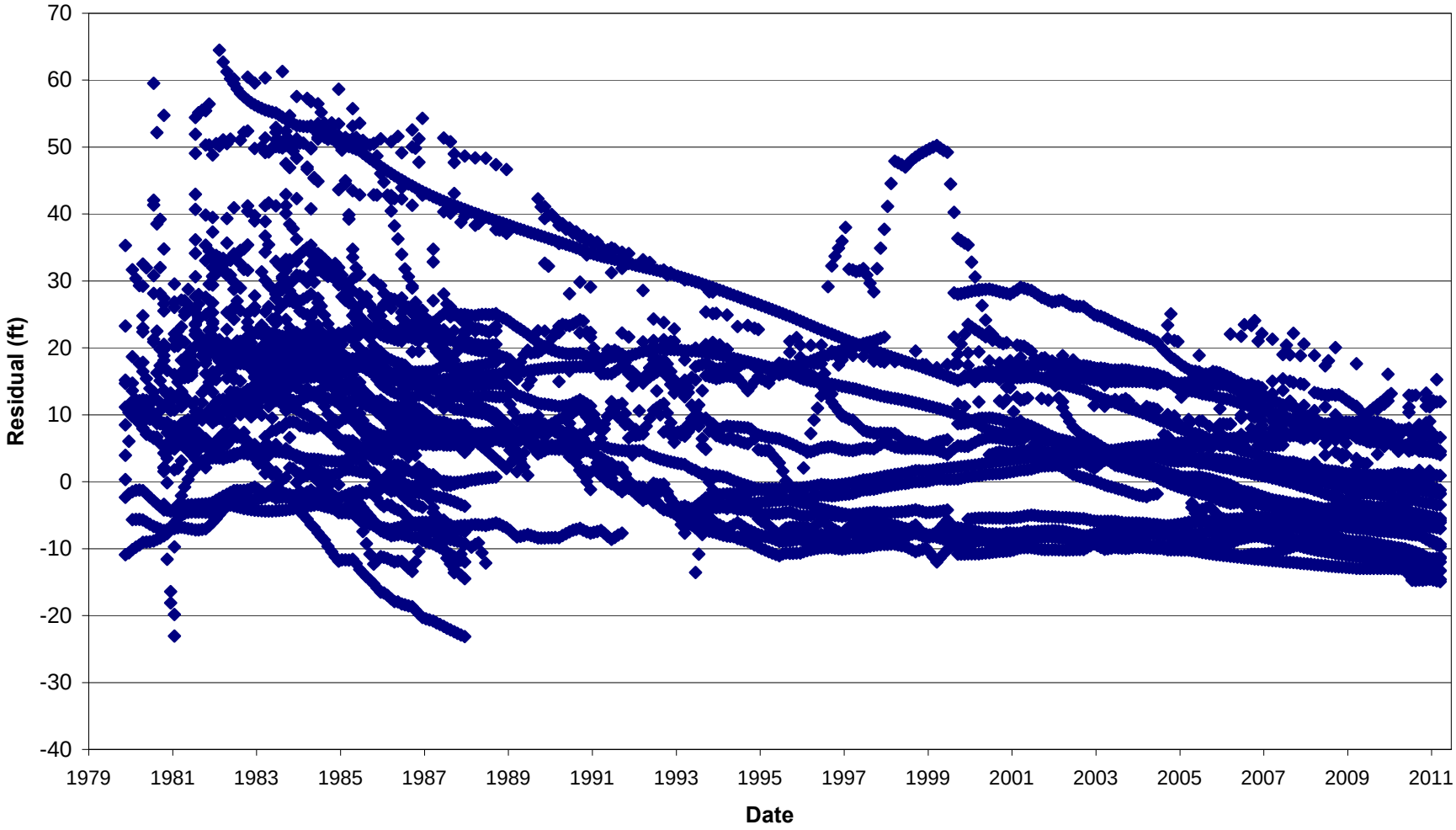

**FIGURE 24B**
**Zone 1 Residuals vs Time**

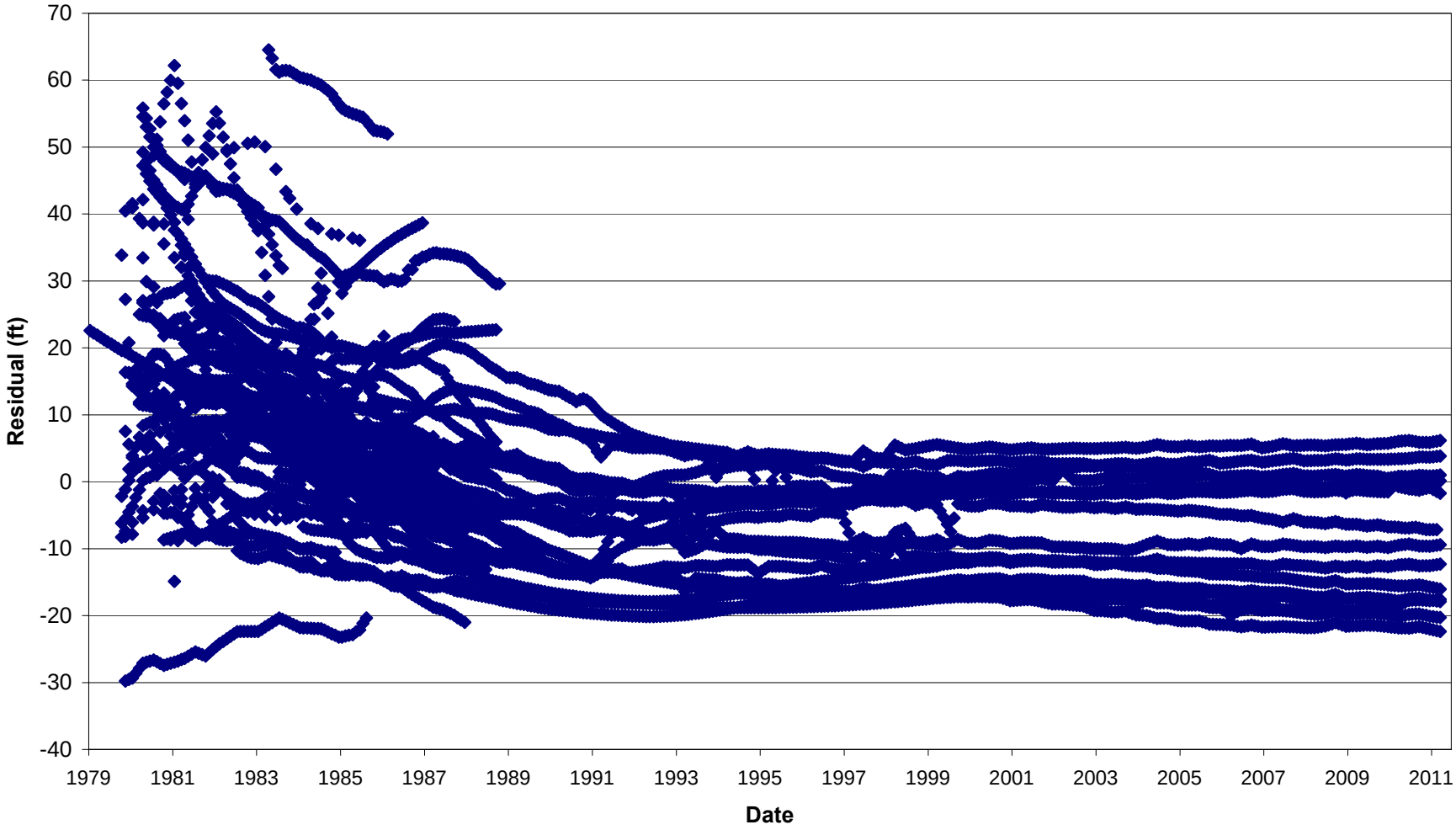

**FIGURE 24C**
**Southwest Alluvium Residuals vs Time**

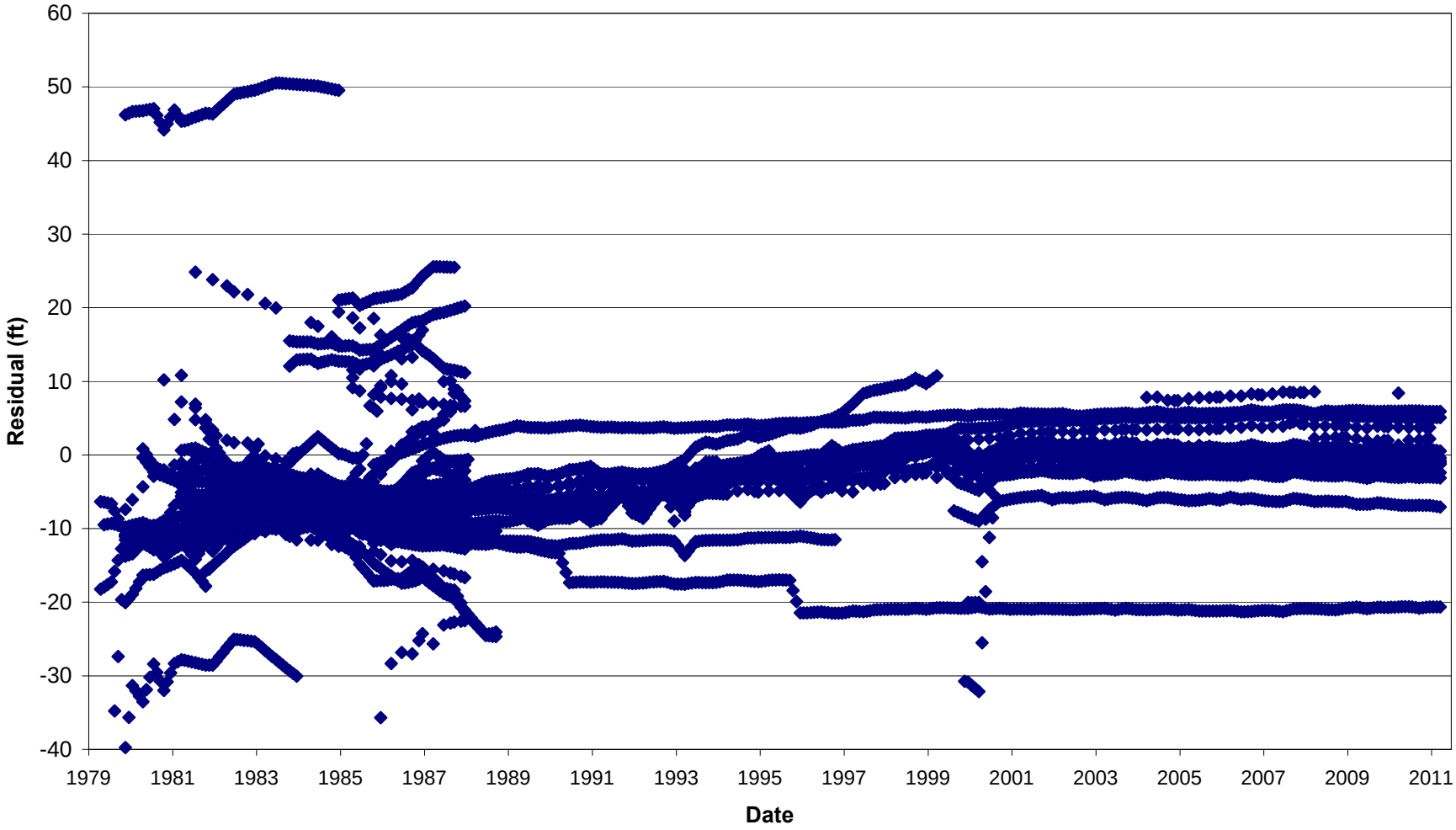

# Appendix A

**RIVER CELLS, DRAIN CELLS AND RELATED ESTIMATES**


FIGURE A-1
Segments of Pipeline Arroyo (blue) represented by river cells in the Flow Model
(see Table A-1 for estimates of transient stage and average conductance for arroyo segments).
Alignment of subsurface drainage boundary within the southwest alluvium (green)
represented by drain cells in the Flow Model. Drain cell hydrograph extrapolated from
measurements at alluvium Well 0627 (see Figure A-2). Weir locations after Raymondi and Conrad (1983).

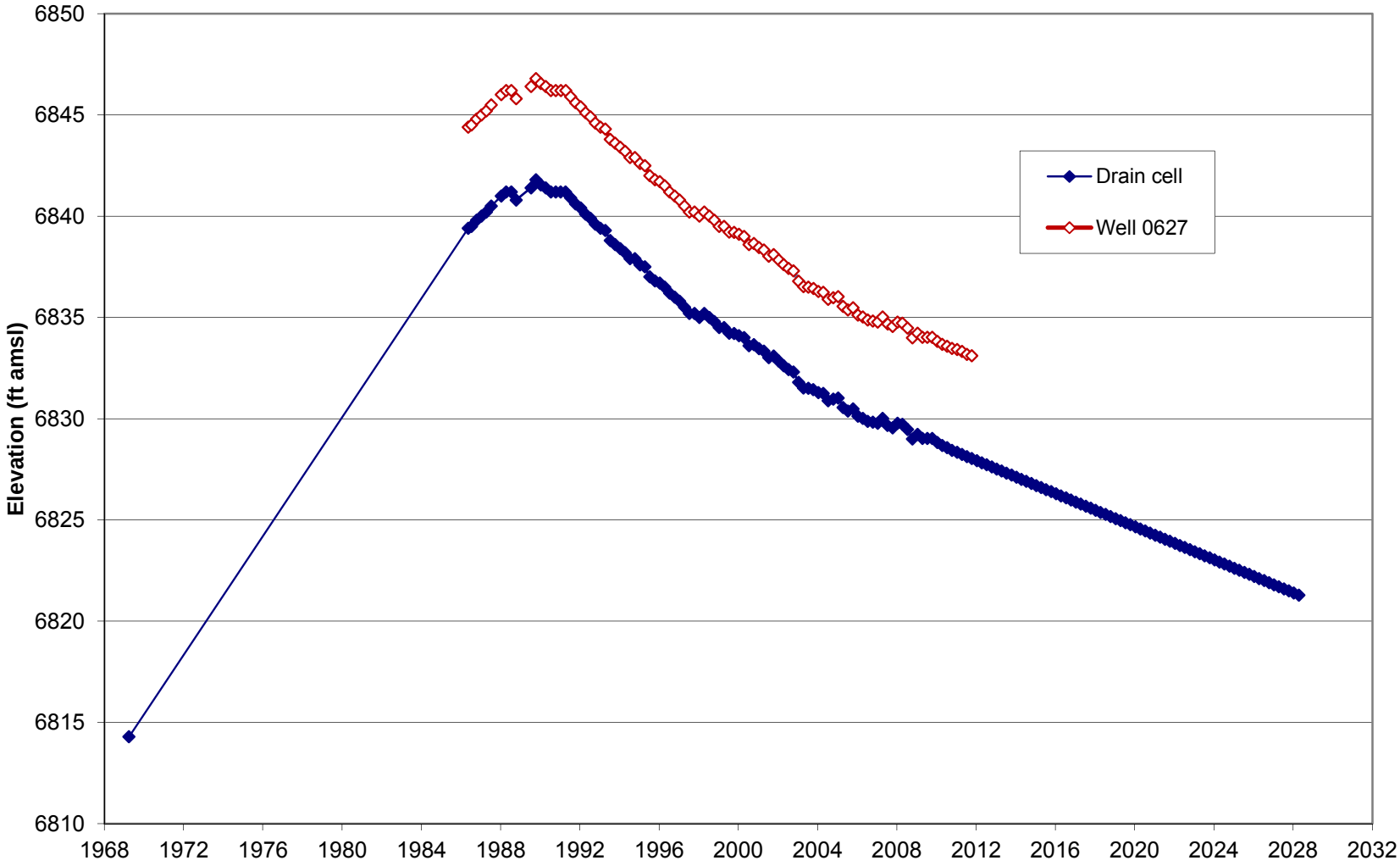


FIGURE A-2
Comparison of extrapolated Flow Model drain cell hydrograph with measurements made in upgradient alluvium Well 0627 (see Figure A-1 for locations)

**Table A-1**
**Calculated Stage (ft)**
**segment ID/channel slope**

| **Year** | **14** | **8** | **15** | **18** | **17** | **9** | **7** | **2** | **5** | **19** | **13** |
|---|---|---|---|---|---|---|---|---|---|---|---|
| (mid-year) | 0.0195 | 0.0186 | 0.0005 | 0.0110 | 0.0002 | 0.0037 | 0.0193 | 0.0148 | 0.0139 | 0.0295 | 0.0028 |
| 3/15/1968 | 0.08 | 0.08 | 0.2 | 0.09 | 0.25 | 0.12 | 0.08 | 0.08 | 0.08 | 0.07 | 0.13 |
| 7/21/1968 | 0.08 | 0.08 | 0.2 | 0.09 | 0.25 | 0.12 | 0.08 | 0.08 | 0.08 | 0.07 | 0.13 |
| 11/24/1968 | 0.33 | 0.34 | 0.87 | 0.39 | 1.09 | 0.52 | 0.33 | 0.36 | 0.37 | 0.3 | 0.56 |
| 7/6/1969 | 0.4 | 0.41 | 1.03 | 0.47 | 1.28 | 0.62 | 0.4 | 0.43 | 0.44 | 0.36 | 0.67 |
| 6/15/1970 | 0.39 | 0.4 | 1 | 0.46 | 1.25 | 0.61 | 0.39 | 0.42 | 0.43 | 0.35 | 0.65 |
| 6/15/1971 | 0.41 | 0.42 | 1.05 | 0.48 | 1.31 | 0.64 | 0.41 | 0.44 | 0.45 | 0.37 | 0.69 |
| 11/15/1971 | 0.42 | 0.43 | 1.07 | 0.49 | 1.33 | 0.65 | 0.42 | 0.46 | 0.46 | 0.38 | 0.7 |
| 6/15/1972 | 0.44 | 0.45 | 1.12 | 0.51 | 1.39 | 0.68 | 0.44 | 0.48 | 0.48 | 0.4 | 0.73 |
| 6/15/1973 | 0.53 | 0.54 | 1.33 | 0.62 | 1.64 | 0.82 | 0.53 | 0.57 | 0.58 | 0.48 | 0.88 |
| 6/15/1974 | 0.49 | 0.49 | 1.22 | 0.56 | 1.51 | 0.74 | 0.49 | 0.52 | 0.53 | 0.44 | 0.8 |
| 6/15/1975 | 0.51 | 0.52 | 1.27 | 0.59 | 1.58 | 0.78 | 0.51 | 0.55 | 0.56 | 0.46 | 0.84 |
| 6/15/1976 | 0.57 | 0.58 | 1.4 | 0.66 | 1.73 | 0.87 | 0.57 | 0.61 | 0.62 | 0.51 | 0.93 |
| 6/15/1977 | 0.61 | 0.62 | 1.49 | 0.71 | 1.84 | 0.93 | 0.61 | 0.66 | 0.67 | 0.55 | 0.99 |
| 6/15/1978 | 0.63 | 0.64 | 1.53 | 0.73 | 1.89 | 0.96 | 0.63 | 0.68 | 0.69 | 0.56 | 1.02 |
| 6/15/1979 | 0.61 | 0.62 | 1.49 | 0.71 | 1.84 | 0.93 | 0.61 | 0.65 | 0.66 | 0.54 | 0.99 |
| 6/15/1980 | 0.58 | 0.59 | 1.43 | 0.67 | 1.76 | 0.88 | 0.58 | 0.62 | 0.63 | 0.52 | 0.95 |
| 6/15/1981 | 0.53 | 0.54 | 1.32 | 0.62 | 1.63 | 0.81 | 0.53 | 0.57 | 0.58 | 0.48 | 0.87 |
| 6/15/1982 | 0.53 | 0.54 | 1.32 | 0.62 | 1.63 | 0.81 | 0.53 | 0.57 | 0.58 | 0.48 | 0.87 |
| 2/15/1983 | 0.47 | 0.48 | 1.18 | 0.54 | 1.47 | 0.72 | 0.47 | 0.5 | 0.51 | 0.42 | 0.77 |
| 2/15/1983 | 0.47 | 0.48 | 1.18 | 0.54 | 1.47 | 0.72 | 0.47 | 0.5 | 0.51 | 0.42 | 0.77 |
| 6/15/1984 | 0.47 | 0.48 | 1.18 | 0.54 | 1.47 | 0.72 | 0.47 | 0.5 | 0.51 | 0.42 | 0.77 |
| 6/15/1985 | 0.49 | 0.49 | 1.23 | 0.57 | 1.52 | 0.75 | 0.49 | 0.53 | 0.53 | 0.44 | 0.81 |
| 2/15/1986 | 0.5 | 0.51 | 1.26 | 0.59 | 1.57 | 0.78 | 0.5 | 0.54 | 0.55 | 0.46 | 0.83 |
| 2/15/1986 | 0 | 0 | 0 | 0 | 0 | 0 | 0 | 0 | 0 | 0 | 0 |

Note:
See Figure A-1 for channel segment locations
Calculations based on assumed trapezoidal channel having a Manning's coefficient of 0.45, side slope of 4, and bottom width of 4 ft (1 ft prior to 11/68).

**Table A-2**

**Calculated Wetted Width (ft) and Average Conductance ($ft^2$/d/ft)**

| **Year** | **segment ID** | | | | | | | | | | |
|---|---|---|---|---|---|---|---|---|---|---|---|
| (mid-year) | **14** | **8** | **15** | **18** | **17** | **9** | **7** | **2** | **5** | **19** | **13** |
| 3/15/1968 | 1.6 | 1.6 | 2.6 | 1.7 | 3.0 | 2.0 | 1.6 | 1.6 | 1.6 | 1.6 | 2.0 |
| 7/21/1968 | 1.6 | 1.6 | 2.6 | 1.7 | 3.0 | 2.0 | 1.6 | 1.6 | 1.6 | 1.6 | 2.0 |
| 11/24/1968 | 6.6 | 6.7 | 11.0 | 7.1 | 12.7 | 8.2 | 6.6 | 6.9 | 7.0 | 6.4 | 8.5 |
| 7/6/1969 | 7.2 | 7.3 | 12.2 | 7.8 | 14.2 | 9.0 | 7.2 | 7.4 | 7.5 | 6.9 | 9.4 |
| 6/15/1970 | 7.1 | 7.2 | 12.0 | 7.7 | 14.0 | 8.9 | 7.1 | 7.4 | 7.4 | 6.8 | 9.2 |
| 6/15/1971 | 7.3 | 7.4 | 12.4 | 7.8 | 14.5 | 9.1 | 7.3 | 7.5 | 7.6 | 7.0 | 9.5 |
| 11/15/1971 | 7.4 | 7.4 | 12.6 | 7.9 | 14.6 | 9.2 | 7.4 | 7.7 | 7.7 | 7.0 | 9.6 |
| 6/15/1972 | 7.5 | 7.6 | 13.0 | 8.1 | 15.1 | 9.4 | 7.5 | 7.8 | 7.8 | 7.2 | 9.8 |
| 6/15/1973 | 8.2 | 8.3 | 14.6 | 9.0 | 17.1 | 10.6 | 8.2 | 8.6 | 8.6 | 7.8 | 11.0 |
| 6/15/1974 | 7.9 | 7.9 | 13.8 | 8.5 | 16.1 | 9.9 | 7.9 | 8.2 | 8.2 | 7.5 | 10.4 |
| 6/15/1975 | 8.1 | 8.2 | 14.2 | 8.7 | 16.6 | 10.2 | 8.1 | 8.4 | 8.5 | 7.7 | 10.7 |
| 6/15/1976 | 8.6 | 8.6 | 15.2 | 9.3 | 17.8 | 11.0 | 8.6 | 8.9 | 9.0 | 8.1 | 11.4 |
| 6/15/1977 | 8.9 | 9.0 | 15.9 | 9.7 | 18.7 | 11.4 | 8.9 | 9.3 | 9.4 | 8.4 | 11.9 |
| 6/15/1978 | 9.0 | 9.1 | 16.2 | 9.8 | 19.1 | 11.7 | 9.0 | 9.4 | 9.5 | 8.5 | 12.2 |
| 6/15/1979 | 8.9 | 9.0 | 15.9 | 9.7 | 18.7 | 11.4 | 8.9 | 9.2 | 9.3 | 8.3 | 11.9 |
| 6/15/1980 | 8.6 | 8.7 | 15.4 | 9.4 | 18.1 | 11.0 | 8.6 | 9.0 | 9.0 | 8.2 | 11.6 |
| 6/15/1981 | 8.2 | 8.3 | 14.6 | 9.0 | 17.0 | 10.5 | 8.2 | 8.6 | 8.6 | 7.8 | 11.0 |
| 6/15/1982 | 8.2 | 8.3 | 14.6 | 9.0 | 17.0 | 10.5 | 8.2 | 8.6 | 8.6 | 7.8 | 11.0 |
| 2/15/1983 | 7.8 | 7.8 | 13.4 | 8.3 | 15.8 | 9.8 | 7.8 | 8.0 | 8.1 | 7.4 | 10.2 |
| 2/15/1983 | 7.8 | 7.8 | 13.4 | 8.3 | 15.8 | 9.8 | 7.8 | 8.0 | 8.1 | 7.4 | 10.2 |
| 6/15/1984 | 7.8 | 7.8 | 13.4 | 8.3 | 15.8 | 9.8 | 7.8 | 8.0 | 8.1 | 7.4 | 10.2 |
| 6/15/1985 | 7.9 | 7.9 | 13.8 | 8.6 | 16.2 | 10.0 | 7.9 | 8.2 | 8.2 | 7.5 | 10.5 |
| 2/15/1986 | 8.0 | 8.1 | 14.1 | 8.7 | 16.6 | 10.2 | 8.0 | 8.3 | 8.4 | 7.7 | 10.6 |
| 2/15/1986 | | | | | | | | | | | |
| **average conductance** | **18.9** | **19.1** | **33.0** | **20.4** | **38.6** | **23.9** | **18.9** | **19.6** | **19.8** | **18.0** | **25.0** |
| average width | 7.95 | 8.03 | 13.89 | 8.60 | 16.27 | 10.07 | 7.95 | 8.25 | 8.32 | 7.56 | 10.51 |

Notes:
See Figure A-1 for channel segment locations
Calculations based on assumed trapezoidal channel having a Manning's coefficient of 0.45, side slope of 4,
and bottom width of 4 ft (1 ft prior to 11/68).
Conductance calculation based on uniform stream bed conductivity equal to alluvium vertical hydraulic conductivity of 2.375 ft/d

# Appendix B

**RECHARGE AREAS AND RELATED ESTIMATES**

Table B-1

Estimation of North and South Pond Infiltration Rates Following July 1979 Cessation of Tailings Discharge

| Pond | Date[1] | Wetted Surface Area | Wetted Surface Elevation[2] | Head above Pond Bottom | Water Level Drop | | Evapotranspiration[3] | | Infiltration Rate[4] | Seepage Flux[5] | |
|---|---|---|---|---|---|---|---|---|---|---|---|
| | | | | | total | avg. rate | total | avg. rate | | | |
| **north** | | ($ft^2$) | (ft amsl) | (ft) | (ft) | (ft/d) | (ft) | (ft/d) | (ft/d) | (ft3/d) | (gal/d) |
| begin | 7/16/1979 | 542,131 | 6960 | 10 | | | | | 0.011 | 6,017 | 45,006 |
| end | 3/30/1980 | 141,113 | 6955 | 5 | 5 | 0.019 | 2.9 | 0.0111 | 0.006 | 1,451 | 10,851 |
| **south** | | | | | | | | | | | |
| begin | 7/16/1979 | 765,804 | 6950 | 22 | | | | | 0.008 | 6,048 | 45,237 |
| end | 3/1/1981 | 71,289 | 6940 | 12 | 10 | 0.017 | 6.4 | 0.0107 | 0.004 | 1,205 | 9,010 |

Notes

1. End dates and wetted surface areas based on aerial photography (see Figures B-4 through B-8)
2. Wetted surface elevations estimated from topographic maps (see Figures B-2 and B-3)
3. Evapotransportation rates based on site observations reported by 1979-1980 seepage study (Science Applications, 1980)
4. Infiltration rate is equal to average rate of water level drop minus average rate of evapotranspiration, adjusted by ratio of head to average head above pond bottom (i.e. infiltration rate assumed to be proportional to head)
5. Seepage flux is shown for information (not a model input value). Equal to average infiltration rate times wetted surface area for begin date. Equal to average infiltration rate times sum of end date wetted surface area plus 0.3 times subsurface wetted area (end date area - begin date area) for end date (calculation accounts for estimated 0.3 tailings porosity)

Table B-2
Estimated Infiltration Rates and Volumes Beneath Tailings Ponds

**north pond**

| Date | Area | elevation | Head | Infiltration Rate | Seepage Flux[1] | | Volume[1] |
|---|---|---|---|---|---|---|---|
| | ($ft^2$) | (ft amsl) | (ft) | (ft/d) | ($ft^3$/day) | (gal./day) | (gal) |
| 3/15/1969 | | 6950.0 | | | | | |
| 6/1/1977 | 141,114 | 6952.0 | 2.0 | 0.0022 | 313 | 2,343 | |
| 4/30/1978 | 542,131 | 6954.5 | 4.5 | 0.0050 | 2,708 | 20,253 | 3,762,217 |
| 1/1/1979 | 542,131 | 6955.0 | 5.0 | 0.0055 | 3,008 | 22,503 | 5,259,005 |
| 6/10/1979 | 542,131 | 6952.0 | 2.0 | 0.0022 | 1,203 | 9,001 | 2,520,362 |
| 7/16/1979 | 602,189 | 6960.0 | 10.0 | 0.0111 | 6,017 | 45,006 | 972,140 |
| 3/30/1980 | 602,189 | 6955.0 | 5.0 | 0.0055 | 1,451 | 10,851 | 7,205,636 |
| 7/15/1982 | 602,189 | 6951.5 | 1.5 | 0.0017 | 435 | 3,255 | 5,903,582 |
| 12/31/1983 | 602,189 | 6960.0 | 10.0 | 0.0111 | 6,017 | 45,006 | 12,885,905 |
| 11/12/1993 | 602,189 | 6950.0 | 0.0 | 0.0000 | 0.000 | 0 | 81,102,798 |
| total | | | | | | | 119,611,645 |

1. Seepage flux and volumes shown for information (not model input values).

**south pond**

| Date | Area | elevation | Head | Infiltration Rate | Seepage Flux[1] | | Volume[1] |
|---|---|---|---|---|---|---|---|
| | ($ft^2$) | (ft amsl) | (ft) | (ft/d) | ($ft^3$/day) | (gal./day) | (gal) |
| 3/15/1969 | | 6928.0 | | | | | |
| 6/1/1977 | 181,112 | 6933.0 | 5.0 | 0.0018 | 325 | 2,431 | |
| 4/30/1978 | 181,112 | 6933.0 | 5.0 | 0.0018 | 325 | 2,431 | 809,689 |
| 1/1/1979 | 778,816 | 6940.0 | 12.0 | 0.0043 | 3,355 | 25,094 | 3,385,658 |
| 6/10/1979 | 932,653 | 6958.0 | 30.0 | 0.0108 | 10,044 | 75,127 | 8,017,722 |
| 7/16/1979 | 932,653 | 6960.0 | 32.0 | 0.0115 | 10,713 | 80,136 | 2,794,738 |
| 7/16/1979 | 765,804 | 6950.0 | 22.0 | 0.0079 | 6,048 | 45,237 | see note |
| 3/30/1980 | 359,645 | 6944.0 | 16.0 | 0.0057 | 2,765 | 20,686 | 8,504,049 |
| 3/1/1981 | 71,289 | 6940.0 | 12.0 | 0.0043 | 1,205 | 9,010 | 4,988,910 |
| 10/15/1988 | 0 | 6928.0 | 0.0 | 0.0000 | 0 | 0 | 12,550,400 |
| total | | | | | | | 41,051,166 |

Note: Estimated height lost in July 1979 breach 13.3 feet; estimated volume lost 12,433,155 gal.

**central pond**

| Date | Area | elevation | Head | Infiltration Rate | Seepage Flux[1] | | Volume[1] |
|---|---|---|---|---|---|---|---|
| | ($ft^2$) | (ft amsl) | (ft) | (ft/d) | ($ft^3$/day) | (gal./day) | (gal) |
| 3/15/1969 | | 6942.0 | | | | | |
| 6/1/1977 | | 6942.0 | 0.0 | 0.00 | 0 | 0 | |
| 4/30/1978 | 370,300 | 6954.4 | 12.4 | 0.0111 | 4,110 | 30,741 | 5,118,452 |
| 1/1/1979 | 370,300 | 6954.4 | 12.4 | 0.0111 | 4,110 | 30,741 | 7,562,397 |
| 6/10/1979 | 370,300 | 6954.4 | 12.4 | 0.0111 | 4,110 | 30,741 | 4,918,632 |
| 7/16/1979 | 454,931 | 6955.2 | 13.2 | 0.0118 | 5,370 | 40,169 | 1,276,380 |
| 3/30/1980 | 454,931 | 6961.6 | 19.6 | 0.0176 | 7,992 | 59,778 | 12,893,155 |
| 6/2/1980 | 454,931 | 6962.2 | 20.2 | 0.0181 | 8,241 | 61,646 | 3,885,582 |
| 11/15/1980 | 454,931 | 6962.5 | 20.5 | 0.0183 | 8,347 | 62,438 | 10,298,966 |
| 2/15/1981 | 454,931 | 6964.0 | 22.0 | 0.0197 | 8,958 | 67,007 | 5,954,445 |
| 12/1/1981 | 454,931 | 6966.0 | 24.0 | 0.0215 | 9,772 | 73,098 | 20,245,112 |
| 6/15/1982 | 454,931 | 6968.0 | 26.0 | 0.0233 | 10,587 | 79,190 | 14,924,183 |
| 7/15/1982 | 454,931 | 6968.0 | 26.0 | 0.0233 | 10,587 | 79,190 | 2,375,686 |
| 10/6/1984 | 370,300 | 6954.4 | 12.4 | 0.0111 | 4,110 | 30,741 | 44,778,507 |
| 11/19/1990 | 0 | 6942.0 | 0.0 | 0.01 | 0 | 0 | 34,346,066 |
| total | | | | | | | 168,577,561 |

Table B-3
Estimated Annual Average Recharge in Arroyo Channels from Periodic Runnoff Events

| Arroyo Segment ID[1] | Watershed Area[2] | Vol. per inch precip. per day | Runoff Rate at Fraction[3] **0.037** | | Channel Slope | Channel Bottom Width | Side Slope | Manning's Coef. | Calculated Stage | Calculated Wetted Width | Conductance per Unit Length[4] | Periodic Recharge Rate per Unit Length[5] | Average Recharge Rate per Unit Length[6] | Average Areal Recharge Rate[7] |
|---|---|---|---|---|---|---|---|---|---|---|---|---|---|---|
| | ($ft^2$) | ($ft^3$/d) | ($ft^3$/s) | ($ft^3$/s) | | (ft) | | | (ft) | (ft) | ($ft^2$/d per ft) | ($ft^3$/d per ft) | ($ft^3$/d per ft) | (ft/d) |
| **18** | 162,920,386 | 13,576,699 | 502,338 | 5.81 | 0.0110 | 4 | 4 | 0.045 | 0.52 | 8.16 | 19.38 | 3.16 | 0.0258 | 0.00260 |
| **3** | 261,430,623 | 21,785,885 | 806,078 | 9.33 | 0.0112 | 4 | 4 | 0.045 | 0.67 | 9.36 | 22.23 | 4.48 | 0.0365 | 0.00663 |
| **17** | 431,426,211 | 35,952,184 | 1,330,231 | 15.40 | 0.0002 | 4 | 4 | 0.045 | 2.2 | 21.6 | 51.30 | 28.16 | 0.2295 | 0.02260 |
| **10** | 4,315,510 | 359,626 | 13,306 | 0.15 | 0.0037 | 2 | 4 | 0.045 | 0.14 | 3.12 | 7.41 | 0.36 | 0.0029 | 0.00064 |
| **6** | 4,315,510 | 359,626 | 13,306 | 0.15 | 0.0391 | 2 | 4 | 0.045 | 0.07 | 2.56 | 6.08 | 0.16 | 0.0013 | 0.00012 |
| **22** | 4,315,510 | 359,626 | 13,306 | 0.15 | 0.0053 | 2 | 4 | 0.045 | 0.12 | 2.96 | 7.03 | 0.30 | 0.0024 | 0.00028 |
| **4** | 12,605,662 | 1,050,472 | 38,867 | 0.45 | 0.0330 | 2 | 4 | 0.045 | 0.13 | 3.04 | 7.22 | 0.33 | 0.0027 | 0.00024 |
| **12** | 25,552,191 | 2,129,349 | 78,786 | 0.91 | 0.0007 | 2 | 4 | 0.045 | 0.52 | 6.16 | 14.63 | 2.12 | 0.0173 | 0.00028 |
| **9** | 472,048,750 | 39,337,396 | 1,455,484 | 16.85 | 0.0037 | 4 | 4 | 0.045 | 1.18 | 13.44 | 31.92 | 10.29 | 0.0839 | 0.00900 |

Notes

1. See Figure B-1 for arroyo segment locations
2. Watershed areas based on digitization of digital elevation model
3. Runnoff rate fraction (0.037) empirically adjusted as Flow Model calibration parameter
4. Conductance per unit length is equal to alluvium vertical conductivity x calculated wetted width.
5. Periodic recharge rate per unit length is equal to average calculated stage (adjusted for channel side depths) x conductance per unit length.
6. Average recharge rate based on annual average of 0.94 months having 2 to 3 in. precip. and 0.37 months having greater than 3 in. precip. (Gallup area, 1960-2011 period of record). Average rate is the periodic rate times a frequency factor equal to (0.37 X 3 + 0.94 X 2)/365.
7. Average areal recharge rate is model input, based on calculated total recharge (annualized recharge rate x arroyo segment length) divided by recharge area (dependent on model cell sizes).

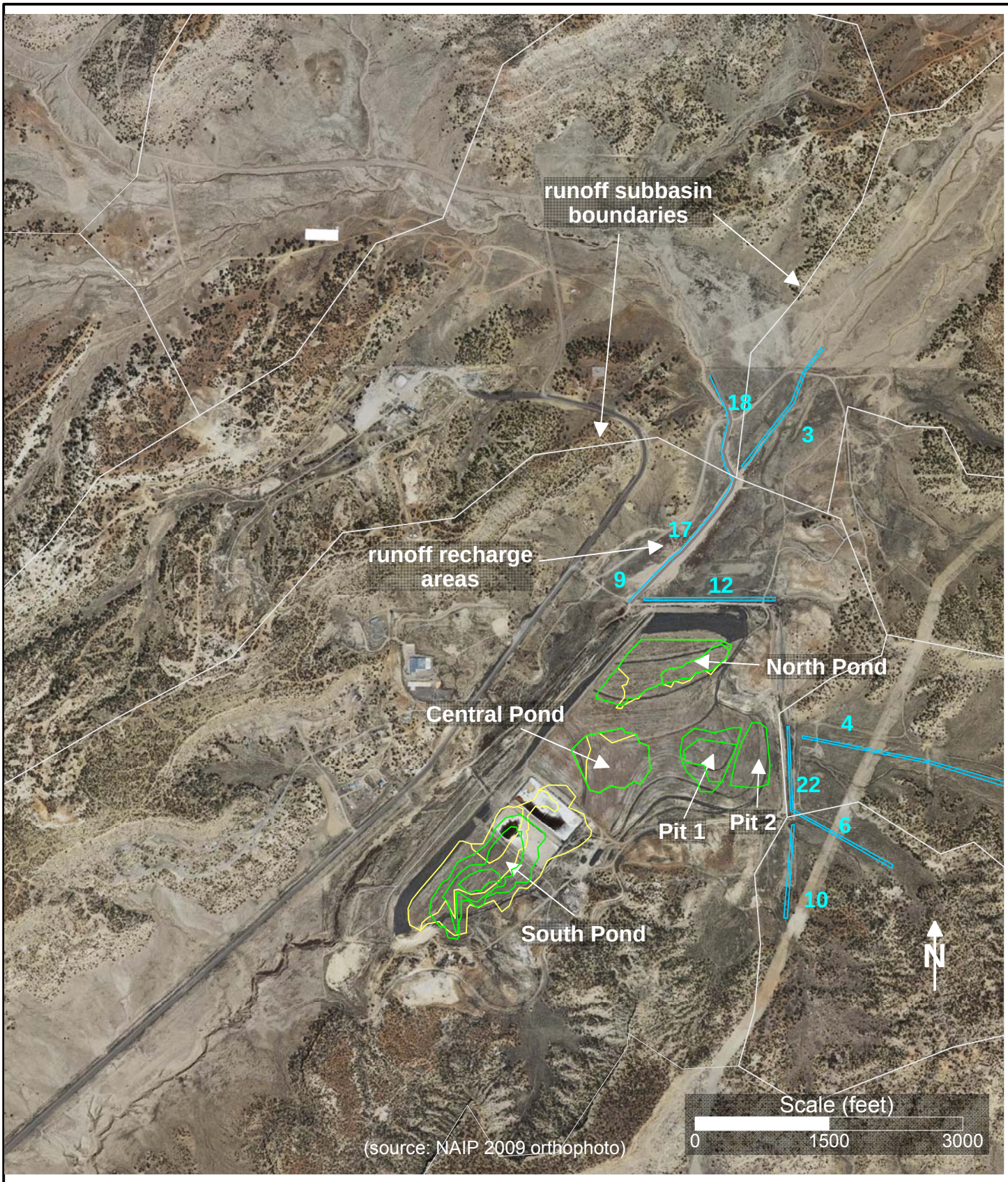


FIGURE B-1
Recharge areas used in Flow Model. Tailings sourced recharge areas outlined in yellow (pre-7/79 configurations) and green (post 7/79 configurations). (see Tables B-1, B-2 for tailings pond recharge estimates), Runoff-sourced recharge areas outlined in blue and portions of runoff subbasins in light grey (see Table B-3 for runoff recharge estimates).

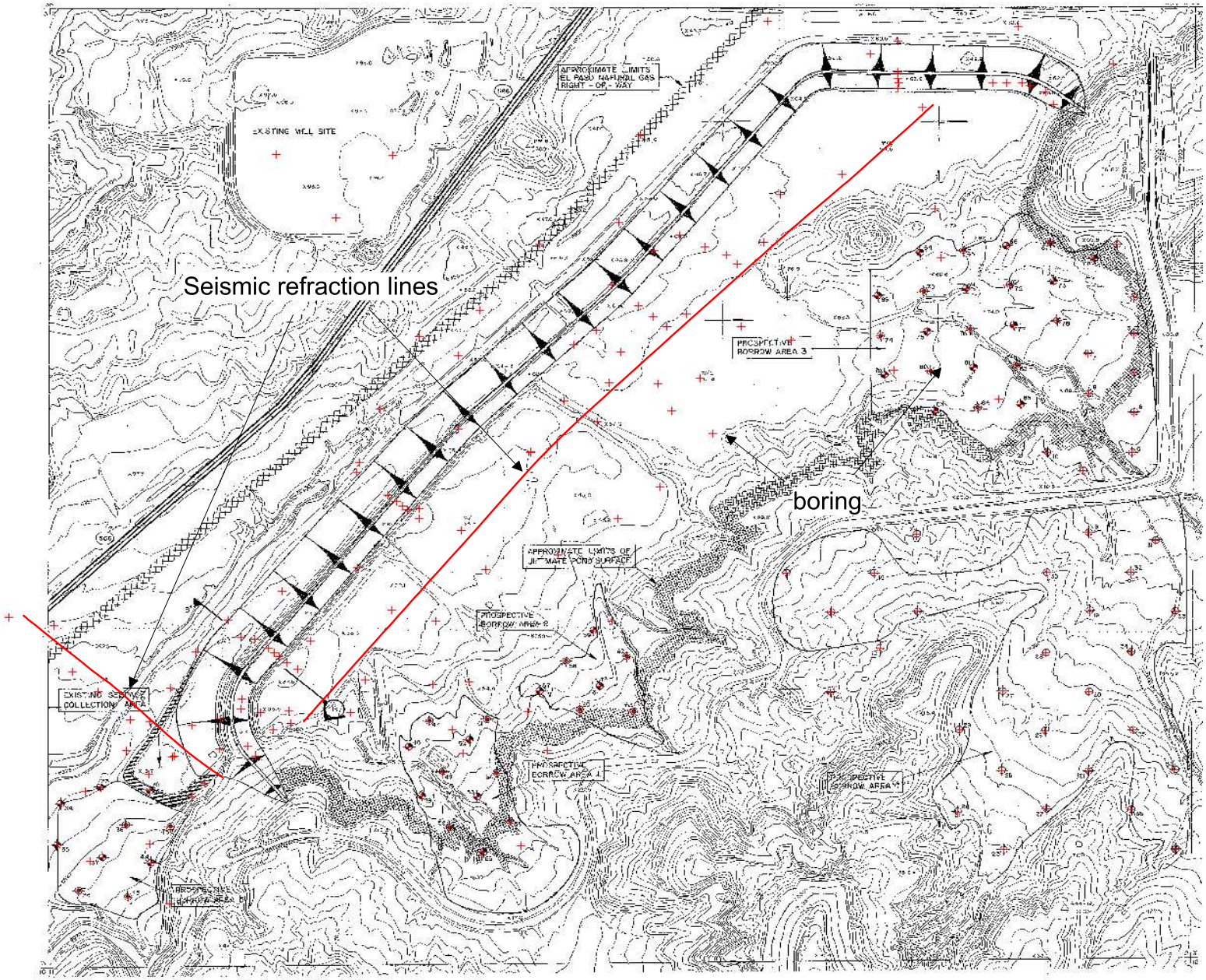


FIGURE B-2

May 1978 Topographic map showing planned modification of the "starter" dam, 1974-1979 borings, and 1976 seismic refraction survey used to estimate top-of-rock and base-of-tailings elevations (topographic base reproduced from Sergent, Hauskins & Beckwith, October 1978; seismic refraction lines from Sergent, Hauskins & Beckwith, July 1976)

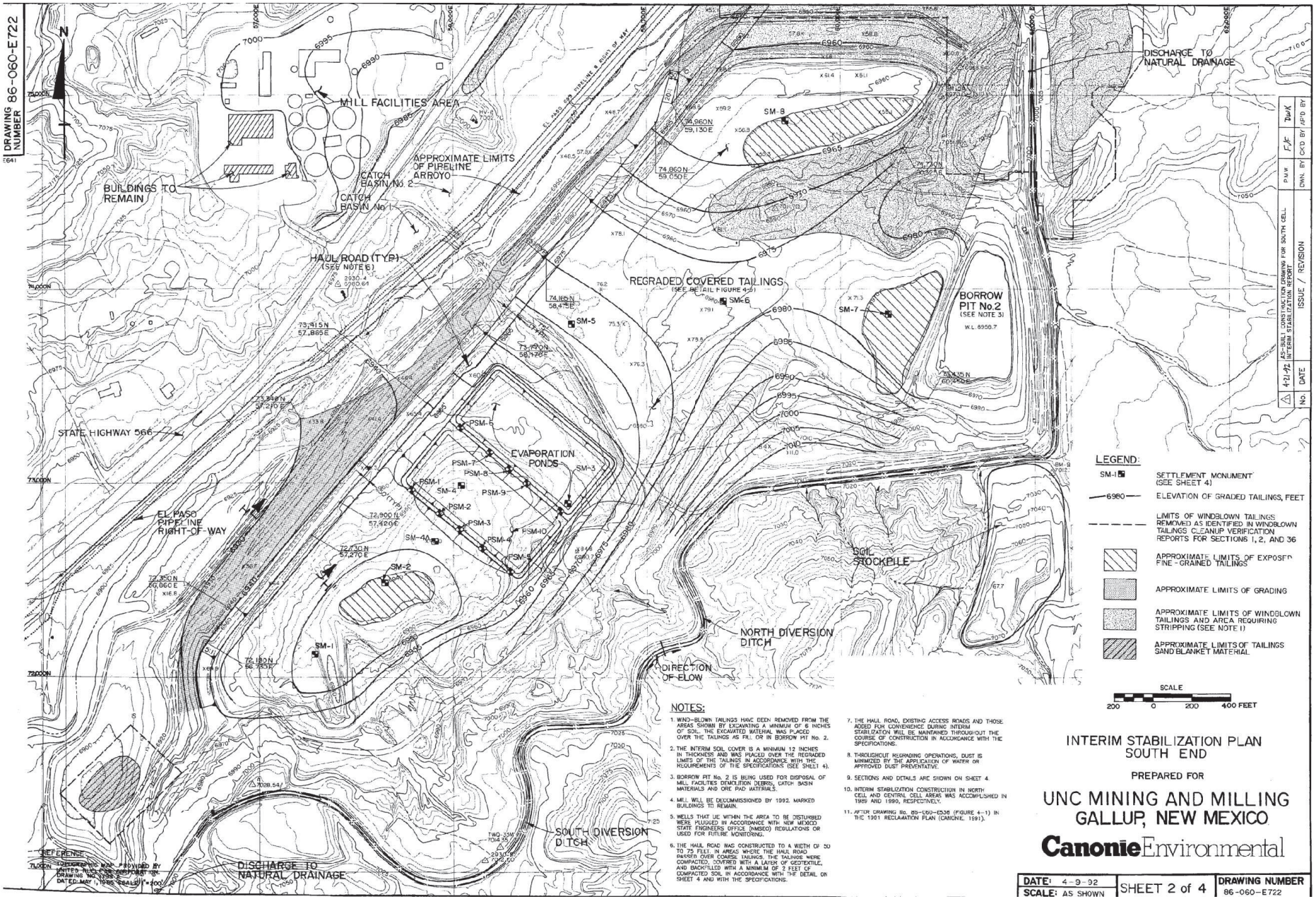


FIGURE B-3
May 1985 Topographic map showing planned elevation contours for the interim reclamation of 1989 - 1991 (reproduced from Canonie, April 1987)

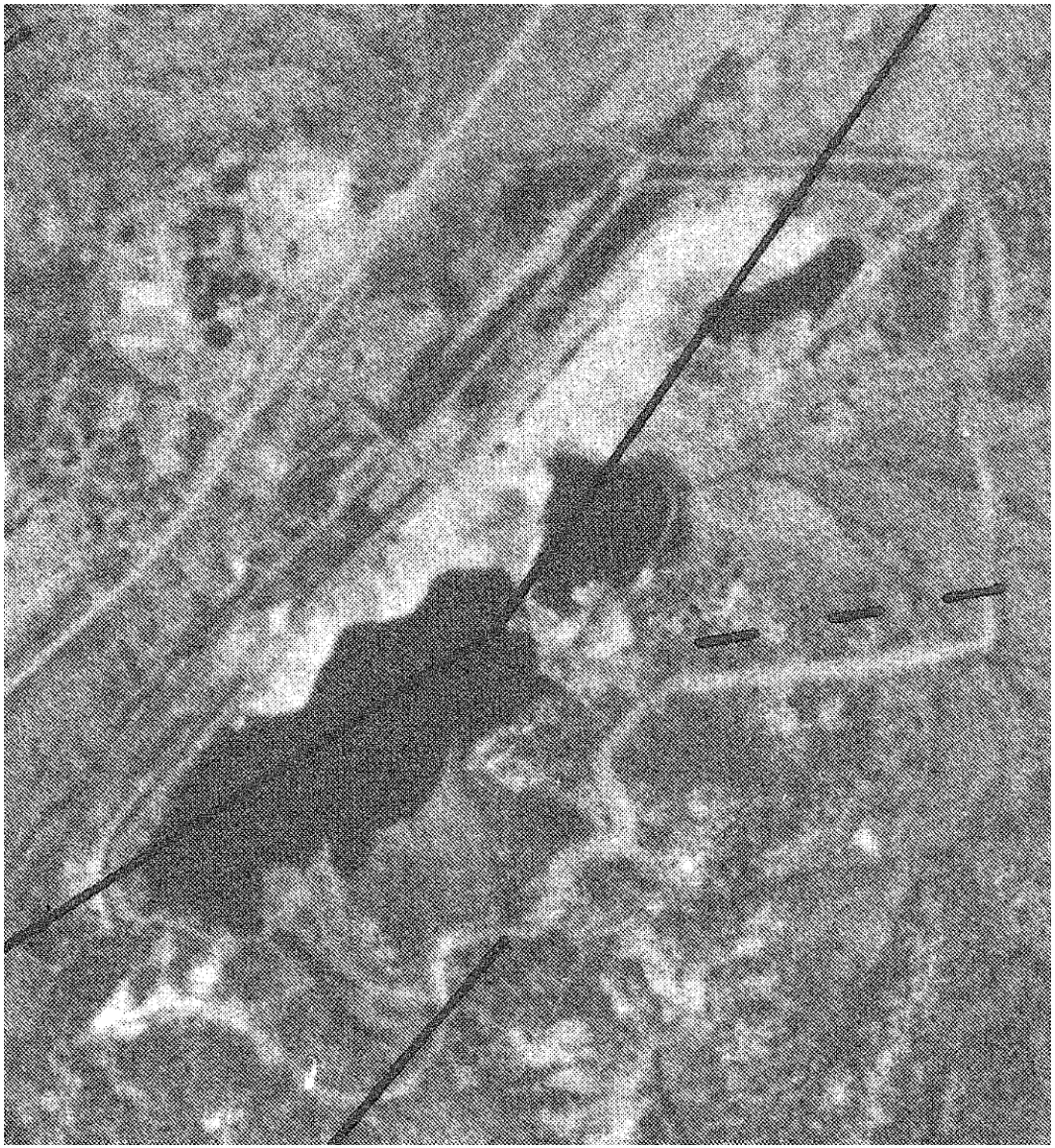

FIGURE B-4
June 10, 1979 aerial photograph, source UNC

FIGURE B-5
Collage of October 23, 1979 aerial photographs, source UNC

FIGURE B-6
January 15, 1980 aerial photograph, source UNC

FIGURE B-7
November 4, 1980 aerial photograph, source UNC


FIGURE B-8
April 7, 1981 aerial photograph, source UNC

# Appendix C

**PUMPING RATE TIME SERIES FOR EXTRACTION WELLS**

Table C-1
Zone 1 Pumped Well Time Series

| Date | Well 666 Rate (gpm) | Well 670 Rate (gpm) | Well 665 Rate (gpm) | Well 669 Rate (gpm) | Well 620 Rate (gpm) | Well 615 Rate (gpm) | Well 616 Rate (gpm) | Well 617 Rate (gpm) | Well EPA 1 Rate (gpm) | Well 607 Rate (gpm) | Well 611 Rate (gpm) | Well 303 Rate (gpm) |
|---|---|---|---|---|---|---|---|---|---|---|---|---|
| 12/5/1983 | | | | | | | | | | 0.00 | 0 | |
| 12/5/1983 | | | | | | | | | | 0.59 | 4.16 | |
| 1/10/1984 | | | | | | | | | | 0.59 | 4.16 | |
| 1/10/1984 | | | | | | | | | | 0.29 | 3.42 | |
| 3/30/1984 | | | | | | | | | | 0.29 | 3.42 | |
| 3/30/1984 | | | | | | | | | | 0.00 | 3.21 | |
| 9/12/1984 | | | | | 0 | | | | | | 3.21 | 0 |
| 9/12/1984 | | | | | 4.66 | | | | | | 3.21 | 0.99 |
| 12/31/1984 | | | | | 4.66 | | | | | | 3.21 | 0.99 |
| 12/31/1984 | | | | | 2.46 | | | | | | 3.21 | 0.52 |
| 10/14/1985 | 0.00 | 0 | 0 | 0 | 2.46 | | | | | | 2.55 | 0.52 |
| 10/14/1985 | 2.94 | 1.98 | 0.87 | 1.33 | 2.46 | | | | | | 2.55 | 0.52 |
| 12/31/1985 | 2.94 | 1.98 | 0.87 | 1.33 | 2.46 | | | | | | 2.55 | 0.52 |
| 12/31/1985 | 3.38 | 2.27 | 1.00 | 1.53 | 1.84 | | | | | | 2.39 | 0.39 |
| 12/31/1986 | 3.38 | 2.27 | 1.00 | 1.53 | 1.84 | | | | | | 2.39 | 0.39 |
| 12/31/1986 | 3.14 | 2.11 | 0.93 | 1.43 | 2.20 | | | | | | 2.19 | 0.47 |
| 12/31/1987 | 3.14 | 2.11 | 0.93 | 1.43 | 2.20 | | | | | | 2.19 | 0.47 |
| 12/31/1987 | 2.19 | 1.48 | 0.65 | 1.00 | 2.02 | | | | | | 2.05 | 0.43 |
| 12/31/1988 | 2.19 | 1.48 | 0.65 | 1.00 | 2.02 | | | | | | 2.05 | 0.43 |
| 12/31/1988 | 1.57 | 1.06 | 0.46 | 0.71 | 1.84 | | | | | | 1.94 | 0.39 |
| 12/31/1989 | 1.57 | 1.06 | 0.46 | 0.71 | 1.84 | | | | | | 1.78 | 0.39 |
| 12/31/1989 | 1.61 | 1.08 | 0.48 | 0.73 | 1.92 | | | | | | 1.57 | 0.41 |
| 9/24/1990 | 1.61 | 1.08 | 0.48 | 0.73 | 1.92 | 0 | 0 | 0 | 0 | | 1.57 | 0.41 |
| 9/24/1990 | 0.00 | 0.00 | 0.00 | 0.00 | 0.00 | 0.27 | 0.22 | 0.11 | 0.25 | | 0.00 | 0.00 |
| 8/12/1991 | 0.00 | 0.00 | | 0.00 | 0.00 | 0.27 | 0.22 | | | | | |
| 8/12/1991 | 1.87 | 1.46 | | 1.19 | 0.41 | 0.21 | 0.22 | | | | | |
| 10/11/1991 | 1.87 | 1.46 | | 1.19 | 0.41 | 0.21 | 0.22 | 0.11 | 0.25 | | | |
| 10/11/1991 | 1.87 | 1.46 | | 1.19 | 0.41 | 0.19 | 0.24 | 0.1 | 0.22 | | | |
| 12/2/1991 | 1.87 | 1.46 | | 1.19 | 0.41 | 0.19 | 0.24 | | | | | |
| 12/2/1991 | 0.00 | 0.00 | | 0.00 | 0.00 | 0.19 | 0.24 | | | | | |
| 10/9/1992 | | | | | | 0.19 | 0.24 | 0.1 | 0.22 | | | |
| 10/9/1992 | | | | | | 0.2 | 0.18 | 0.09 | 0.21 | | | |
| 10/8/1993 | | | | | | 0.2 | 0.18 | 0.09 | 0.21 | | | |
| 10/8/1993 | | | | | | 0.21 | 0.18 | 0.1 | 0.21 | | | |
| 10/14/1994 | | | | | | 0.21 | 0.18 | 0.1 | 0.21 | | | |

Table C-1
Zone 1 Pumped Well Time Series

| | Well 666 | Well 670 | Well 665 | Well 669 | Well 620 | Well 615 | Well 616 | Well 617 | Well EPA 1 | Well 607 | Well 611 | Well 303 |
|---|---|---|---|---|---|---|---|---|---|---|---|---|
| 10/14/1994 | | | | | | 0.19 | 0.15 | 0.13 | 0 | | | |
| 9/30/1995 | | | | | | 0.19 | 0.15 | 0.13 | | | | |
| 9/30/1995 | | | | | | 0.16 | 0.19 | 0.11 | | | | |
| 9/30/1996 | | | | | | 0.16 | 0.19 | 0.11 | | | | |
| 9/30/1996 | | | | | | 0.15 | 0.12 | 0.1 | | | | |
| 10/3/1997 | | | | | | 0.15 | 0.12 | 0.1 | | | | |
| 10/3/1997 | | | | | | 0.13 | 0.58 | 0.09 | | | | |
| 9/25/1998 | | | | | | 0.13 | 0.58 | 0.09 | | | | |
| 9/25/1998 | | | | | | 0 | 0.59 | 0.09 | | | | |
| 7/27/1999 | | | | | | | 0.59 | 0.09 | | | | |
| 7/27/1999 | | | | | | | | 0 | | | | |

Table C-1
Zone 1 Pumped Well Time Series

| Date | Well 636 Rate (gpm) | Well 301 Rate (gpm) | Well 312A Rate (gpm) | Well 304 Rate (gpm) | Well 622 Rate (gpm) | Well 306 Rate (gpm) | Well 621 Rate (gpm) | Well 623 Rate (gpm) | Well 302 Rate (gpm) |
|---|---|---|---|---|---|---|---|---|---|
| 12/5/1983 | | | | | | | | | |
| 12/5/1983 | | | | | | | | | |
| 1/10/1984 | | | | | | | | | |
| 1/10/1984 | | | | | | | | | |
| 3/30/1984 | | | | | | | | | |
| 3/30/1984 | | | | | | | | | |
| 9/12/1984 | 0 | 0 | 0 | 0 | 0 | 0 | 0 | 0 | 0 |
| 9/12/1984 | 0.99 | 0.66 | 0.58 | 0.55 | 0.47 | 0.41 | 0.33 | 0.33 | 0.11 |
| 12/31/1984 | 0.99 | 0.66 | 0.58 | 0.55 | 0.47 | 0.41 | 0.33 | 0.33 | 0.11 |
| 12/31/1984 | 0.52 | 0.35 | 0.31 | 0.29 | 0.25 | 0.22 | 0.17 | 0.17 | 0.06 |
| 10/14/1985 | 0.52 | 0.35 | 0.31 | 0.29 | 0.25 | 0.22 | 0.17 | | |
| 10/14/1985 | 0.52 | 0.35 | 0.31 | 0.29 | 0.25 | 0.22 | 0.17 | | |
| 12/31/1985 | 0.52 | 0.35 | 0.31 | 0.29 | 0.25 | 0.22 | 0.17 | 0.17 | 0.06 |
| 12/31/1985 | 0.39 | 0.26 | 0.23 | 0.22 | 0.19 | 0.16 | 0.13 | 0.13 | 0.04 |
| 12/31/1986 | 0.39 | 0.26 | 0.23 | 0.22 | 0.19 | 0.16 | 0.13 | 0.13 | 0.04 |
| 12/31/1986 | 0.47 | 0.31 | 0.27 | 0.26 | 0.22 | 0.19 | 0.16 | 0.16 | 0.05 |
| 12/31/1987 | 0.47 | 0.31 | 0.27 | 0.26 | 0.22 | 0.19 | 0.16 | 0.16 | 0.05 |
| 12/31/1987 | 0.43 | 0.29 | 0.25 | 0.24 | 0.20 | 0.18 | 0.14 | 0.14 | 0.05 |
| 12/31/1988 | 0.43 | 0.29 | 0.25 | 0.24 | 0.20 | 0.18 | 0.14 | 0.14 | 0.05 |
| 12/31/1988 | 0.39 | 0.26 | 0.23 | 0.22 | 0.19 | 0.16 | 0.13 | 0.13 | 0.04 |
| 12/31/1989 | 0.39 | 0.26 | 0.23 | 0.22 | 0.19 | 0.16 | 0.13 | 0.13 | 0.04 |
| 12/31/1989 | 0.41 | 0.27 | 0.24 | 0.23 | 0.19 | 0.17 | 0.14 | 0.14 | 0.05 |
| 9/24/1990 | 0.41 | 0.27 | 0.24 | 0.23 | 0.19 | 0.17 | 0.14 | 0.14 | 0.05 |
| 9/24/1990 | 0.00 | 0.00 | 0.00 | 0.00 | 0.00 | 0.00 | 0.00 | 0.00 | 0.00 |
| 8/12/1991 | | | | | | | | | |
| 8/12/1991 | | | | | | | | | |
| 10/11/1991 | | | | | | | | | |
| 10/11/1991 | | | | | | | | | |
| 12/2/1991 | | | | | | | | | |
| 12/2/1991 | | | | | | | | | |
| 10/9/1992 | | | | | | | | | |
| 10/9/1992 | | | | | | | | | |
| 10/8/1993 | | | | | | | | | |
| 10/8/1993 | | | | | | | | | |
| 10/14/1994 | | | | | | | | | |

Table C-2
Southwest Alluvium Pumped Well Time Series

| Well 801 | | Well 802 | | Well 803 | | Well 808 | |
|---|---|---|---|---|---|---|---|
| Date | Rate (gpm) | Date | Rate (gpm) | Date | Rate (gpm) | Date | Rate (gpm) |
| 10/13/1989 | | 10/13/1989 | | 10/13/1989 | | 6/26/1991 | |
| 10/13/1989 | 1.20 | 10/13/1989 | 11.10 | 10/13/1989 | 2.00 | 6/26/1991 | 10.00 |
| 10/12/1990 | 1.20 | 10/12/1990 | 11.10 | 10/12/1990 | 2.00 | 10/11/1991 | 10.00 |
| 10/12/1990 | 0.50 | 10/12/1990 | 12.50 | 10/12/1990 | 2.00 | 10/11/1991 | 15.50 |
| 10/11/1991 | 0.50 | 10/11/1991 | 12.50 | 10/11/1991 | 2.00 | 10/8/1992 | 15.50 |
| 10/11/1991 | 0.40 | 10/11/1991 | 11.90 | 10/11/1991 | 2.50 | 10/8/1992 | 19.90 |
| 10/8/1992 | 0.40 | 10/8/1992 | 11.90 | 10/8/1992 | 2.50 | 10/8/1993 | 19.90 |
| 10/8/1992 | 0.20 | 10/8/1992 | 9.00 | 10/8/1992 | 3.00 | 10/8/1993 | 15.60 |
| 10/8/1993 | 0.20 | 10/8/1993 | 9.00 | 10/8/1993 | 3.00 | 10/14/1994 | 15.60 |
| 10/8/1993 | 0.20 | 10/8/1993 | 9.80 | 10/8/1993 | 3.20 | 10/14/1994 | 12.30 |
| 10/14/1994 | 0.20 | 10/14/1994 | 9.80 | 10/14/1994 | 3.20 | 9/29/1995 | 12.30 |
| 10/14/1994 | 0.13 | 10/14/1994 | 9.74 | 10/14/1994 | 3.46 | 9/29/1995 | 12.20 |
| 9/29/1995 | 0.13 | 9/29/1995 | 9.74 | 9/29/1995 | 3.46 | 9/27/1996 | 12.20 |
| 9/29/1995 | 0.12 | 9/29/1995 | 9.08 | 9/29/1995 | 3.11 | 9/27/1996 | 7.20 |
| 9/27/1996 | 0.12 | 9/27/1996 | 9.08 | 9/27/1996 | 3.11 | 9/26/1997 | 7.20 |
| 9/27/1996 | 0.10 | 9/27/1996 | 10.10 | 9/27/1996 | 2.90 | 9/26/1997 | 4.34 |
| 9/26/1997 | 0.10 | 9/26/1997 | 10.10 | 9/26/1997 | 2.90 | 9/25/1998 | 4.34 |
| 9/26/1997 | 0.08 | 9/26/1997 | 11.02 | 9/26/1997 | 3.84 | 9/25/1998 | 3.50 |
| 9/25/1998 | 0.08 | 9/25/1998 | 11.02 | 9/25/1998 | 3.84 | 9/27/1999 | 3.50 |
| 9/25/1998 | 0.08 | 9/25/1998 | 9.62 | 9/25/1998 | 3.56 | 9/27/1999 | 2.50 |
| 7/30/1999 | 0.08 | 9/27/1999 | 9.62 | 9/27/1999 | 3.56 | 9/29/2000 | 2.50 |
| 7/30/1999 | 0.00 | 9/27/1999 | 9.31 | 9/27/1999 | 3.83 | 9/29/2000 | 3.35 |
| | | 9/29/2000 | 9.31 | 9/29/2000 | 3.83 | 1/12/2001 | 3.35 |
| | | 9/29/2000 | 5.80 | 9/29/2000 | 3.68 | 1/12/2001 | 0.00 |
| | | 1/12/2001 | 5.80 | 1/12/2001 | 3.68 | | |
| | | 1/12/2001 | 0.00 | 1/12/2001 | 0.00 | | |

# Appendix D

**PIEZOMETRIC SURFACE MAPS FOR JANUARY 1987 (AFTER CANONIE, 1987)**

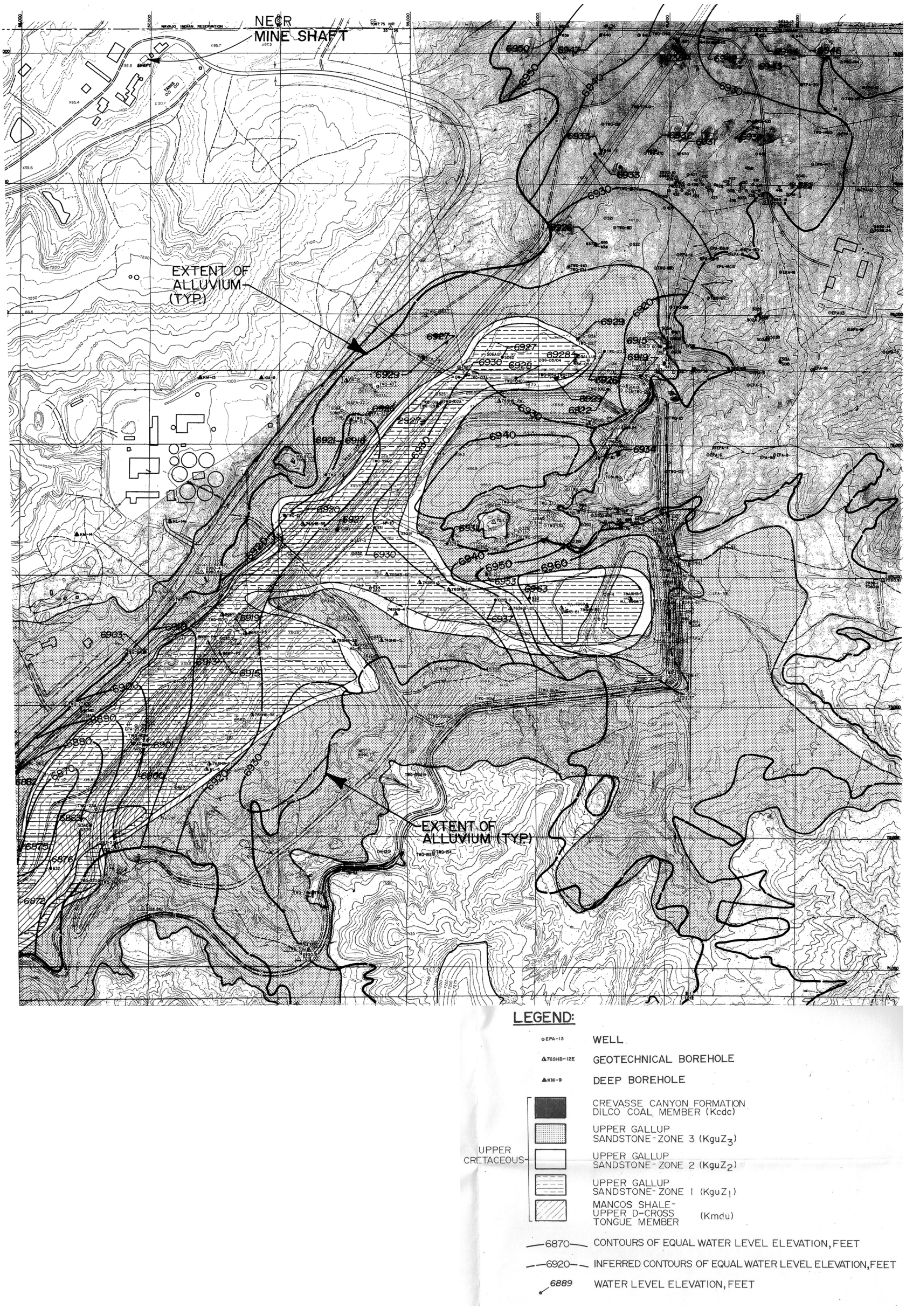


FIGURE D-1
Piezometric surface map of alluvium, January 1987.
Reproduced from Canonie (1987), 1985 topography composited from UNC maps

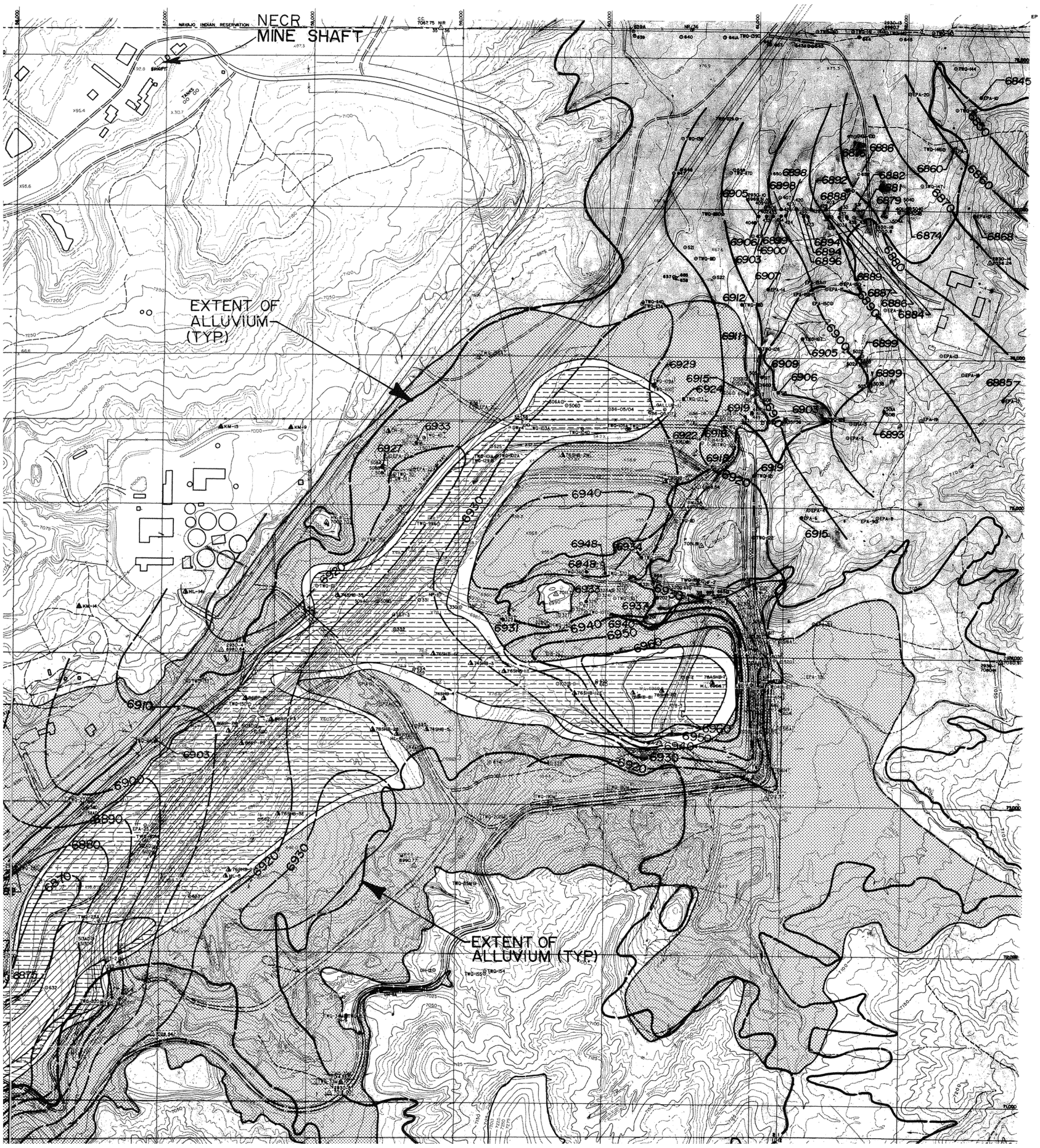


FIGURE D-2
Piezometric surface map of Zone 3, January 1987.
Reproduced from Canonie (1987), 1985 topography composited from UNC maps

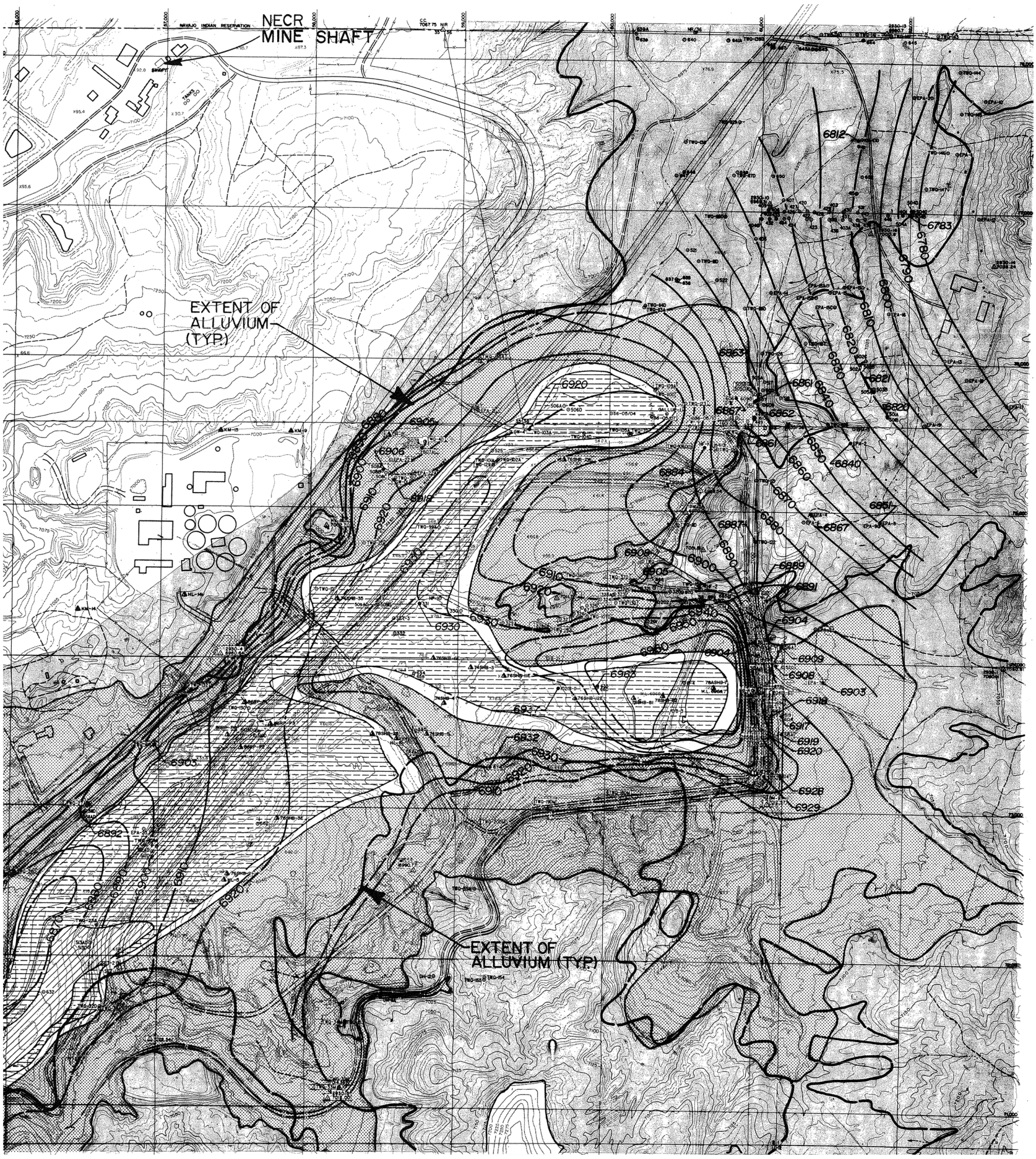


FIGURE D-3
Piezometric surface map of Zone 1, January 1987.
Reproduced from Canonie (1987), 1985 topography composited from UNC maps